11-1-1993

A Log NEQ based comparison of several silver halide and electronic pictorial imaging systems

Jack Holm

A Log NEQ Based Comparison of Several Silver Halide and Electronic Pictorial Imaging Systems

by

Jack Holm

B.S. Texas A&M University

(1981)

A thesis submitted in partial fulfillment of the
requirements for the degree of Master of Science
in the Center for Imaging Science in the
College of Imaging Arts & Sciences of the
Rochester Institute of Technology

November 1993

Signature of the Author Jack Holm

Accepted by Dana G. Marsh Nov. 8, 1993
Coordinator, M.S. Degree Program

COLLEGE OF IMAGING ARTS & SCIENCES
ROCHESTER INSTITUTE OF TECHNOLOGY
ROCHESTER, NEW YORK

CERTIFICATE OF APPROVAL

M.S. DEGREE THESIS

The M.S. Degree Thesis of Jack M. Holm
has been examined and approved by the
thesis committee as satisfactory for the
thesis requirement for the
Master of Science degree.

Dr. Zoran Ninkov, Thesis Advisor

Dr. Roger Easton

Prof. Richard Hailstone

11/7/93
Date

THESIS RELEASE PERMISSION
ROCHESTER INSTITUTE OF TECHNOLOGY
COLLEGE OF IMAGING ARTS & SCIENCES

Title of Thesis: A Log NEQ Based Comparison of Several Silver Halide and Electronic Pictorial Imaging Systems.

I, Jack M. Holm, hereby grant permission to the Wallace Memorial Library of R.I.T. to reproduce my thesis, with proper accreditation, in whole or part. Any such reproduction shall be for educational purposes only, and at no charge to the recipient, other than normal and proper duplicating charges. The permission granted herein does not constitute a transfer of copyright.

Date: 11/7/93

A LOG NEQ BASED COMPARISON OF SEVERAL
SILVER HALIDE AND ELECTRONIC PICTORIAL IMAGING SYSTEMS

by
Jack M. Holm

Submitted to the
Center for Imaging Science
in partial fulfillment of the requirements
for the Master of Science Degree
at the Rochester Institute of Technology

ABSTRACT

A protocol for determining log NEQ and a new metric, the Equivalent Image Quality or EIQ, are presented for the generalized experimental evaluation of noise related monochrome pictorial image quality. These metrics are then applied to the evaluation of a pictorial CCD camera and several pictorial films. Emphasis is placed on the development and verification of experimental techniques which do not require elaborate equipment or support facilities. Data analysis is conducted using only available software packages and personal computers. Conclusions are drawn concerning the performance of CCD based and silver halide imaging systems which allow for the objective comparison of the images they produce, and the fundamental differences in the characteristics and requirements of the two systems as applied to pictorial imaging are noted.

TABLE OF CONTENTS

TABLES

FIGURES

I. Introduction

The advent of electronic technologies is significantly impacting all aspects of imaging. New devices for image capture and output are introduced almost daily. These developments are synchronous with rapid advances in micro- and mini-computers and image processing software. Clearly, much of the future of imaging will be electronic, and this future will not be limited to high-end users. Within the next decade, it will be possible for the average consumer to purchase an entirely electronic imaging system, from the camera to the printer, and perform all of his/her own acquisition, processing, and output. Additionally, the motivation for this purchase will be enhanced by interconnectivity between still cameras, video, audio, and computers. We are at a new frontier in information management.

In view of these developments, it is surprising that so little work has been presented which compares the quality of electronic and conventional silver-halide imaging systems. It is possible that proprietary studies have been conducted and are not generally available, but it is also possible that the emphasis has been placed on the development of new technologies rather than comparison. One aspect of this development is that despite the increasing importance of electronic imaging, it is apparent that the silver-halide process possesses a number of extremely valuable and unique characteristics. Historically, silver-halide imaging has provided much of the framework for photographic science. The future of imaging will include

silver-halide technology as a very important part of the whole.

At this time, the need for objective comparison protocols and results is high. In particular, standards are under development for electronic photography which ideally will work in much the same way as those for conventional photography. Unfortunately, many of the metrics and standards developed for use with silver-halide images, such as Granularity and Resolving Power, are elegant in their use of the specific characteristics of the process. For example, the Granularity standard assumes data from a continuous, analog microdensitometer scan and noise that is relatively independent of spatial frequency. However electronic images are discrete, and detector characteristics result in fundamentally different noise profiles. Metrics currently used with electronic images frequently were developed for the analysis of electrical signals, and may not correlate well with familiar imaging metrics or with the perception of images. The comparison proposed requires the re-examination of some fundamental imaging metrics with a view to the development of new protocols for objective and general imaging system characterization.

The work presented here is the result of one such re-examination. It does not build on a specific, previously developed approach, but is the result of an overall view of the past fifty years work in this area. To this end, the concepts developed over this period were reviewed and evaluated according to the following criteria:

1. General application to all pictorial imaging systems.
2. Correlation to subjective imaging system quality characteristics.
3. Correlation to fundamental physical imaging system characteristics.
4. Simplicity of conception and application.

A number of the methodologies reviewed were excellent for a particular application, but did not meet one or more of the criteria. A few did meet all four criteria, and have been adopted to some extent, but are not universally accepted. There are also a few areas which have not been fully developed.

The goal of this work is to contribute to the development of a set of generalized pictorial image evaluation protocols. To this end, most of this work deals with noise-related image evaluation. It was found that this area was the least developed, although development in a number of areas is important. In some cases, the theoretical development in an area has advanced to the point where the conceptual behavior of systems is well understood, but this understanding has yet to be widely applied. Also, in some cases an excellent metric is available, but is generally not used due to a lack of widespread understanding or because of difficulties involved in the translation between system engineering metrics and evaluation metrics. For this reason, the work presented here is biased toward experimental results and the application of these results to image evaluation.

This work also emphasizes the evaluation of pictorial imaging systems in the simplest manner consistent with significant accuracy. In many cases, the lack of application of image evaluation protocols appears to stem from approaches which use rather sophisticated and uncommon equipment and custom software. The individuals conducting the evaluation frequently have only secondary interest in the practical application of the results, and others who are interested in practical application are frequently unable to conduct an evaluation. Rapid developments in electronic imaging are making it possible for much larger numbers of individuals to conduct meaningful evaluations on accessible equipment. Every effort was made in the development of the procedures presented to make them accessible to thousands, rather than dozens, of imaging professionals.

Complete establishment of general image evaluation protocols will be a monumental task far beyond the scope of this work. It is the hope of the author that the strategy presented here will fill in a major gap and outline a course to take to this end. The experimental results are an attempt to support the course outlined as an appropriate one, and to provide useful information concerning the relative advantages of silver-halide versus electronic image capture.

II. Background

Ultimately, the majority of pictorial images are evaluated subjectively. Images can also be used to represent data arrays, but in this case it is the data that has significance; the representation is primarily a tool for understanding. For this reason, true pictorial image evaluation must be subjective, or at least correlate with subjective evaluations. Unfortunately, differing perceptions and opinions result in significant variability with subjective evaluations. This variability must be described statistically, which makes subjective evaluation extremely cumbersome, especially when small differences between systems are to be detected.

The common approach to resolving this difficulty is to develop objective metrics, and then to establish correlations with subjective characteristics. The cumbersome subjective evaluations are carried out one time, to establish the correlation, allowing the objective metrics to be used for subsequent evaluation. A great deal of work has been done to establish objective metrics for image evaluation. For pictorial imaging systems, this work can be grouped into four areas: Tone Reproduction,[B&C; 1-13] Color Reproduction,[B-D; 14-17] Detail Reproduction,[A-D; 18-55] and Signal-to-Noise Characteristics.[A-D; 56-113] A listing of some of these metrics, also grouped according to application, is provided in Table 1. A significant amount of work has also been done to establish subjective correlations.[B&C; 114-142]

Table 1: Common Image Evaluation Metrics.

	Silver-Halide Systems	Electronic Imaging Systems	Generalized Metrics
Tone Reproduction	Quadrant Diagrams (Jones Diagrams) & Preferred Curves for Different Viewing Conditions*.	Gamma (Television); Printing Industry Standards (generally similar to the silver-halide metrics).	None established, although the silver halide metrics are applicable.
Color Reproduction	RGB Status Densitometry.	Various Colorimetric approaches.	CIELab* (although not correlated with RGB Status Densitometry).
Detail Reproduction	Resolving Power (lp./mm.) & Acutance*; SMT Acutance*.	Resolution (lines/picture dimension).	Modulation Transfer Function (MTF); Subjective Quality Factor (SQF)*.
Signal-to-Noise (S/N) Characteristics	Granularity & Density Range*; RMS Fluctuation*.	S/N (dB)*; various noise measurement schemes and Wiener Spectra (WS) & Gain*.	Noise Equivalent Quanta (NEQ); Information Capacity (IC).

*Indicates subjective correlation established.

The metrics listed above are widely varied in terms of both the degree of development of the subjective correlation and the generality. In particular, work is needed in the following areas:

1. Expansion of the silver-halide tone reproduction protocols to other types of imaging. The problem here is that the television standards have evolved to be significantly different from hard copy standards. In particular log values are not used, and the transfer function curves have fixed shapes which are not optimal for other imaging systems. At the same time the existing television standards as developed are appropriate

for the television industry. The best solution is probably a means for converting television "gamma" into four-quadrant tone reproduction space to allow comparison, while retaining the television standards for that specific use.

2. Correlation between Tricolor (RGB) measurements and CIELab coordinates. The reverse of the tone reproduction condition exists here. The tricolor metrics are essential to silver-halide and other types of tricolor imaging systems engineering, but are not applicable to other systems, and therefore are not subjectively correlatable. Standardized transformations from the various RGB spaces to CIELab space are needed.

3. More general adoption of the well developed Modulation Transfer Function (MTF) and Subjective Quality Factor (SQF) metrics.

4. A generalized, subjectively correlatable metric related to signal-to-noise (S/N) perception is needed. Specific metrics exist for specific imaging system types, but they are not comparable. Generalized metrics, such as Noise Equivalent Quanta (NEQ) exist, but are typically not considered for practical evaluation. The exact nature of the subjective correlation of this metric has also not been fully explored.

Of the choices listed above, it is currently possible to perform general objective image evaluation measurements in the areas of tone reproduction,

color reproduction, and detail reproduction. The protocols employed may not be universally accepted, and the details of the experimental procedure may need development, but the work could be done. It would be difficult, however, to conduct such an evaluation of noise-related image quality based solely on previously published literature. The work presented here is an attempt to fill this gap.

The lack of common but general S/N metrics is due primarily to a lack of application. A great deal has been published concerning the NEQ metric, and in particular the related Detective Quantum Efficiency (DQE) metric,[A, B, D; 143-170] but the emphasis of this work has been primarily on the use of the DQE metric to evaluate the efficiency of imaging systems. This metric has been applied successfully to a wide variety of systems, thus verifying its generality. However in pictorial photography the efficiency of the imaging system, while important, is not always directly related to image quality. It is frequently possible to increase the amount of light, thereby increasing image quality even with a relatively low efficiency system. Also, the quality of the final image is directly related to the size of the detector as well as to its DQE. The NEQ criterion is more useful for pictorial image evaluation than the DQE.

Another S/N metric of interest is the information capacity (IC) of a system. Again, a significant amount of work exists in this area,[A, B, D; 171-187] but it is mostly theoretical. Only a few publications exist containing experimental measurements of IC. Also, the IC of a system is related not only to the S/N,

but also to the information density, which is a function of the MTF.

In summary, a great deal of work has been done concerning image evaluation, but most of the work in the S/N area is either specifically related to a particular imaging system, or not immediately applicable to pictorial image evaluation. It should be possible, however, to build on generalized metrics such as the NEQ or IC to develop a protocol for such evaluation.

Having chosen a goal for the research to be conducted, the next step in the literature review is to evaluate different experimental procedures. By far the largest amount of work in the areas of interest has been done on film using microdensitometers,[A&B; 188, 189, 193, 194] but microdensitometry is not necessary with electronic images -- the data are already accessible. On the other hand, it is necessary in a comparative experiment to assure that the data obtained for one system are substantially equivalent to the data obtained for the other. Also, recent work indicates that newer techniques may allow for much faster microdensitometry on silver-halide materials by using array detectors.[190-192, 195-197] One of the major impediments to S/N evaluation is the number of data points required for statistically accurate results; faster measurement techniques can be of significant benefit. Finally, the goal of simplified data analysis must be considered.

III. Approach

The major aspects of the work presented here are the development of a strategy for noise related image quality evaluation, and the utilization of the strategy for comparison. During the course of the research, both aspects were conducted simultaneously. Various theoretical models were considered and compared to the experimental data. Additionally, the experimental data were viewed independently as the prime source of information for the development of empirical strategies. The strategy which resulted therefore has a theoretical and empirical basis. However it would be awkward to present the results in the manner in which they were obtained. For this reason, the theoretical presentation will precede the empirical one.

Theoretical:

The desired comparison requires the development of metrics applicable to all images, but correlatable, at least to some extent, with perceptual characteristics. The fundamental subjective characteristics of silver-halide images are tone and color reproduction, graininess, sharpness, and detail. The fundamental subjective characteristics of electronic images are tone and color reproduction, noise, dynamic range, pixel size, and inter-pixel effects. Of these characteristics, schemes for the objective evaluation of tone and color reproduction are well established for silver-halide images, and these schemes

are directly applicable and appropriate to electronic images (although this is not always done). Of the remaining characteristics, the objective correspondent to graininess is granularity (which is similar to noise), and sharpness and detail correlate with the objective MTF. The MTF of an electronic image relates to the pixel size and inter-pixel effects. In summary, the general objective characteristics of an image are tone and color reproduction, noise, MTF, and dynamic range.

In silver-halide imaging, the density ranges typically used for pictorial imaging are relatively constant. This means that even though the output dynamic range capabilities of various silver-halide materials and processes are different, practical considerations require that the dynamic range utilized be approximately the same. As a result, comparisons of noise measurements for silver-halide materials correlate well with comparisons of S/N measurements.

The motivation for the utilization of a constant dynamic range in silver-halide imaging lies in the effects of factors independent of the noise, in particular optical flare (stray light). Once the dynamic range has reached a certain level, generally on the order of 10:1, the advantages of increasing dynamic range are outweighed by flare degradation. Also, for a particular film, increasing the dynamic range is accomplished by increasing development. Increased development increases noise, and therefore no advantage is obtained with regard to S/N. Unfortunately, in other types of

imaging, noise is not a perceptual characteristic in itself. High levels of noise are compensated for by increasing signal strength. For this reason, the S/N ratio is often considered to be more significant than the actual noise level.

Another theoretical indicator of the importance of S/N relative to noise alone arises from information theory. The following relation for the information capacity (IC) of photographic film has been established:[172, 175-179]

$$IC = \pi\int_0^\infty \log_2\left[1+\frac{S(k)}{N(k)}\right]dk \qquad (1)$$

where S(k) and N(k) are the spectral (spatial frequency dependent) signal and noise associated with the system, and k is the spatial frequency. If images are viewed as a means of transmitting information, the quality of the image relates to the amount of information contained.

The final metric common to the measurement of noise is the NEQ criterion, defined by Rose[144, 145] as follows:

$$NEQ = \left[(S/N)_{out}\right]^2 \qquad (2)$$

In the above equation, S and N can be spectral quantities or integrated. The motivation for squaring the signal-to-noise ratio lies in the fact that for photons (which are Poissonly distributed) the number of photons is equal to

the square of the S/N. The NEQ criterion therefore indicates how many "imaginary" photons would be required to make an image with a specific S/N. Since the NEQ quanta are fictitious, the distribution of the actual physical elements making up the image is unimportant to the criterion. The NEQ is based solely on the S/N.

The concept of DQE is related to the NEQ and is also of interest in image evaluation. DQE is defined as follows:[A]

$$DQE = \left[\frac{(S/N)_{out}}{(S/N)_{in}}\right]^2 = NEQ / H_q \qquad (3)$$

where H_q is the number of actual exposure quanta input to the system. The DQE criterion characterizes imaging *systems*, not images, and is therefore not classified as an image characteristic. It is nevertheless important as a measure of the efficiency of an imaging process. The DQE concept may be extended to individual stages of an imaging process if the definition is generalized as follows:

$$DQE_j = NEQ_j / NEQ_i \qquad (4)$$

where DQE_j is the DQE of stage j, NEQ_j is the NEQ of stage j, and NEQ_i is the NEQ of stage i, or the input NEQ to stage j.

Note that the following relationship exists between information capacity and integrated (with respect to spatial frequency) NEQ, for S/N values much greater than unity:

$$IC \propto \log_{10}[NEQ], \quad S/N >> 1 \tag{5}$$

Also note that:

$$\log_{10}\left[NEQ_{system}\right] = \log_{10}\left[H_q\right] + \sum_{stages} \log_{10}\left[DQE_{of\ each\ stage}\right] \tag{6}$$

Therefore it is possible to determine the log NEQ of an image and the information content, given the number of input quanta and the log DQE values of the various stages of the system. Base-ten logarithms are not required for this computation, but are used here because they are commonly used in imaging system evaluation.

The concepts of NEQ and DQE presented above follow from the definitions, but in silver-halide imaging the equation for DQE is conventionally written as follows:[D]

$$DQE\left(H_q, k\right) = \frac{0.189\ \gamma^2\left(\log_{10} H_q\right)\ MTF(k)}{H_q\ WS\left(H_q, k\right)} \tag{7}$$

where γ is the pointwise slope of the characteristic curve of the material

under consideration, and WS is the Wiener or noise power spectrum. The 0.189 constant factor is $\log_{10}e^2$, which compensates for the change of slope brought about by the conventional use of $\log_{10}$ values on the input axis. The above equation gives DQE as a function of both exposure* and spatial frequency. It is also useful to simplify equation 7 by integrating over spatial frequency to obtain the following equation:[A]

$$DQE(H_q) = \frac{0.189\ \gamma^2(\log_{10} H_q)}{H_q\ G(H_q)} \tag{8}$$

where G is the granularity of the material.

The derivation of these expressions for the DQE of silver-halide materials is relatively straightforward, except for the definition of the "signal". The signal is considered to be the product of the input to the system and the gain, rather than the density above base plus fog. This definition departs from standard silver-halide imaging conventions, but makes sense if the imaging process is viewed as a means of conveying information. In any case, comparisons can be carried forward by using either definition as long as the same definition is used for all processes considered.

*Note: The exposure units used here are actual exposure quanta. In practice, other units are frequently used, in particular photometric units, in which case the input is measured in lux-seconds, and radiometric units, in which case the input is measured in joules (or ergs).

Unfortunately, equations 7 and 8 make use of a unique characteristic of silver-halide materials, notably the fact that:

$$G = N^2A = WS(0) = \text{integrated noise} \tag{9}$$

where N is the RMS noise measured using an aperture of area A. This characteristic results in the DQE being relatively independent of frequency. Electronic imaging detectors do not possess this characteristic. An integrated DQE value can be obtained, but theoretically only through the use of the Wiener spectrum.

However the purpose of this work is to obtain the simplest significant means of comparison. Two approaches allow for removal of the frequency dependence of the S/N:

1. Weighted integration of the S/N over the range of spatial frequencies visible to the eye.
2. Examination of the Wiener spectrum to determine its "flatness" over the visible spatial frequency range. If the spectrum is sufficiently flat, choice of an appropriate "pixel size" allows for the use of frequency independent noise values.

In this study, it was found that the Wiener spectra of the CCD camera, while not completely flat, had gradual slopes and no strong features (see Figures 7-

10). In another study, Juenger[111] used the first method and several sets of integration limits. The different limits resulted in only small changes in the integrated noise value. This result is particularly significant in view of the fact that the Wiener spectra of the CCD camera system used by Juenger were sloped more steeply than for the one studied here.

It is therefore possible to write an equation for DQE which is the result of either the appropriate choice of pixel size or integration between visually perceptible limits:

$$DQE\left(H_q\right) = \frac{0.189\ \gamma^2(\log_{10} H_q)}{H_q\ N^2(H_q)} \tag{10}$$

Or, using g for gain instead of γ:

$$DQE\left(H_q\right) = \frac{H_q\ g^2(H_q)}{N^2\left(H_q\right)} \tag{11}$$

Equations 10 and 11 are applicable to all imaging systems, but only for a specific final image magnification or magnification range, as the magnification determines the visual frequency response.

The range of magnifications over which equations 10 and 11 are applicable for a particular imaging system depends on the flatness of the Wiener spectra. With silver-halide imaging systems, the Wiener spectra are quite flat out to

very high spatial frequencies and consequently the equations are general. Noise levels are so objectionable at the magnifications required to make the sloped regions of the Wiener spectrum visible with silver-halide images that such magnifications are never used in pictorial applications. However CCD imaging systems are typically used at magnifications where the pixels are just small enough to be indistinguishable. The high cost of CCD chips which even approach the size of a standard 35mm film frame, and the non-existence of larger sizes requires that CCD based systems be used over a relatively limited range of magnifications for optimal results. It is too expensive in terms of equipment and memory requirements to capture and save a 12 Mb image unless a moderately large print is to be made. This limited practical magnification range allows equations 10 and 11 to be used for CCD systems, despite Wiener spectra which are typically more sloped than for silver-halide systems.

In summary, it is possible to obtain meaningful non-frequency-dependent DQE and NEQ values for both silver halide and CCD based imaging systems, although the conditions used in obtaining the values are somewhat different and must be considered in comparisons. Consequently, the optimal evaluation criteria for image characterization appear to be as follows:

Table 2: Criteria for Image System Characterization.

Characteristic	Criterion
Tone Reproduction	Characteristic Curve - Output (density or digital level) vs. Log Exposure (H, H_e, or H_q)
Color Reproduction	CIELab
Definition	MTF, SQF
Information Content	Log NEQ/pixel (or aperture area)
Efficiency	Log DQE/pixel (or aperture area)

Of course, even relatively robust metrics require intelligent application to produce meaningful results. The above metrics should correlate with subjective image quality provided they are applied appropriately to reasonably well designed systems. The subjective quality of images in poorly designed systems may still produce different subjective impressions even with the same objective results, as was demonstrated by Metz, *et al.*[127] In that work, however, it is important to note that some of the objective values were obtained for different pixel sizes, a condition that is prohibited with the proposed approach.

Experimental:

Currently, the standard for pictorial electronic image acquisition is the two-dimensional CCD array. Photoelectric scanners and various other

devices are used in some instances, but it is clear that the CCD detector is establishing dominance, and it seems reasonable to expect this dominance to increase as larger and cheaper arrays are constructed. The experimental comparison presented here is therefore between four monochrome pictorial negative films and a monochrome CCD camera. The following readily available Kodak films were chosen: Technical Pan, T-Max 100, T-Max 400, and T-Max P3200. The CCD camera used was the Kodak DCS200mi, which offers four quantization schemes designated by the exposure index values E.I. 100, E.I. 200, E.I. 400, and E.I. 800. Although it was discovered that the optimal exposure for the quantization schemes did not match the E.I. designation, the digital camera still encompassed most of the sensitivity range represented by the films.

It is noteworthy that the DCS200mi camera *system* is the subject of the evaluation for comparison. Undoubtedly, steps could be taken to improve the performance of the CCD chip and the digital file produced with respect to the characteristics measured, but the goal of these experiments was to compare real pictorial imaging systems. For this reason, the unaltered output of the camera system was evaluated, and this output was treated in the same way as a typical pictorial image. The digital file was considered to be the analog of the photographic negative. Ultimately, both the file and the negative must be printed (and the electronic file could be processed to improve the information contained), but the effects of these stages have been left for subsequent investigation.

The primary goal of this experimental investigation is to compare the quality of the images produced using the CCD camera and film. The secondary goal is to accomplish this in as simple a manner as possible. Consequently, some distillation of the characteristics to be measured is necessary. The emphasis of most of the literature in this area, however, has been on the characterization and modeling of systems. Little work has been done to simplify experimental approaches. The basis of the following discussion therefore rests largely upon the experimental results obtained in this study. These results are presented in subsequent sections.

Probably the most significant factor affecting the quality of a single image (electronic or film) is the degree to which it can be enlarged while maintaining a specified amount of definition. The degree to which an electronic image can be enlarged is a function of the number of pixels making up the image, and therefore of the amount of information contained. The maximum number of pixels currently available in electronic sensors is on the order of four million (2k x 2k). Larger sensors are being developed, and mosaics of sensors are used to form larger arrays, but the largest sensors available are generally not used for pictorial applications because of cost. These larger sensors will almost certainly become less expensive, but storage considerations may then become significant. It appears that the definition of electronic images will always be limited by the size of the image file that can be economically captured and stored.

However the degree of enlargement for silver-halide images is primarily related to the noise level of the image. Graininess is the major consideration in choosing a pictorial film for a specific degree of enlargement. MTF characteristics are important, but noise becomes apparent before the loss of sharpness and detail as enlargement increases for most conventional photographic systems. Also, the sharpness and detail capabilities of a particular film are directly tied to grain size, which also determines the noise. As the grain size (and therefore the noise) is reduced, the sharpness and detail automatically improve. This fundamental difference in the limitations of electronic and silver-halide processes is a great impediment to the comparison of images produced using the two systems.

In this study, this difficulty will be resolved by assuming that electronic images will be enlarged by a factor that depends on the number of pixels making up the image, and the final image sharpness and detail desired.

$$(\text{Enlargement Factor})^2 \propto (\text{Final Image Area}) \propto (\text{Number of Pixels}) \quad (12)$$

This assumption, while rather strict, is reasonable in view of the cost of capturing and storing the pixels of the image. Economic factors will strongly motivate consumers to settle upon a fixed information capacity for an imaging system. Once decided upon, it will generally be desirable to take advantage of its full capability.

The exact degree to which an image can be enlarged is subjective and variable, and need not be defined specifically. It is sufficient to say that a specific enlargement factor exists, and that it is directly related to the number of pixels contained in the image. In reality, this degree of enlargement will be related to the capabilities of the printer used, and the preferences of the viewer. Once decided upon, this degree of enlargement will result in the maximum spatial frequencies accurately represented in the image being reproduced at spatial frequencies corresponding to the highest sensitivity region of the eye. In other words, because of the scarcity of pixels in an electronic image, the pixels themselves optimally function as the aperture by which the noise of the image is most appropriately measured.

If this assumption is accepted, electronic and silver-halide images may be relatively easily compared. The pixels of the CCD are considered to be discrete apertures for the determination of CCD noise, and the same CCD is then used on a microscope to determine the film noise. The size of the data sample aperture for the film noise measurements is then chosen to match the actual CCD pixel size, considering the magnification of the microscope system. In this manner, direct comparison is possible between systems.

The above scenario allows for the determination of per pixel noise levels, and consequently S/N, NEQ, and DQE values. The values obtained in this manner will be effectively integrated over a specific spatial frequency range by the choice of aperture size. Under the assumption made above, this aperture

size is chosen to be optimal in relation to the spatial frequency sensitivity of the eye, and cost considerations. The approach presented does not specifically allow for the varying degrees of enlargement, and the resultingly different per pixel noise levels possible with silver-halide images. In other words, this comparison is somewhat biased in terms of flexibility toward electronic images, in that it allows constraints exclusive to electronic systems to dictate parameters for the measurement of all systems. However this bias need not reduce the significance of the results obtained, as it is possible to use the characteristic relationship between aperture and noise level to extrapolate to other degrees of enlargement for silver-halide materials. The only consideration is that the aperture must remain sufficiently large so that the MTF values for the range of spatial frequencies measured are comparable to those for the CCD.

IV. Procedure

Photometric/Quantumetric Relationship:

The first item considered was to establish a relationship between photometric exposure and exposure quanta. Standard sensitometric evaluation utilizes photometric measures, but the DQE criterion requires knowledge of the number of exposure quanta to obtain information about the input noise levels. To facilitate this determination, tungsten sources were

used for all exposures. Film exposures were made using a Kodak Model 101 sensitometer calibrated to 2850K. CCD exposures were made using a small (35 watt) tungsten-halogen source with a color temperature of 3100K at a distance of 144 cm. Shielding and baffles were used to prevent stray light from reaching the camera for the CCD exposures. All color temperatures were determined by using a Minolta Color Meter II.

A significant consideration involved when correlating photometric quantities with radiometric or quantumetric measures is the fact that photometric quantities are defined only at visible wavelengths (wavelengths between 390 and 760 nm.). This consideration does not cause a problem with the film exposures, because the response of the film to the 2850K source is minimal outside of this bandwidth. (At wavelengths shorter than 390 nm. the output of the source is very low, and at wavelengths longer than 760 nm. the films tested exhibit no measurable sensitivity.) The response of the CCD to the 3100K source at wavelengths longer than 760 nm., however, is large. For this reason a Kodak Wratten #301 infrared cutoff filter was placed in the light path for the CCD exposures.

Except for the effects of the infrared cutoff filter, the output of the tungsten sources was assumed to approximate that of a blackbody source at the same color temperature. The spectral distribution of a blackbody source at an absolute temperature of T can be calculated using Planck's Radiation Law:

$$E(\lambda) = \frac{2\pi hc^2}{\lambda^5}\left[\frac{1}{e^{hc/\lambda kT} - 1}\right] \qquad (13)$$

where $h = 6.626 \times 10^{-34}$ J-sec. (Planck's constant), $k = 1.381 \times 10^{-23}$ J/K (Boltzmann's constant), and $c = 2.9979 \times 10^{8}$ m/sec. (the speed of light). The power emitted (exitance) from a blackbody over a specific wavelength region is the integral of $E(\lambda)$ over the region of interest. Also, the number of photons emitted at a specific wavelength per unit time (photon exitance) is given by the equation:

$$N(\lambda) = \frac{E(\lambda)}{E_{photon}} = \frac{\lambda\, E(\lambda)}{hc} \qquad (14)$$

Data on the visual response function and infrared cutoff filter are not available in functional form. For this reason, equation 13 had to be integrated numerically to provide energy quantities for 10 nm. bandwidths. These values were then entered into a spreadsheet for subsequent manipulations. The results of these calculations are provided below in Table 3. Appendix B contains the details of these calculations along with plots of the various relationships. Note that the absolute number of exposure quanta per lux-sec. does not vary much for moderate changes in color temperature with typical blackbody-type sources. The primary cause of the decrease in photons/lux-sec. at 3100K was the infrared cutoff filter.

Table 3: Photon/Lux-Second Conversion Factors.

Color Temp.	photons/lumen-sec.	aperture area (μm^2)	photons/lux-sec.	log (photons/lux-sec.)
2850 K	1.91×10^{16}	82.1	1568110	6.20
3100 K	1.06×10^{16}	82.8	881098	5.95

Exposures:

The sensitometer shutter (exposure time 0.2 sec.) was used for the film exposures, with the step tablet modulating the exposures. A piece of clear plastic was placed between the film and the step tablet to reduce the imaging of step tablet noise patterns on the film. An inconel step tablet would have been preferable in this respect, in that it would not contribute to the noise level at all, but one was not available. To evaluate the magnitude of the step tablet noise contribution, a comparison of image noise levels was conducted between a sample of film exposed using the step tablet and another piece of film (from the same package) exposed to a similar amount of even illumination using a camera (see Table 4).

Both film samples were processed together, and ten sets of measurements were made from each sample by using the microdensitometry techniques described in the Microdensitometry System section. Data sample areas of 31 and 82 square microns were used. Though a difference in the noise levels for the two samples was observed, it was small relative to the overall noise level.

The contribution of the step tablet to the granularity was assumed to be insignificant for subsequent calculations. The raw data from which the values in Table 4 were obtained are in Appendix C.

Table 4: Step Tablet Noise Contribution Test.
(T-Max 400 samples, identically processed)

	Sensitometer Sample		Camera Sample	
Sample Diffuse Density:	0.88		0.85	
Data sample area (μm^2):	82	31	82	31
Mean Variance (output levels, 10 samples each):	89.0	221.1	77.6	212.4
Standard Deviation in Output Level Variance:	4.2	8.8	3.6	6.3
Mean Density Variance:	0.0028	0.0070	0.0023	0.0063
Mean Granularity:	0.231	0.218	0.188	0.195
Density Variance Contribution from Step Tablet	0.0005		0.0007	
Granularity Contribution from Step Tablet	0.043		0.023	

The DCS200mi camera shutter was used to control the CCD exposures. In the past, it has generally been considered inappropriate to use a camera shutter for sensitometric testing because of inaccuracies and variability. Modern electronic shutters, however, are far more accurate than their mechanical predecessors. The accuracy of the response curve fits attests to the reliability of this shutter (see Figure 1). The details of the acquisition of the electronic images used in this study are provided in Appendix I.

CCD Camera Response and Variance:

The CCD chip in the DCS200mi camera contains over 1.5 million pixels (1012 x 1524). It would be possible to use every pixel as a data point, but statistically this is unnecessary, and using the entire frame significantly increases memory requirements and computational time on small computers. Also, film measurements typically do not include an entire frame. A "clean" section is chosen from which measurements are made. For these reasons, a 114 x 76 pixel section of the top left corner of the DCS200mi images was chosen for analysis. This section appeared visually clean in views of the images, and still contains 8664 data points -- enough for significant statistical accuracy.

The analysis of the DCS200mi images consisted of direct calculation of the mean and variance of the selected sections of the image files. No attempts were made to "clean up" the files through bias subtraction, flat field division, *etc.* The results of the calculations are therefore representative of the images as they are delivered by the camera. The results of these calculations are presented in Table 5.

The next step was to determine the input-output response functions for the DCS200mi. This was accomplished by plotting the points and visually estimating the approximate form of the response function. The functional form chosen was as follows:

$$\text{output digital level} = a + b(\text{input exposure})^c + d(\text{input exposure}) \qquad (15)$$

where a, b, c, and d are constants. These constants were then determined using a linear regression fit in the Mathematica™ software package. The results are provided in Table 6 and Figure 1, and the raw data and calculations are provided in Appendices D and E. Note that the abscissa is input exposure rather than log exposure. This allowed the use of gain as opposed to γ in the DQE and NEQ equations.

Table 5: CCD Means and Variances.

	E.I. 100		E.I. 200		E.I. 400		E.I. 800	
Log Exposure	Mean	Variance	Mean	Variance	Mean	Variance	Mean	Variance
-4.45	1.04	6.19	5.10	15.35	3.58	22.97	9.70	80.78
-4.15	0.04	0.30	1.80	9.88	5.93	30.67	7.81	65.65
-3.85	3.44	12.28	1.79	9.80	7.41	33.63	9.81	73.04
-3.54			2.41	11.87	6.90	34.41	13.51	74.47
-3.24	6.12	6.01	5.14	14.68	11.40	37.52	19.43	63.00
-2.94	2.92	11.97	9.68	10.81	19.28	19.57	26.32	65.73
-2.64	9.61	3.81	16.64	5.43	29.93	19.62		
-2.32	16.28	2.04	27.44	3.72				
-2.02	27.08	1.07	43.32	3.40				
-2.59	13.32	1.85	19.24	5.30	32.43	13.54	55.01	34.08
-2.29	18.24	2.34	29.93	2.61	51.27	10.35	82.63	21.35
-1.99	27.02	1.05	47.44	2.14			125.6	19.43
-1.68	45.91	0.85	73.12	3.53	122.6	7.45	198.1	17.80
-1.38	73.62	0.70	111.0	2.08	195.9	5.66	255	0
-1.08	114.3	1.13	179.7	2.63	254	0		
-0.78	182.1	2.82	254	0				
-0.46	254	0						

Table 6: DCS200mi Response Curve Fits.

Exposure Index Setting	Response Equation
100	output digital level = $-4.72 + 380(\text{exposure})^{0.55} + 274(\text{exposure})$
200	output digital level = $-3.60 + 548(\text{exposure})^{0.55} + 525(\text{exposure})$
400	output digital level = $-2.85 + 849(\text{exposure})^{0.55} + 1238(\text{exposure})$
800	output digital level = $-2.56 + 1308(\text{exposure})^{0.55} + 2208(\text{exposure})$

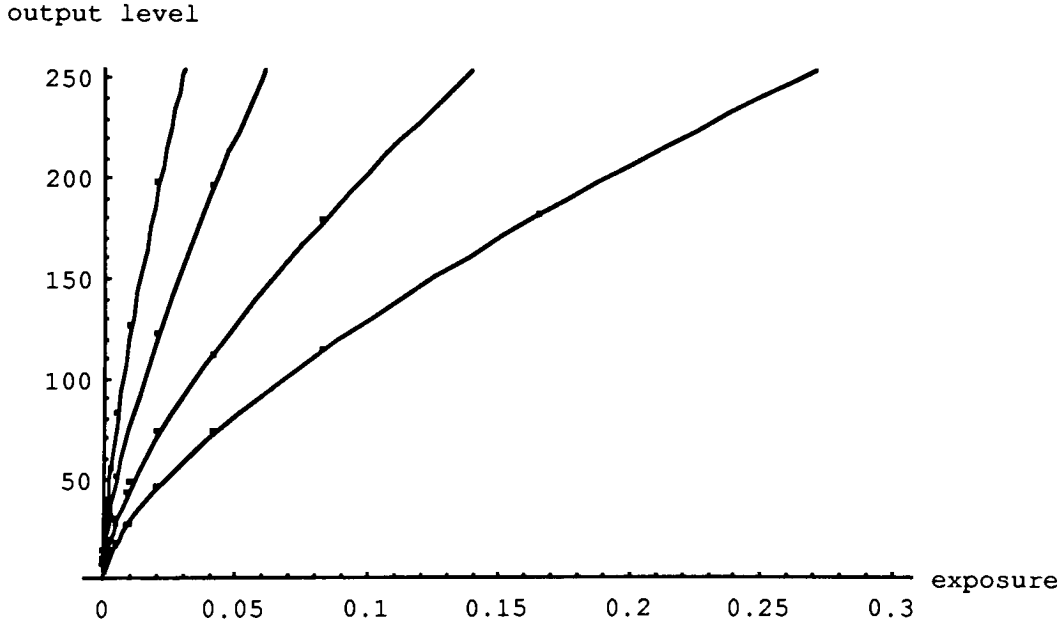

Figure 1: DCS200mi Response Curves.
(points = data points; lines = curve fits)

The final measurements of the DCS200mi performance consisted of the determination of the bias and flat-field characteristics. The bias values for the DCS200mi were obtained by averaging the mean output level for all frames

which received log exposures of -3.85 log lux sec. or less. No significant signal levels were observed at these log exposure values, and the response functions obtained using these bias values indicated that the response at these exposure levels should be below the cutoff for the first quantization level. The resulting bias values are provided in Table 7.

Table 7: Bias values for Dark CCD Frames.

Frame #	145	146	147	Mean
Quantization E.I.	100	100	100	100
Mean Digital Count	1.04	0.04	3.44	1.51
Frame #	164	165	166	Mean
Quantization E.I.	200	200	200	200
Mean Digital Count	5.10	1.80	1.79	2.90
Frame #	181	182	183	Mean
Quantization E.I.	400	400	400	400
Mean Digital Count	3.58	5.93	7.41	5.64
Frame #	197	198	199	Mean
Quantization E.I.	800	800	800	800
Mean Digital Count	9.70	7.81	9.81	9.11

The reason for determining the DCS200mi fixed pattern noise is to allow for a more accurate determination of the microscopic film characteristics using the DCS200mi camera/microscope system. To this end, ten clear-field

(uniform) exposures were made using this system at a speed setting of 100. These exposures were then reduced (by averaging pixels) in the same manner as for the images of the film samples, and averaged together. The resulting "flat field" was then normalized to a mean value of unity. The bias value of 1.51 for the E.I. 100 quantization scheme was considered to be so low as to be insignificant, and was not included in the calculations.

The size of even the reduced flat field precludes its tabular presentation in the body of this report, but a plot of the levels is provided in Figure 2.

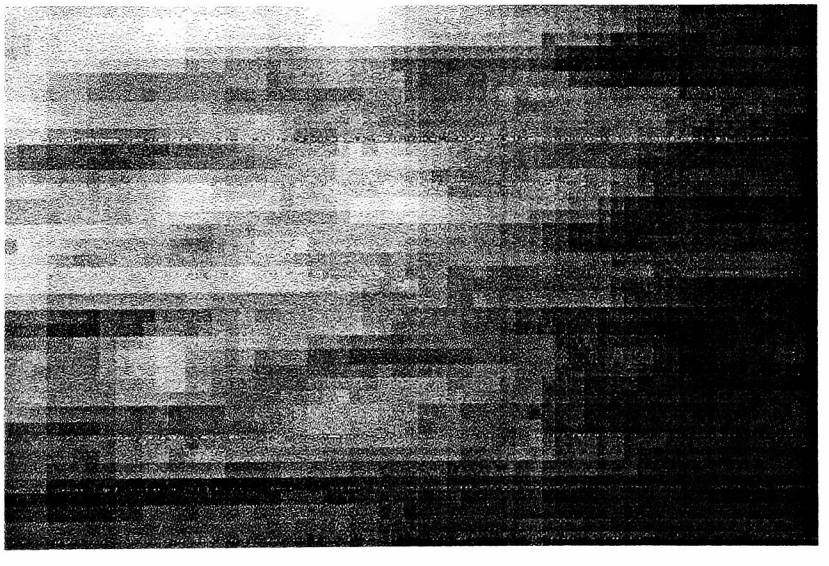

Figure 2: DCS200mi Flat Field; Microscope Illumination.
(tones expanded to go from black to white)

The contrast in the above figure is greatly expanded. If the image were presented at normal contrast, it would appear to be even. It is also likely that much of the observed fluctuation is due to unevenness in the microscope illumination. The bias and flat field characteristics of the DCS200mi camera/microscope system appear to be quite good, even without external bias subtraction and flat field division. However flat field division is not difficult, and the observed fluctuation is more significant than the bias. For these reasons, flat field division was employed in the analysis of the camera/microscope system data. The actual flat field, along with some analysis of its characteristics, is provided in Appendix F.

Microdensitometry System:

The pixels of the DCS200mi CCD are rectangular with an approximate area of 82 square microns. The microdensitometry system consists of this camera mounted atop a Nikon Optiphot microscope with a 10X 0.45 N.A. plan-apochromatic objective, a 1.4 N.A. apochromatic condenser stopped down to a N.A. of 0.30, and 2.5X and 4X eyepiece-camera systems.

Most of the film sample images were obtained using the 2.5X eyepiece-camera system, providing a total magnification of 26X on the CCD. The 1012 x 1524 pixel images were then reduced through pixel averaging to 39 x 59 pixel images, with the pixels in the reduced images corresponding to a rectangular

aperture with an area of approximately 82 square microns on the film samples. The second set of film sample images was obtained using the 4.0X eyepiece-camera system, resulting in a total magnification of 42X. These images were reduced to both 39 x 59 and 24 x 36, providing for data sample aperture areas of 31 and 82 square microns respectively.

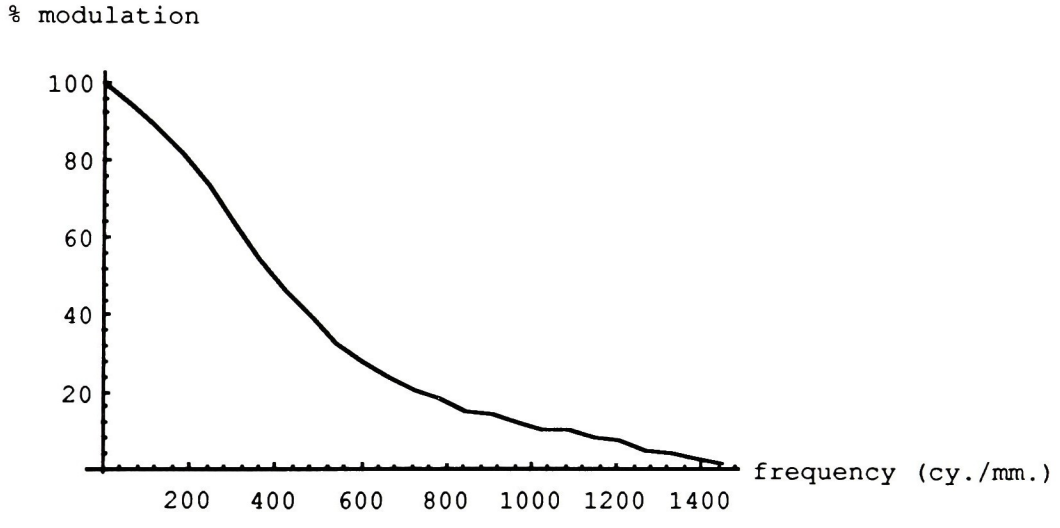

Figure 3: Combination DCS200mi/Microscope MTF Curve.

Hertel and Topfer, *et. al.*[195-197] have used CCD arrays on microscope systems as microdensitometers, so the technique has been applied previously. In such systems there are three important effects which must be considered: the system MTF, the effects of flare light, and the effects of quantization.

With the system used, extensive pixel averaging reduces the significance of these effects. At the spatial frequencies of interest, the MTF is assumed to be approximately unity. The flare light, which significantly affects only the darkest areas of the image, is also assumed to make a negligible contribution as the small dark areas are averaged with larger midtone and light areas. Finally, the quantization to 256 levels is assumed to be sufficient to adequately represent the random fluctuations to be measured in the film samples. These assumptions, while seemingly reasonable, require at least some validation. To this end, an MTF curve for the DCS200mi/Microscope system was obtained (see Figure 3). The calculations for this MTF curve can be found in Appendix G.

Effect of Data Sample Area on Mean Square Density Fluctuation:

A final check on the validity of the microdensitometer system utilized lies in the verification of the granularity relationship for silver-halide films. It has been established that the product of the aperture area and the mean square density fluctuation should be a constant for a moderate range of apertures (see equation 9). Given the nature of the images obtained of the film samples, it is a relatively simple matter to construct a range of data sample apertures and determine if this relationship holds. Figure 4 is a plot of the granularity of step 16 (density = 0.88) of the T-Max 400 sample as a function of aperture size. The data points in this plot were obtained from

images taken using the 2.5X eyepiece-camera system. These points do not form a horizontal line partially because the data files from which they were produced were not corrected by flat field division. This was done to speed up the determination the approximate range of aperture sizes over which the correctly calculated granularity relationship should hold. As the aperture becomes very small, the effect of flare becomes more significant because the darkest pixels are averaged in with fewer others, resulting in a decrease in granularity. As the aperture becomes large, the quantization limits the accuracy with which the small differences in density can be reproduced, increasing the measured granularity.

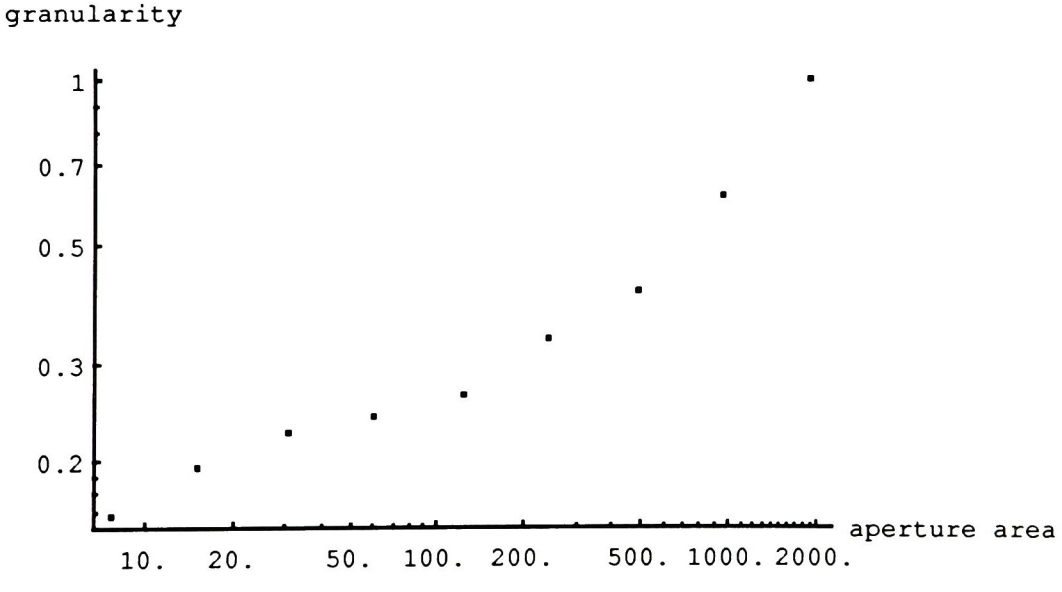

Figure 4: T-Max 400 Granularity vs. Data Sample Aperture Area (sq. μm.).
(wide aperture range, no flat field division, one sample per aperture size)

Examination of the above figure suggests that problems with flare begin to appear with aperture sizes less than about 30 square microns (5.5 x 5.5 μm.), with the 2.5X eyepiece-camera system. Quantization effects appear at aperture sizes larger than 120 square microns (11 x 11 μm.). Figure 5 is a plot of the same relationship over a more limited range of aperture sizes. In this case, twenty flat field corrected data files were used to obtain twenty data points at each aperture size (the vertical "lines" in the plot). These points were obtained using the 4.0X eyepiece-camera system. Three other points are also plotted in Figure 5. They were obtained using the 2.5X eyepiece-camera system. A best-fit line is drawn through the data points. Note that, as expected, its slope is relatively flat. Figure 6 shows the same relationship for the DCS200mi camera. The calculations on which these figures are based are included in Appendix H. Other data on the acquisition of the images used for the noise measurements are provided in the Image Log, Appendix I.

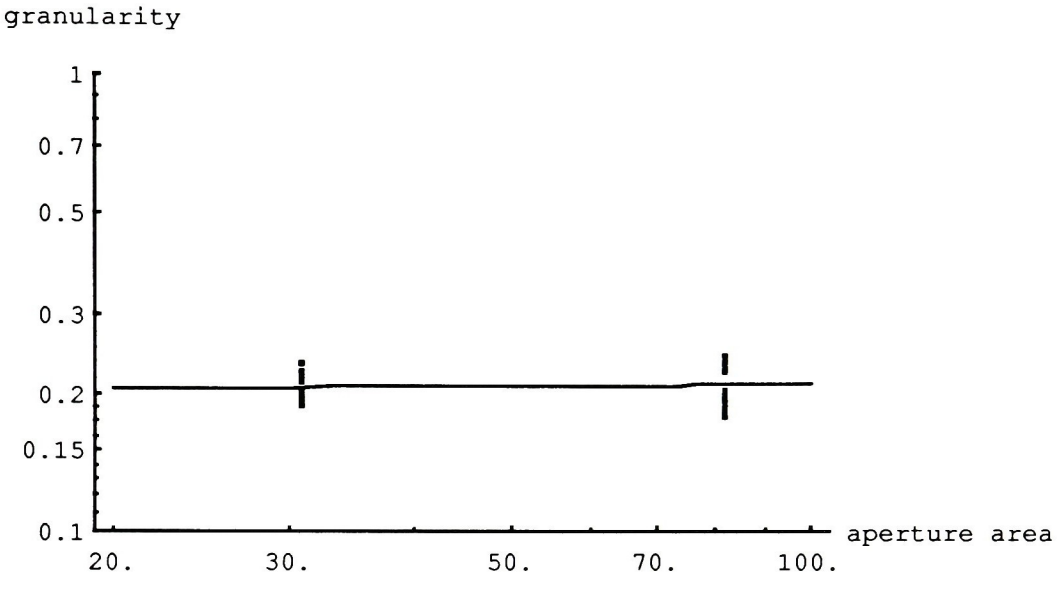

Figure 5: T-Max 400 Granularity vs. Data Sample Aperture Area.
(apertures of 31 and 82 square microns, with flat field division)

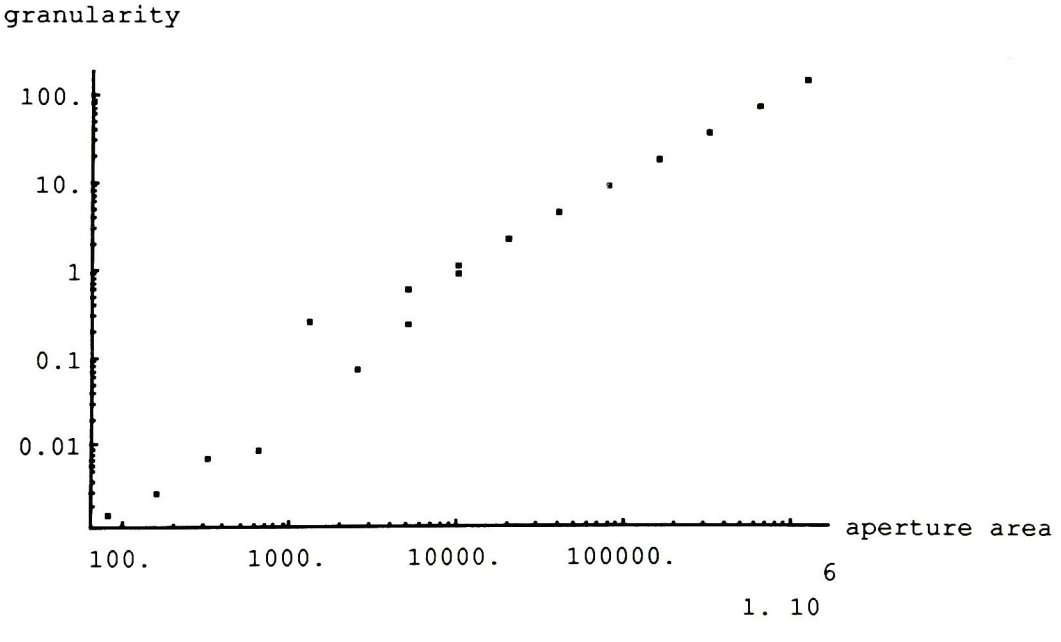

Figure 6: DCS200mi "Granularity" vs. Data Sample Aperture Area.

Film Sample Response and Variance:

Once the validity of the microdensitometer system is established, it can be used to obtain information about the noise characteristics of the film samples. Table 8 lists the results of these measurements (also see Appendix J).

Table 8: Film Sample Mean Response and Variance.

Log Exposure	Density	Density Standard Deviation	Granularity	DQE (%)	log NEQ
Technical Pan:					
-1.69	0.23	0.01532	0.019	0.167	1.73
-1.55	0.28	0.01739	0.025	0.200	1.95
-1.40	0.34	0.02046	0.034	0.205	2.11
-1.27	0.43	0.02277	0.043	0.199	2.23
-1.12	0.53	0.02560	0.054	0.110	2.12
-0.97	0.63	0.02761	0.063	0.065	2.04
-0.83	0.72	0.02951	0.071	0.035	1.92
-0.66	0.82	0.03124	0.080	0.018	1.80
-0.49	0.91	0.03415	0.096	0.011	1.76
-0.34	1.01	0.03540	0.103	0.007	1.71
-0.17	1.09	0.03913	0.126	0.004	1.59
T-Max 100:					
-2.31	0.30	0.03238	0.086	0.181	1.14
-2.14	0.35	0.03385	0.094	0.157	1.25
-2.00	0.40	0.03583	0.105	0.153	1.38
-1.85	0.47	0.03810	0.119	0.193	1.63
-1.72	0.56	0.03974	0.129	0.170	1.71
-1.57	0.65	0.04265	0.149	0.082	1.54
-1.42	0.73	0.04813	0.190	0.047	1.45
-1.28	0.82	0.04298	0.151	0.044	1.55
-1.11	0.91	0.04639	0.176	0.021	1.40
-0.94	1.00	0.04600	0.173	0.019	1.54
-0.79	1.11	0.04641	0.177	0.016	1.60

Table 8 (continued).

Log Exposure	Density	Density Standard Deviation	Granularity	DQE (%)	log NEQ
T-Max 400:					
-2.41	0.20	0.04753	0.185	0.155	0.98
-2.26	0.25	0.04688	0.180	0.113	0.99
-2.11	0.30	0.04902	0.197	0.086	1.02
-1.96	0.36	0.04820	0.190	0.088	1.18
-1.81	0.43	0.04853	0.193	0.073	1.25
-1.66	0.50	0.05010	0.206	0.049	1.22
-1.51	0.57	0.04909	0.198	0.036	1.24
-1.36	0.64	0.04759	0.186	0.030	1.32
-1.21	0.72	0.04986	0.204	0.023	1.34
-1.06	0.80	0.04859	0.194	0.017	1.37
-0.91	0.88	0.05125	0.215	0.012	1.36
T-Max P3200:					
-3.17	0.36	0.10038	0.826	0.187	0.30
-3.02	0.42	0.10453	0.896	0.215	0.51
-2.87	0.49	0.09961	0.814	0.250	0.72
-2.72	0.58	0.09786	0.785	0.242	0.86
-2.57	0.67	0.09204	0.695	0.194	0.91
-2.42	0.76	0.09437	0.730	0.119	0.85
-2.27	0.84	0.09744	0.779	0.076	0.80
-2.12	0.93	0.09890	0.802	0.071	0.93
-1.97	1.04	0.10380	0.884	0.053	0.95
-1.82	1.14	0.10391	0.885	0.036	0.93
-1.67	1.25	0.10999	0.992	0.026	0.93

DCS200mi Response and Variance:

The shape of the Wiener spectrum for photographic film insures that granularity is a good measure of the noise present. However, we have already seen in Figure 6 that the product of the aperture area and the measured mean square fluctuation for the DCS200mi is not constant over even a limited range as the aperture size is varied (although it is reasonable to suspect that at least some of this slope results from the re-quantization of the

aperture values). The use of an aperture with an area equivalent to the CCD pixel area allows for direct comparison at a fixed magnification regardless of the effect of changing aperture areas, however an ideal comparison would provide values quantifying the noise level in a manner independent of the magnification. The question then becomes: can a parameter similar to film granularity be calculated for a CCD camera system. The answer to this question lies in the shape of the CCD Wiener spectrum. For a given magnification, the observed noise is the spectral noise weighted by the spectral noise sensitivity of the eye. Different magnifications result in different limits and weighting values at different spatial frequencies. However if the Wiener spectra are flat, moving the visual spectral weighting function up and down the spatial frequency axis will have no effect. Figures 7 - 10 display some experimental Wiener spectra of mid-range uniform exposures using two different quantization schemes. Appendix K contains the calculations.

These plots indicates that the Wiener spectra for the DCS200mi are relatively flat, with only a slight negative slope. Consequently, for this CCD camera, direct comparison of the log NEQ values as calculated from the MSF should be valid over a reasonable range of magnifications. Table 9 lists the response, variance, DQE, and log NEQ for the DCS200mi at all four quantizations over the useful exposure range for each. The supporting calculations can be found in Appendix L.

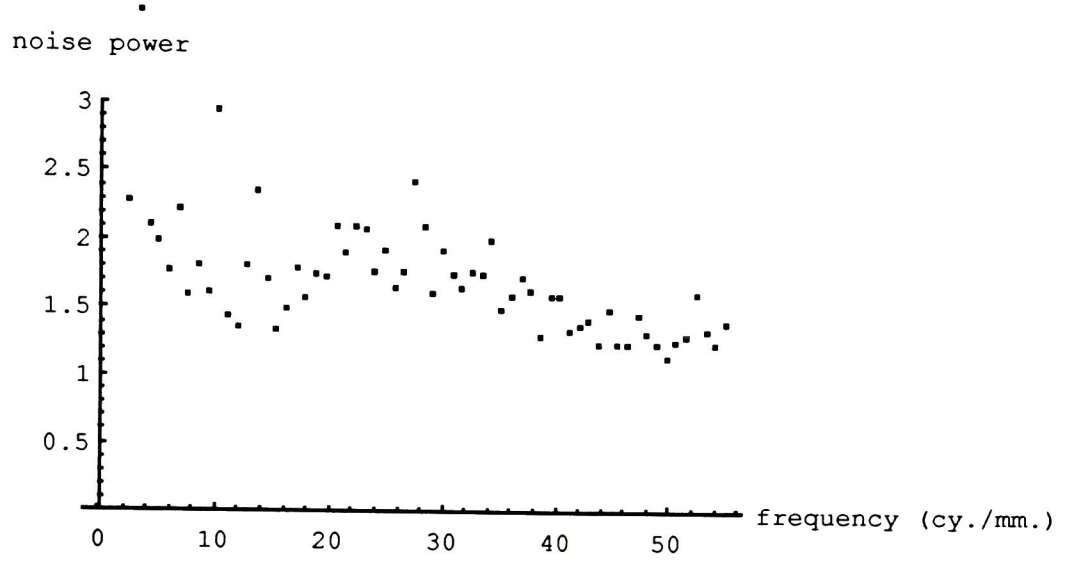

Figure 7: Horizontal Wiener Spectrum Values, E.I. 100 Quantization.
(Data points are from midtone exposures.)

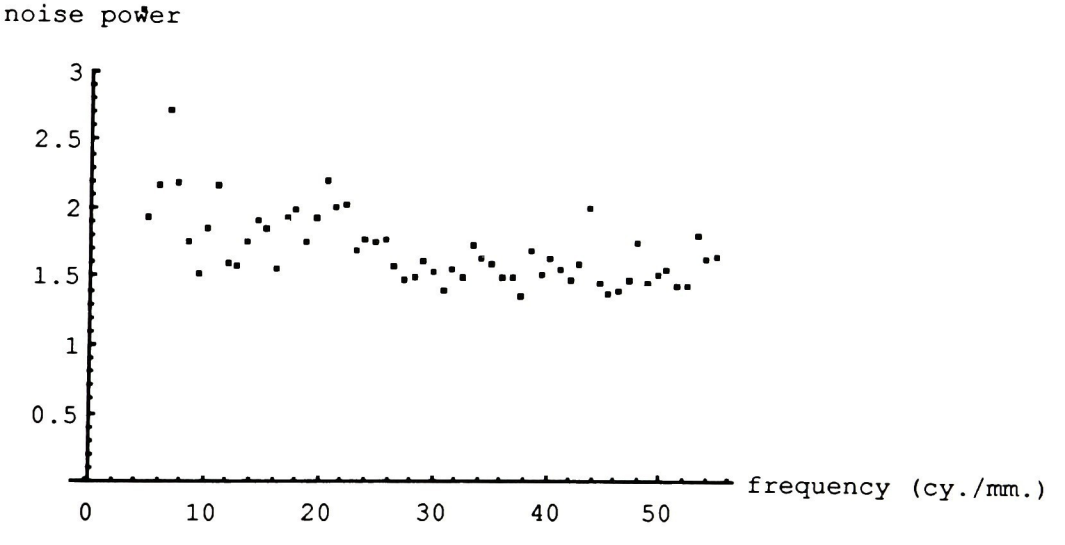

Figure 8: Vertical Wiener Spectrum Values, E.I. 100 Quantization.

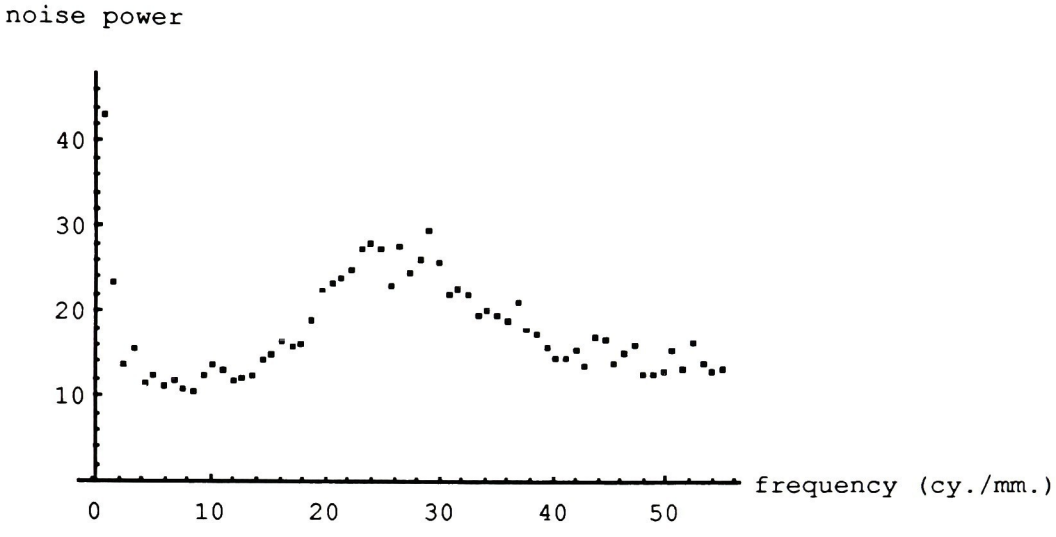

Figure 9: Horizontal Wiener Spectrum Values, E.I. 800 Quantization.

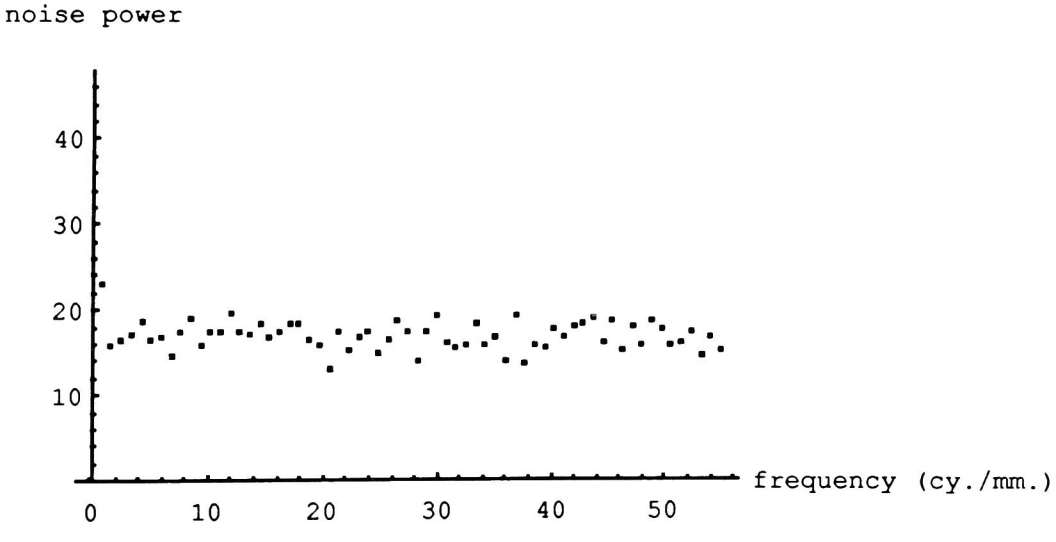

Figure 10: Horizontal Wiener Spectrum Values, E.I. 800 Quantization.

Table 9: DCS200mi Mean Response and Variance.

Log Exposure	Output Level	Output Level Variance	DQE (%)	log NEQ
Quantization Scheme 1 (nominal E.I. = 100):				
-2.64	9.61	3.81	0.84	1.23
-2.59	13.32	1.85	1.76	1.60
-2.32	16.28	2.04	1.78	1.87
-2.29	18.24	2.34	1.58	1.86
-2.02	27.1	1.07	3.95	2.52
-1.99	27.0	1.05	4.08	2.57
-1.68	45.9	0.85	5.97	3.04
-1.38	73.6	0.70	8.86	3.51
-1.08	114.3	1.13	7.00	3.71
-0.78	182.1	2.82	3.69	3.73
Quantization Scheme 2 (nominal E.I. = 200):				
-2.94	9.68	10.80	0.57	0.76
-2.64	16.64	5.43	1.28	1.41
-2.59	19.24	5.30	1.34	1.49
-2.32	27.4	3.72	2.17	1.96
-2.29	29.9	2.61	3.16	2.16
-2.02	43.3	3.40	2.81	2.37
-1.99	47.4	2.14	4.54	2.62
-1.68	73.1	3.53	3.36	2.79
-1.38	111.0	2.08	7.22	3.42
-1.08	180.0	2.63	7.49	3.74
Quantization Scheme 3 (nominal E.I. = 400):				
-3.24	11.40	37.5	0.37	0.27
-2.94	19.28	19.57	0.81	0.91
-2.64	29.9	19.62	0.94	1.28
-2.59	32.4	13.54	1.41	1.51
-2.29	51.3	10.35	2.20	2.00
-1.68	122.6	7.45	4.82	2.94
-1.38	195.9	5.66	8.46	3.49
Quantization Scheme 4 (nominal E.I. = 800):				
-3.54	13.51	74.5	0.41	0.01
-3.24	19.43	63.0	0.54	0.44
-2.94	26.3	65.7	0.60	0.78
-2.59	55.0	34.1	1.39	1.50
-2.29	82.6	21.4	2.69	2.09
-1.99	125.6	19.43	3.71	2.53
-1.68	198.1	17.80	5.28	2.98

V. Results

Film Response:

The characteristic curves for the four films tested are shown in Figure 11. These curves are typical for pictorial monochrome negative films and are provided for comparison purposes. The processing conditions are described in Appendix I.

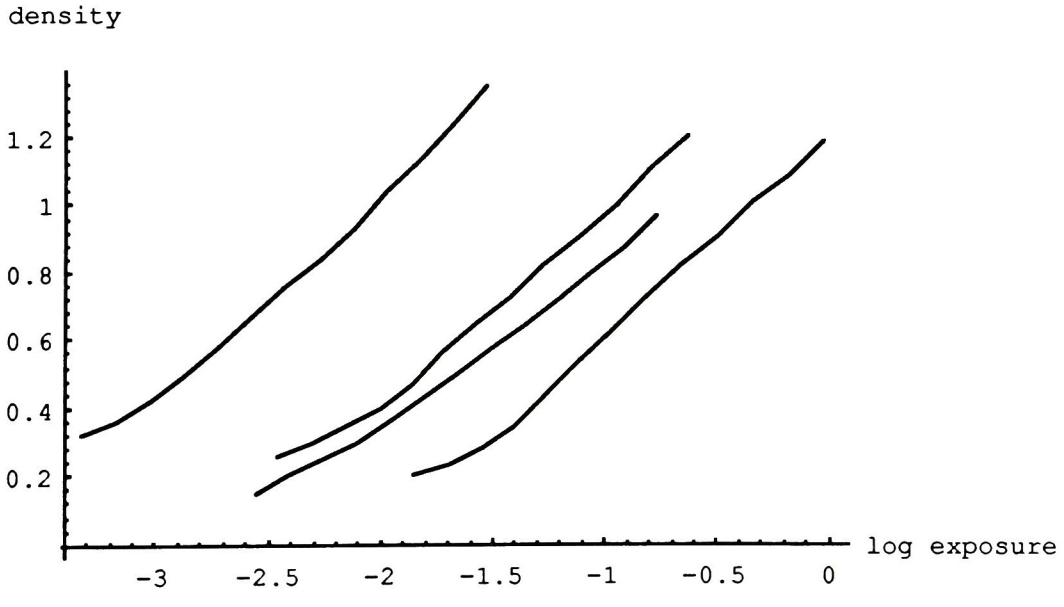

Figure 11: Film Characteristic Curves.
(from left to right: T-Max P3200, T-Max 400, T-Max 100, Technical Pan)

DCS200mi Response:

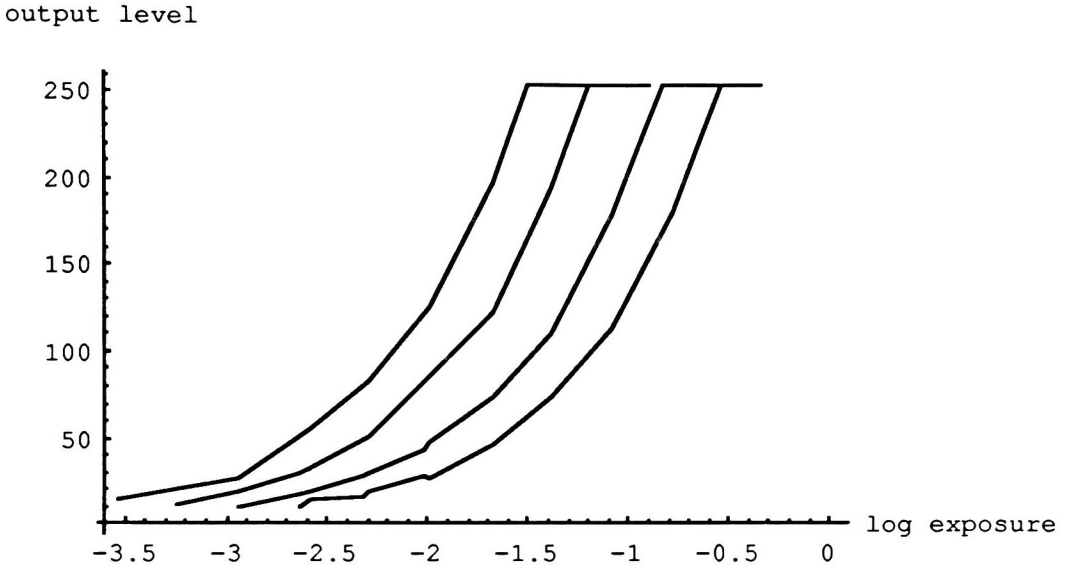

Figure 12: DCS200mi Characteristic Curves.
(quantization schemes, from left to right: E.I. 800, E.I. 400, E.I. 200, E.I. 100)

The characteristic curves for the DCS200mi camera are shown in Figure 12. These curves illustrate an important but often neglected consideration in the electronic photography, the system response. The response of CCD detectors is typically linear with exposure, so the response of a camera system is largely determined by the quantization scheme employed. Memory is divided into 8-bit bytes or 16-bit words, so the image is most efficiently quantized at these levels. Quantization to 8 bits is attractive in that it requires less memory, and the resulting 256 levels can be sufficient for high quality. The problem with 8-

bit quantization lies in the placement and spacing of the levels. The eye does not perceive linearly, so linear quantization results in too few low levels and too many high levels. Log quantization solves this problem. The eye does not perceive exactly logarithmically, but the human visual response function is complex, and is much closer to the log response than the linear response. For over a century, photographic sensitometry has been based successfully on log measures. The problem with log measures is that for CCD's, unlike film, the quantization interval varies much more strongly with the exposure than the noise level.

The ultimate solution to the quantization problem is 16-bit linear quantization, which results in a sufficient number of gray levels to hold all the information captured by the CCD. Linear quantization allows the sampling interval to remain approximately proportional to the noise throughout the sensitivity range of the CCD. Processing software can then operate on the captured image to logarithmically re-quantize the exposure region of interest to 8 bits for output. It is even possible that this could be accomplished automatically in the camera. For now, however, the 8-bit quantization dilemma remains. The strategy employed in the DCS200mi camera is a compromise between logarithmic and linear quantization. This strategy results in a hard ceiling being placed on the sensitivity range of the camera, but only a soft floor (see Appendix D). Consequently, the optimum exposure places the maximum scene luminance at the hard ceiling. Applying this exposure placement strategy, along with conventional photographic

speed determination rationale, results in the following speed determinations for the DCS200mi:

Table 10: Optimal DCS200mI Speed Settings.

Camera E.I. Setting:	100	200	400	800
Exposure of Output Level 255 (white, in lux-sec., from Appendix C):	0.289	0.148	0.0638	0.0317
Average Pictorial Scene Range:	160:1	160:1	160:1	160:1
Average Pictorial Scene Log Range:	2.2	2.2	2.2	2.2
Average Pictorial Imaging System Flare Factor:	2	2	2	2
Average Pictorial Image Log Range:	1.9	1.9	1.9	1.9
Average Scene Reflectance:	10-18%	10-18%	10-18%	10-18%
Maximum Ratio Between Image Highlight (~100% reflectance) and Mean Reflectance (10%):	10:1	10:1	10:1	10:1
Distance on Log Exposure Axis from Highlight to Mean Reflectance:	1.0	1.0	1.0	1.0
Safety Factor (allows for scene ranges slightly above 160:1):	0.1	0.1	0.1	0.1
Optimal Speed Setting (standard speed values):	320	640	1600	3200

The above speed settings were determined using the equation:

$$\text{Speed} = \frac{100}{H_{255}} \tag{16}$$

where H_{255} is the exposure required to produce an output level of 255. The constant of 100 was obtained as follows:

Light Meter Equation (used by light meters to calculate shutter speed and f-number):

$$\frac{t}{f\#^2} = \frac{12.4}{<L> FS} \tag{17}$$

where t is the shutter speed, f# is the f-number, <L> is the mean scene luminance, and FS is the film speed.

Relation between Mean Exposure <H> and Mean Scene Luminance:

$$<H> = \frac{0.65 <L> t}{f\#^2} \tag{18}$$

Resulting General Speed Equation:

$$<H> = \frac{8}{FS} \tag{19}$$

Relation between Mean Exposure and Speed Point Exposure:

$$H_{255} = 12.5 <H> \tag{20}$$

Note that this speed equation derivation is applicable only to quantization schemes which are sub-logarithmic. Also, the sole motivation for this equation is to place the input exposure range so that scenes with approximately normal ranges have the maximum S/N without truncation. Practically speaking, this speed criterion has limited utility because many scenes differ significantly from normal in contrast.

In general, metering for 8-bit quantization will remain a problem because of the diverse nature of the scenes encountered in general pictorial photography. Ultimately, 16-bit initial quantization will have to be adopted for optimum quality, followed by some form of adaptive subsequent quantization which takes into account the actual scene range. A secondary advantage of such adaptive re-quantization is the possibility for the correction of exposure errors due to intentional under- or over-exposure, metering errors, or errors resulting from scenes with unusual average reflectances. The "hard" truncation at the white level which is characteristic of sub-logarithmically quantized CCD images can make exposure more critical than for films.

Another consideration in speed determination is spectral sensitivity. Most exposure meters are designed to approximate visual response, but most films do not. This is generally not a problem because the blue-red balance of the films is not very different from the blue-red visual response, and the blue-red balance is the most variable characteristic with typical light sources. The classic example is between tungsten and daylight illumination. Older monochrome films typically had somewhat higher blue sensitivity than red sensitivity, and somewhat higher daylight speeds than tungsten speeds. Modern films have approximately equal blue and red sensitivities and daylight and tungsten speeds. CCD's, however, have significantly greater red sensitivity than blue sensitivity. This may be a partial explanation of the

difference between the nominal E.I.'s and the calculated speeds presented in Table 10.

Noise Analysis:

For the CCD exposures, the purpose of this investigation was to analyze the actual image files generated by the camera. The in-camera processing of the DCS200mi image files appeared to be minimal, and as a result the information present in these files is somewhat obscured by fixed pattern noise. This noise can be removed relatively easily by using digital image processing techniques, but since it has not been removed it will be considered part of the image noise. Subsequent processing to remove this noise may improve the information content of the images, but this processing is external to the "camera". In electronic imaging systems, many processing algorithms and devices may be used to produce the final image. Each of these devices may affect the information content of the image, and can be analyzed independently. The DQE and NEQ metrics are ideally suited to such analysis. The NEQ of the image at any stage can be determined from the NEQ at a previous stage by multiplying it by the DQE values of the intermediate operations. If log values are used, log DQE values are added to the log NEQ. It is interesting to note that in electronic systems, the DQE value for a particular stage may be significantly greater than one, although the combined DQE value for all the stages of an imaging process must remain less than one.

In the case of the film exposures, the microscope microdensitometer system gave experimental values which were as expected for the films tested. The most interesting thing about the results in this area was that the log NEQ values for the films were typically lower than for the DCS200mi at equivalent exposures. If the DCS200mi had been cooled to reduce the thermal noise level, and if flat field division had been employed, this difference could have been much greater. The results obtained for the film also confirm the validity of the procedure employed. It does not appear necessary to use an elaborate microdensitometer system to obtain meaningful data on film image structure, especially in view of the fact that differences on the order of 5 to 10 percent are required for differences in noise level to be perceptible. The use of the system described also allowed the same analysis techniques to be used on both the film and CCD data.

Plots of the log NEQ values for the films studied, as a function of exposure, are provided in Figure 13. In these plots, the dots indicate the data points, and the solid curves are least-squares quadratic fits. The limits of the fit curves were chosen to represent the minimum and maximum exposure values resulting from an average scene range and flare, and conventional exposure placement.

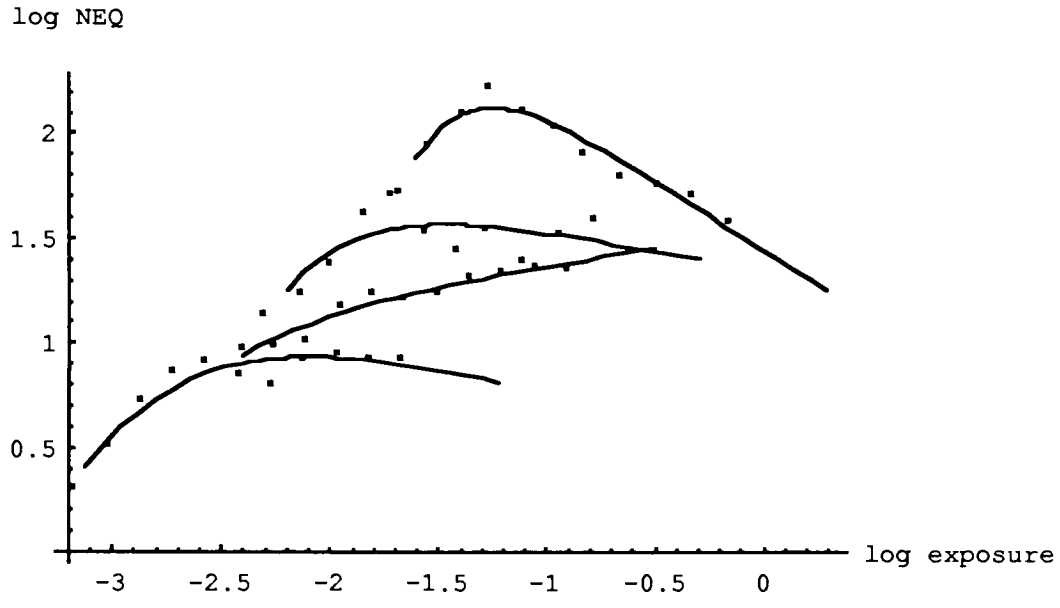

Figure 13: Film Log NEQ Curves.
(from top to bottom: Technical Pan, T-Max 100, T-Max 400, T-Max P3200)

A plot of the log NEQ values for the DCS200mi is provided in Figure 14. This plot contains data from all the quantizations (see Appendix M). An interesting feature of the log NEQ metric is that it is relatively independent of quantization. Note also the large linear region. It is the contention of the author that the curves in Figures 13 and 14 represent not only a means of comparison between systems but also an objective measure of the image quality obtained.

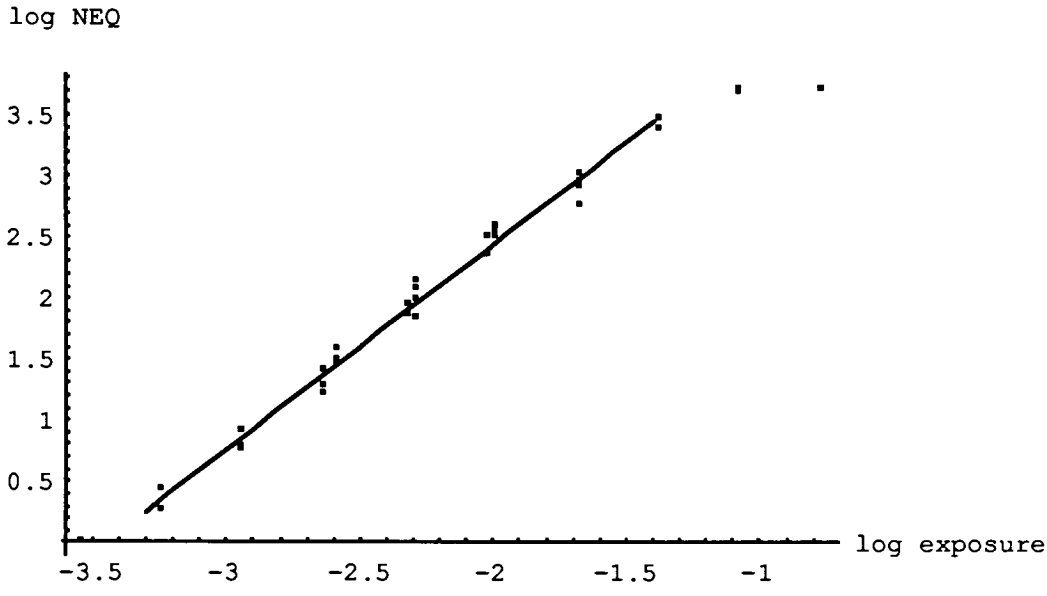

Figure 14: DCS200mi Log NEQ Values.

Equivalent Image Quality:

At this point it is convenient to introduce a new metric for comparing the quality of conventional and electronic images. This metric will be termed the Equivalent Image Quality (EIQ). The EIQ is defined as the weighted mean of the log NEQ values over the range of exposures used for the scene. The advantage of the EIQ is that it provides a single figure of merit for a specific imaging system configuration which should correlate well with the noise-related subjective quality. For the purposes of this comparison an exposure range of 80:1 was used, which is typical of an average scene. The weight values used for the different tones (gray levels) were derived from the

perceptual sensitivity to graininess at different density levels, as determined by Zwick,[119] and are provided in Table 11.

Table 11: Perceptual Response to Graininess at Different Densities.

Tone:	White		Gray				Black
Relative Log Exposure	1.9	1.6	1.3	1.0	0.7	0.4	0.1
Negative Density	1.15	1.0	0.85	0.6	0.45	0.3	0.15
Print Density	0.1	0.4	0.7	1.0	1.3	1.6	1.9
Noise Weight	4	16	16	11	8	5	3

The weighting values presented above are as determined for monochrome photographic prints. In the same study, Zwick also found that the exact weighing values depend on the output medium. Specifically, the values for color prints were found to be somewhat different than for monochrome prints. A number of output media are used in electronic photography. Consequently, the determination of the exact EIQ for a particular type of output image requires knowledge of the noise perception characteristics of the media in addition to knowledge of the printer noise contribution. This study deals only with the digital image files created by the camera. Determination of EIQ values for output images will require further study of both the noise characteristics of output devices and the visibility of the noise produced as a function of output medium, gray level, and spatial frequency.

The weighting values for monochrome silver prints were chosen for the digital file EIQ calculations for two reasons:

1. All weighting values yet determined give more weight to the perceptual midtones than the very light or dark areas. The weighting values used are therefore somewhat typical. The differences between the EIQ values obtained for negatives and digital files and the resulting prints will be less if typical values are chosen, as opposed to weighting all the gray levels equally or choosing some other arbitrary values.

2. The comparison conducted in this study is between monochrome silver halide negatives and monochrome digital image files. Negatives are typically printed on monochrome photographic paper. Therefore, if one wanted to produce output images which removed as much of the printing effect as possible, monochrome photographic paper would be the best choice. A comparison of silver prints of photographic negatives and electronic images written onto photographic paper should provide results close to those obtained by studying the negatives and digital files.

The weights presented in Table 11 result in the following EIQ values for the imaging systems tested:

Table 12: EIQ Values.
(film negative size 24 x 36 mm)

Imaging System	Tested Speed	Fixed Magnification (18X)	Fixed Print Size (150 x225 mm)
Technical Pan	32	1.71	2.61
T-Max 100	125	1.50	2.40
T-Max 400	200	1.31	2.21
T-Max P3200	1000	0.87	1.77
DCS200mi (100)	320	3.19	3.26
DCS200mi (200)	640	2.82	2.89
DCS200mi (400)	1600	2.22	2.29
DCS200mi (800)	3200	1.71	1.78

The EIQ values for the silver-halide materials were also used to calculate the maximum print sizes which could be made from a 35mm negative. The results, presented below in Table 13, agree well with common subjective values for the films tested. The calculations on which Tables 12 and 13 are based can be found in Appendix M.

Table 13: Print Sizes to Produce 2.0 EIQ per Pixel on a Print.
(164x164 µm pixels from a 35mm negative;
Calculations assume the granularity is invariant over a limited aperture size range.)

Film	Print Size (mm.)	Print Size (in.)
Technical Pan	310 x 464	12 x 18
T-Max 100	243 x 364	9.6 x 14.4
T-Max 400	195 x 292	7.7 x 11.5
T-Max P3200	118 x 177	4.6 x 7.0

VI. Conclusions

CCD cameras may not have the resolving power of film cameras due to the relatively large pixel sizes, but the information content, and therefore quality, of each pixel can be significantly higher than for film. Based on this information, the following conclusions were drawn for pictorial images:

1. Enlargement of CCD images is limited by the MTF more than by the noise, whereas for silver-halide images the opposite is true.

2. Log NEQ/pixel values of 2.0 are typically required for acceptable image quality if the pixel size is chosen so that it is just smaller than is visually perceptible (~ 0.15 x 0.15 mm.).

3. For silver-halide images, log NEQ depends on enlargement, but less so for CCD images. This is because the "pixel size" for silver-halide images depends on the print magnification and viewing distance.

4. The optimum enlargement for CCD images is related to the actual pixel size, and is much more rigid than for silver-halide images.

5. The ultimate quality of an imaging system depends on all the components of the system. The effects of these components can be taken into account

by adding the log DQE of each subsequent component or algorithm to the log NEQ of the original camera.

6. Electronic imaging detectors show great promise for pictorial imaging, particularly if large CCD chips can be manufactured at reasonable costs. Quantization schemes need to be developed which allow for the unclipped capture of wide scene ranges (1000:1). Linear quantization optimizes the characteristics of the CCD but requires more than 8 bits/color for storage. Log quantization facilitates 8-bit storage but does not maximize log NEQ. Ultimately, 16-bit initial quantization may be required, possibly followed by adaptive 8-bit re-quantization or some other form of compression. Standards need to be developed to make tone reproduction manageable.

7. The old adage: "It is safer to overexpose than to underexpose." does not apply with CCD cameras. In fact, with the DCS200mi camera the opposite is true. This is largely due to the quantization scheme employed, but 8-bit quantization is attractive -- 256 gray levels are generally sufficient in the final output. As digital memory becomes cheaper and smaller, 16-bit quantization may become more popular, but this will probably not happen too quickly as initial reductions in memory costs will be applied to reductions in system costs. With 8-bit schemes, manufacturers will always be compromising between linear quantization, which follows from the

nature of the output of the CCD chip, and the log quantization more common to photographic processes. This compromise will result in generally more latitude on the underexposure side.

VII. Acknowledgements

I would like to thank Rodney Shaw for his ongoing advice, review, and support of this work, Andy Davidhazy for his support as a colleague, Sabine Süsstrunk for her support and help in obtaining the DCS200mi camera and her help with a subjective correlation study (currently underway), and the members of the ANSI/NAPM IT10 Technical Committee for their valuable comments. I would also like to thank my thesis committee members, Zoran Ninkov, Rich Hailstone, and in particular Roger Easton, for their comments which have led to this final version of the manuscript. Finally, I would like to thank my wife Rachel Goss, and my daughters Stephanie and Christina for their support and tolerance of yet another project in difficult times. Hopefully I will get to be with you more in the future.

Appendix A: Nomenclature.

An attempt was made to use standard nomenclature throughout this work, but for convenience sake a list of the symbols and abbreviations used is provided below.

A - data sample aperture area (square microns).
DQE - detective quantum efficiency.
EIQ - equivalent image quality (weighted mean log NEQ).
FS - film speed.
G - granularity, the product of the scanning aperture area and the mean square fluctuation for a silver halide material; generally a constant for a particular material.
H - the photometric exposure (lux-seconds).
H_e - the radiometric exposure (joules).
H_q - the number of exposure quanta (photons).
IC - information capacity (bits).
k - spatial frequency.
L - the scene luminance.
MSF - mean square fluctuation (N^2).
MTF - modulation transfer function.
N - noise, the random RMS fluctuation in the signal.
NEQ - noise equivalent quanta.
RMS - root-mean-square.
S - Signal, the meaningful input to or output from a system or device
S/N - Signal to Noise Ratio.
SQF - subjective quality factor.
WS - Wiener Spectrum, the noise power plotted as a function of spatial frequency (k).
γ - Gamma, the pointwise slope of the input-output curve for a particular device or system.
γ_{max} - The maximum value of γ for a particular characteristic curve. In some literature, γ_{max} is called γ.
λ - Lambda, the wavelength of electromagnetic radiation (in meters).

Appendix B: Lumen/Photon Conversion.

(Wratten #301 filter transmittance data from Kodak publication No. U-73, *Special Filters from Kodak for Technical Applications.*)

```
energy[l_] :=
2 Pi h c^2/l^5 (1/(E^(h c/(l k T)) - 1))

h=6.626 10^(-34);

c=2.9979 10^8;

k=1.381 10^(-23);

T=3100;

dw=10^(-8);

exitance[w_] := NIntegrate[energy[l],
{l, w-dw/2, w+dw/2}]

EnlargerExitance = Round[Table[exitance[w],
{w, 3.9 10^(-7), 7.6 10^(-7), dw}]]

{2826, 3352, 3931, 4562, 5243, 5973, 6747, 7564,
  8418, 9307, 10226, 11171, 12137, 13120, 14115,
  15118, 16126, 17133, 18136, 19131, 20115, 21085,
  22038, 22970, 23880, 24766, 25625, 26456, 27257,
  28028, 28766, 29472, 30145, 30784, 31388, 31959,
  32496, 32999}

T=2850;

SensitometerExitance = Round[Table[exitance[w],
{w, 3.9 10^(-7), 7.6 10^(-7), dw}]]

{996, 1212, 1457, 1731, 2035, 2369, 2731, 3123,
  3541, 3987. 4457, 4950, 5464, 5998, 6549, 7115,
  7693, 8282, 8879, 9482, 10089, 10698, 11306,
  11911, 12512, 13108, 13695, 14273, 14841, 15397,
  15939, 16468, 16981, 17479, 17960, 18424, 18870,
  19298}
```

Wavelength (nm.)	2850K Exitance	lumens/watt	photons/joule	photons/lum.-sec.
390	996	0.082	1.96375E+18	2.39481E+19
400	1212	0.27	2.0141E+18	7.45962E+18
410	1457	0.826	2.06445E+18	2.49934E+18
420	1731	2.732	2.1148E+18	7.74086E+17
430	2035	7.923	2.16516E+18	2.73275E+17
440	2369	15.71	2.21551E+18	1.41025E+17
450	2731	25.95	2.26586E+18	8.73164E+16
460	3123	40.98	2.31621E+18	5.65206E+16
470	3541	62.14	2.36657E+18	3.80844E+16
480	3987	94.95	2.41692E+18	2.54546E+16
490	4457	142.1	2.46727E+18	1.73629E+16
500	4950	220.6	2.51762E+18	1.14126E+16
510	5464	343.5	2.56798E+18	7.47591E+15
520	5998	484.9	2.61833E+18	5.39973E+15
530	6549	588.7	2.66868E+18	4.53318E+15
540	7115	651.6	2.71903E+18	4.17286E+15
550	7693	679.5	2.76939E+18	4.07562E+15
560	8282	679.6	2.81974E+18	4.14911E+15
570	8879	650.2	2.87009E+18	4.41417E+15
580	9482	594.2	2.92044E+18	4.91492E+15
590	10089	517	2.9708E+18	5.74622E+15
600	10698	431	3.02115E+18	7.00962E+15
610	11306	343.5	3.0715E+18	8.94178E+15
620	11911	260.2	3.12185E+18	1.19979E+16
630	12512	181	3.17221E+18	1.7526E+16
640	13108	119.5	3.22256E+18	2.6967E+16
650	13695	73.08	3.27291E+18	4.47853E+16
660	14273	41.66	3.32326E+18	7.97711E+16
670	14841	21.86	3.37362E+18	1.54328E+17
680	15397	11.61	3.42397E+18	2.94915E+17
690	15939	5.607	3.47432E+18	6.1964E+17
700	16468	2.802	3.52467E+18	1.25791E+18
710	16981	1.428	3.57503E+18	2.50352E+18
720	17479	0.715	3.62538E+18	5.07046E+18
730	17960	0.355	3.67573E+18	1.03542E+19
740	18424	0.17	3.72608E+18	2.19181E+19
750	18870	0.082	3.77644E+18	4.60541E+19
760	19298	0.041	3.82679E+18	9.33363E+19
Mean	9507.894737	192.05455	2.89527E+18	5.71413E+18
Sum	361300	7298.073	1.1002E+20	2.17137E+20
Photons/Lumen				1.50752E+16

2850K lumens	2850K photons
81.672	1.95589E+21
327.24	2.44109E+21
1203.482	3.00791E+21
4729.092	3.66073E+21
16123.305	4.40609E+21
37216.99	5.24854E+21
70869.45	6.18807E+21
127980.54	7.23353E+21
220037.74	8.38001E+21
378565.65	9.63625E+21
633339.7	1.09966E+22
1091970	1.24622E+22
1876884	1.40314E+22
2908430.2	1.57047E+22
3855396.3	1.74772E+22
4636134	1.93459E+22
5227393.5	2.13049E+22
5628447.2	2.33531E+22
5773125.8	2.54835E+22
5634204.4	2.76916E+22
5216013	2.99724E+22
4610838	3.23202E+22
3883611	3.47264E+22
3099242.2	3.71844E+22
2264672	3.96906E+22
1566406	4.22413E+22
1000830.6	4.48225E+22
594613.18	4.74329E+22
324424.26	5.00678E+22
178759.17	5.27188E+22
89369.973	5.53772E+22
46143.336	5.80443E+22
24248.868	6.07075E+22
12497.485	6.3368E+22
6375.8	6.60161E+22
3132.08	6.86493E+22
1547.34	7.12613E+22
791.218	7.38493E+22
1606473.047	3.07489E+22
61045975.77	1.16846E+24
	1.91407E+16

Wavelength (nm.)	3100K Exitance	#301A Trans.	lumens/watt	photons/joule
390	2826	0.670	0.082	1.96375E+18
400	3352	0.740	0.27	2.0141E+18
410	3931	0.780	0.826	2.06445E+18
420	4562	0.810	2.732	2.1148E+18
430	5243	0.830	7.923	2.16516E+18
440	5973	0.855	15.71	2.21551E+18
450	6747	0.870	25.95	2.26586E+18
460	7564	0.880	40.98	2.31621E+18
470	8418	0.890	62.14	2.36657E+18
480	9307	0.890	94.95	2.41692E+18
490	10226	0.885	142.1	2.46727E+18
500	11171	0.880	220.6	2.51762E+18
510	12137	0.880	343.5	2.56798E+18
520	13120	0.885	484.9	2.61833E+18
530	14115	0.890	588.7	2.66868E+18
540	15118	0.885	651.6	2.71903E+18
550	16126	0.875	679.5	2.76939E+18
560	17133	0.865	679.6	2.81974E+18
570	18136	0.865	650.2	2.87009E+18
580	19131	0.870	594.2	2.92044E+18
590	20115	0.850	517	2.9708E+18
600	21085	0.800	431	3.02115E+18
610	22038	0.780	343.5	3.0715E+18
620	22970	0.770	260.2	3.12185E+18
630	23880	0.780	181	3.17221E+18
640	24766	0.810	119.5	3.22256E+18
650	25625	0.820	73.08	3.27291E+18
660	26456	0.805	41.66	3.32326E+18
670	27257	0.700	21.86	3.37362E+18
680	28028	0.400	11.61	3.42397E+18
690	28766	0.260	5.607	3.47432E+18
700	29472	0.170	2.802	3.52467E+18
710	30145	0.120	1.428	3.57503E+18
720	30784	0.090	0.715	3.62538E+18
730	31388	0.070	0.355	3.67573E+18
740	31959	0.055	0.17	3.72608E+18
750	32496	0.045	0.082	3.77644E+18
760	32999	0.035	0.041	3.82679E+18
Mean	18278.02632	0.667	192.05455	2.89527E+18
Sum	694565	25.355	7298.073	1.1002E+20
Photons/Lumen				

photons/lum.-sec.	3100K lumens	3100K photons
2.39481E+19	155.26044	3.7182E+21
7.45962E+18	669.7296	4.99593E+21
2.49934E+18	2532.66468	6.32998E+21
7.74086E+17	10095.34104	7.81466E+21
2.73275E+17	34478.43987	9.42209E+21
1.41025E+17	80229.63465	1.13144E+22
8.73164E+16	152323.6455	1.33004E+22
5.65206E+16	272775.9936	1.54175E+22
3.80844E+16	465554.1228	1.77304E+22
2.54546E+16	786492.6885	2.00199E+22
1.73629E+16	1286006.421	2.23288E+22
1.14126E+16	2168603.888	2.47494E+22
7.47591E+15	3668772.36	2.74274E+22
5.39973E+15	5630270.88	3.04019E+22
4.53318E+15	7395455.445	3.35249E+22
4.17286E+15	8718036.588	3.63791E+22
4.07562E+15	9587914.875	3.90767E+22
4.14911E+15	10071702.58	4.17886E+22
4.41417E+15	10200103.53	4.50249E+22
4.91492E+15	9889846.974	4.86078E+22
5.74622E+15	8839536.75	5.07939E+22
7.00962E+15	7270108	5.09607E+22
8.94178E+15	5904641.34	5.2798E+22
1.19979E+16	4602131.38	5.52159E+22
1.7526E+16	3371378.4	5.90868E+22
2.6967E+16	2397224.97	6.4646E+22
4.47853E+16	1535593.5	6.8772E+22
7.97711E+16	887236.3528	7.07758E+22
1.54328E+17	417086.614	6.43682E+22
2.94915E+17	130162.032	3.83868E+22
6.1964E+17	41935.65012	2.5985E+22
1.25791E+18	14038.69248	1.76595E+22
2.50352E+18	5165.6472	1.29323E+22
5.07046E+18	1980.9504	1.00443E+22
1.03542E+19	779.9918	8.07617E+21
2.19181E+19	298.81665	6.5495E+21
4.60541E+19	119.91024	5.52236E+21
9.33363E+19	47.353565	4.41981E+21
5.71413E+18	2785302.3	2.96412E+22
2.17137E+20	105841487.4	1.12637E+24
1.50752E+16		1.0642E+16

Color temperature (K)	photons/lum.-sec.	aperture area (μm^2)	photons/lux-sec.	log (photons/lux-sec.)
3100	1.06E+16	82.81	881098	5.95
2850	1.91E+16	82.1	1568110	6.20
			per aperture area	per aperture area

Radiant Exitance Plot

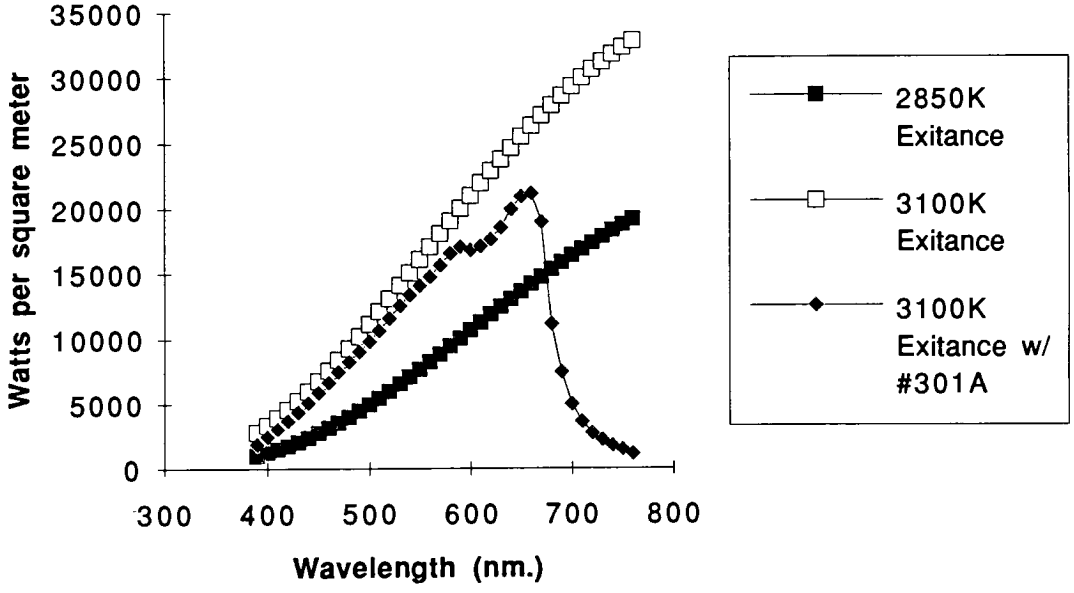

Lumens/Watt Plot

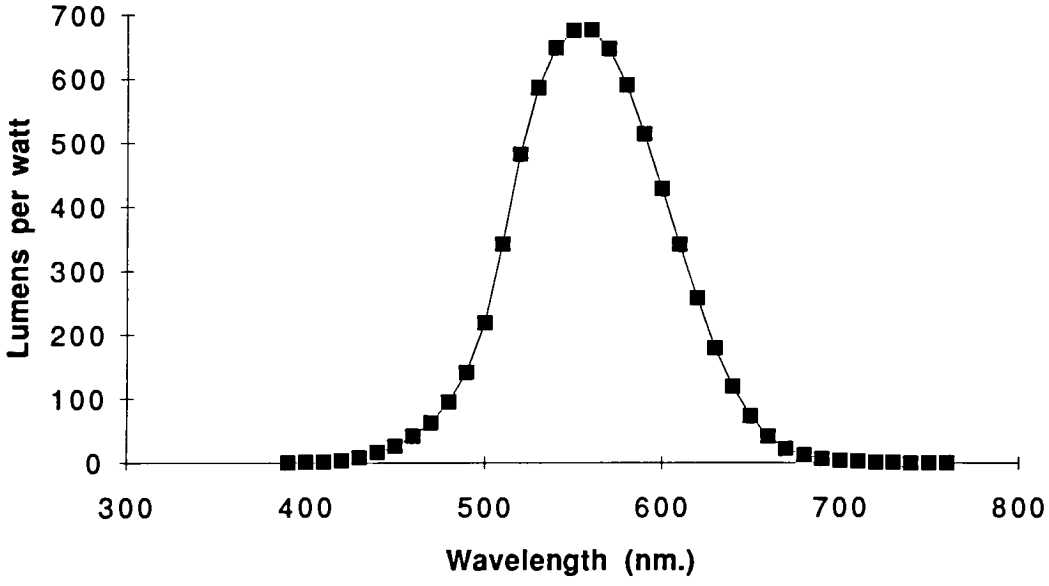

Photons/Joule Plot

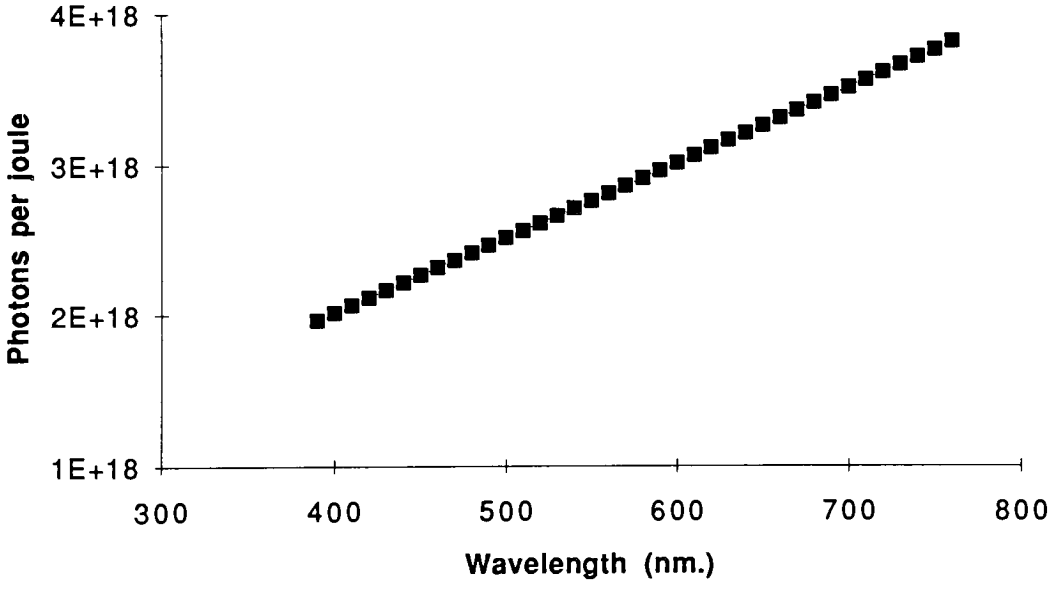

Lumens/Sq. M. Plot

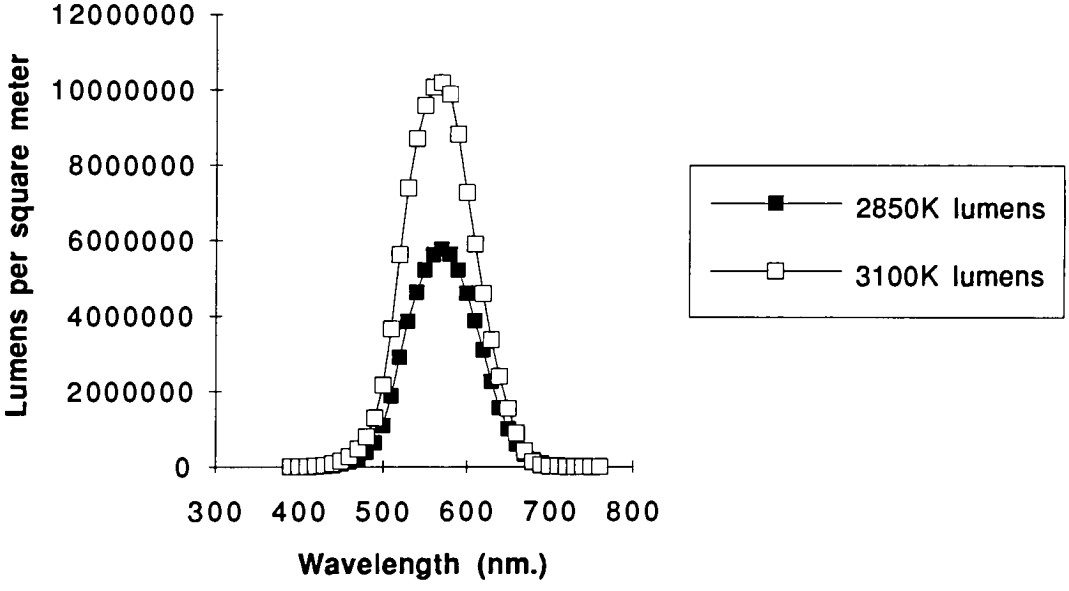

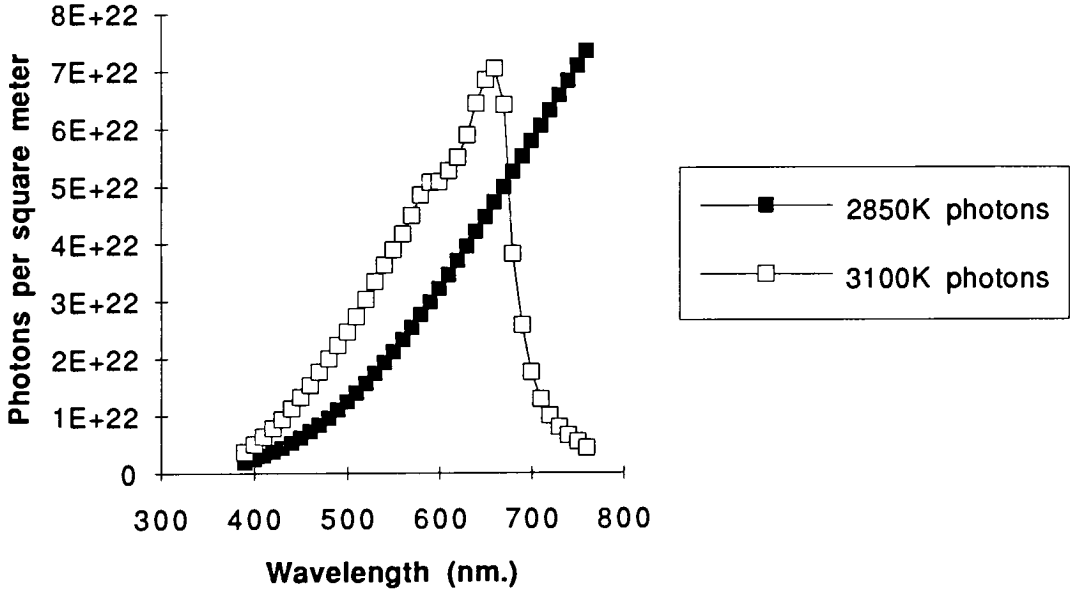
Photons per square meter
8E+22
7E+22
6E+22
5E+22
4E+22
3E+22
2E+22
1E+22
0
300
400
500
600
700
800
Wavelength (nm.)
2850K photons
3100K photons

Appendix C: Step Tablet Noise Contribution.

Trial	Camera 82 mean	Camera 82 variance	Sensi. 82 mean
1	119	72	117
2	125	84	114
3	120	77	116
4	124	80	114
5	121	80	121
6	121	72	121
7	122	78	119
8	123	78	119
9	123	77	116
10	121	78	114
Mean	121.9	77.6	117.1
S.D.	1.852925615	3.596294389	2.766867463
Sample Density	0.85		0.88
Mean Transmittance	0.141253754		0.131825674
Mean CCD Exposure	0.088731646		0.083477685
Output Level S.D.	8.809086218		9.433981132
Minus 1 S.D. Exposure	0.079194731		0.073551834
Plus 1 S.D. Exposure	0.098731274		0.093934224
Minus 1 S.D. Trans.	0.12607174		0.116151041
Plus 1 S.D. Trans	0.157172369		0.148338354
Minus 1 S.D. Density	0.899382252		0.934976894
Plus 1 S.D. Density	0.803623801		0.828746545
Density Variance	0.00229242		0.002821222
Granularity	0.187978462		0.231340182

Sensi. 82 variance	Camera 31 mean	Camera 31 variance	Sensi. 31 mean	Sensi. 31 variance
93	119	202	117	225
84	125	221	114	208
91	120	213	116	221
84	124	212	114	208
92	121	213	121	225
94	121	201	121	229
90	122	215	119	228
89	123	215	119	226
91	123	216	116	230
82	121	216	114	211
89	121.9	212.4	117.1	221.1
4.18993503	1.852925615	6.257440016	2.766867463	8.748968193
	0.85		0.88	
	0.141253754		0.131825674	
	0.088731646		0.083477685	
	14.57394936		14.86943173	
	0.073204047		0.068073951	
	0.10552574		0.10019979	
	0.116535046		0.107500518	
	0.167988622		0.158232764	
	0.933543449		0.968589442	
	0.774720132		0.800703585	
	0.006306211		0.007046415	
	0.195492556		0.218438871	

Appendix D: DCS200mi Back Regression.

(A regressive determination of the function relating the input exposure to the gray level obtained for the DCS200mi camera.)

```
CCDBackAA = {{2.92486, 0.00114},
             {9.60988, 0.00229},
             {13.3202, 0.00259},
             {16.2846, 0.00476},
             {18.2393, 0.00518},
             {27.0770, 0.00952},
             {27.0167, 0.01035},
             {45.9052, 0.0207},
             {73.6219, 0.0414},
             {114.293, 0.0828},
             {182.109, 0.1656}};

<<Statistics`LinearRegression`
```

```
Regress[CCDBackAA, {1, x, x^2}, x]

{ParameterTable ->

        Estimate          SE              TStat       PValue    ,
   1    -0.00213925       0.000761819     -2.80808    0.0229109

   x    0.000382023       0.0000286583    13.3303     0

    2              -6               -7
   x    2.98139 10        1.56794 10      19.0147     0

  RSquared -> 0.999449, AdjustedRSquared -> 0.999311,

                                    -6
  EstimatedVariance -> 1.77681 10    ,

  ANOVATable ->

   Model                                                          }

   Error

   Total

      DoF   SoS              MeanSS           FRatio     PValue
      2     0.0257639        0.0128819        7250.03    0

                                        -6
      8     0.0000142145     1.77681 10

      10    0.0257781

BackFitAA[x_] :=
-0.00213925 + 0.000382023 x + 0.00000298139 x^2

Table[BackFitAA[x], {x, 254, 255}]

{0.287242, 0.289141}
```

```
Show[Plot[BackFitAA[x], {x, 0, 255},
AxesLabel -> {"digital count", "input exposure"}],
ListPlot[CCDBackAA]]
```

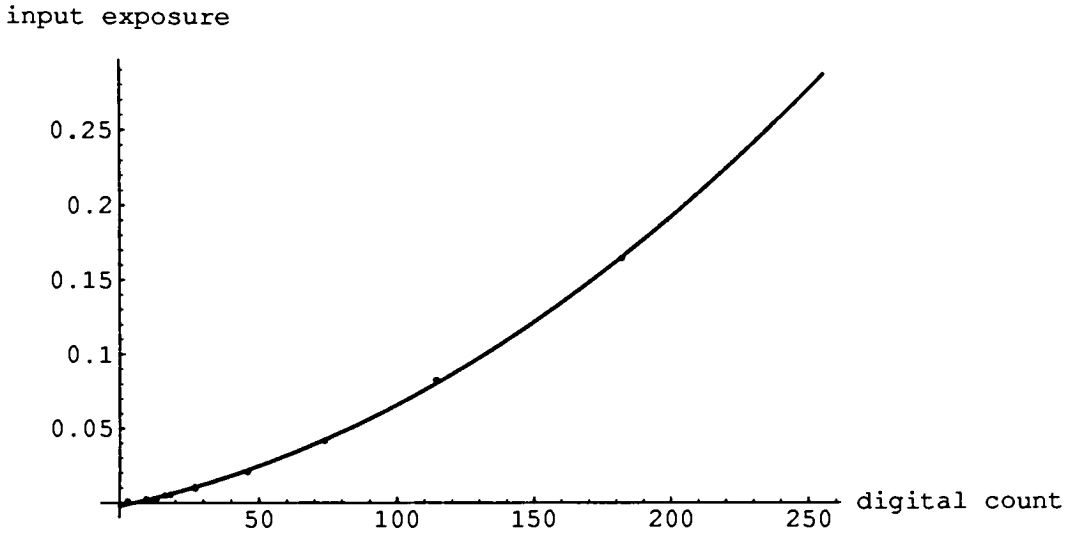


```
-Graphics-
```

```
CCDBackBB = {{5.13516, 0.000571},
             {9.6834, 0.00114},
             {16.6442, 0.00229},
             {19.2363, 0.00259},
             {27.4443, 0.00476},
             {29.9266, 0.00518},
             {43.3152, 0.00952},
             {47.444, 0.01035},
             {73.1155, 0.0207},
             {110.953, 0.0414},
             {179.651, 0.0828}};
```

```
Regress[CCDBackBB, {1, x, x^2}, x]
{ParameterTable ->

   1

   x

    2
   x

      Estimate        SE              TStat       PValue
      -0.00153142     0.00064223      -2.38454    0.0442311

      0.000199672     0.0000221859    8.99997     0.0000185317

                -6              -7
      1.51966 10      1.20317 10      12.6304     0

   , RSquared -> 0.998707, AdjustedRSquared -> 0.998383,

                                      -6
  EstimatedVariance -> 1.01383 10    ,

  ANOVATable ->

   Model

   Error

   Total

      DoF   SoS             MeanSS          FRatio    PValue
      2     0.00626281      0.00313141      3088.7    0

                    -6              -6
      8     8.11061 10      1.01383 10

      10    0.00627092

BackFitBB[x_] :=
-0.00153142 + 0.000199672 x + 0.00000151966 x^2
```

```
Table[BackFitBB[x], {x, 254, 255}]

{0.147228, 0.148201}

CCDBackCC = {{6.898, 0.000286},
             {11.397, 0.000571},
             {19.28, 0.00114},
             {29.927, 0.00229},
             {32.433, 0.00259},
             {51.273, 0.00518},
             {122.627, 0.0207},
             {195.938, 0.0414}};
```

```
Regress[CCDBackCC, {1, x, x^2}, x]
{ParameterTable ->

   1

   x

    2
   x

      Estimate          SE                TStat        PValue
      -0.000823203      0.00032315        -2.54743     0.0514263

      0.0000939156      0.0000112406      8.35502      0.00040189

                -7                  -8
      6.2546 10         5.52807 10        11.3143      0.00009429

   , RSquared -> 0.999325, AdjustedRSquared -> 0.999056,

                                        -7
  EstimatedVariance -> 2.01751 10    ,

  ANOVATable ->

   Model

   Error

   Total

      DoF   SoS               MeanSS            FRatio     PValue
      2     0.00149453        0.000747263       3703.89    0

                      -6                  -7
      5     1.00875 10        2.01751 10

      7     0.00149553

BackFitCC[x_] :=
-0.000823203 + 0.0000939156 x + 0.00000062546 x^2
```

```
Table[BackFitCC[x], {x, 254, 255}]

{0.0633835, 0.0637958}

CCDBackDD = {{9.814, 0.000143},
             {13.508, 0.000286},
             {19.429, 0.000571},
             {26.317, 0.00114},
             {55.009, 0.00259},
             {82.631, 0.00518},
             {125.592, 0.01035},
             {198.061, 0.0207}};
```

```
Regress[CCDBackDD, {1, x, x^2}, x]

{ParameterTable ->

        Estimate          SE                TStat       PValue
   1    -0.000335089      0.000165584       -2.02368    0.098905
                                      -6
   x    0.0000407843      4.94603 10        8.24585     0.000427
    2                -7                -8
   x    3.32461 10       2.42051 10        13.7352     0.000036

   , RSquared -> 0.999276, AdjustedRSquared -> 0.998987,

                                     -8
  EstimatedVariance -> 5.22903 10   ,

  ANOVATable ->

   Model

   Error

   Total

      DoF   SoS               MeanSS            FRatio     PValue
      2     0.000360904       0.000180452       3450.97    0

                        -7                -8
      5     2.61451 10        5.22903 10

      7     0.000361166

BackFitDD[x_] :=
-0.000335089 + 0.0000407843 x + 0.000000332461 x^2

Table[BackFitDD[x], {x, 254, 255}]

{0.0314732, 0.0316832}
```

Appendix E: DCS200mi Response.

```
CCDS100 = {{0.00114, 2.92486},
           {0.00229, 9.60988},
           {0.00259, 13.3202},
           {0.00476, 16.2846},
           {0.00518, 18.2393},
           {0.00952, 27.077},
           {0.01035, 27.0167},
           {0.0207, 45.9052},
           {0.0414, 73.6219},
           {0.0828, 114.293},
           {0.1656, 182.109}};

<<Statistics`LinearRegression`

Regress[CCDS100, {1, x^0.55, x}, x]

{ParameterTable ->

            Estimate    SE          TStat       PValue      ,
   1        -4.71636    1.14717     -4.11129    0.00338462

    0.55
   x        380.306     20.2585     18.7727     0

   x        273.983     43.5928     6.28506     0.000236568

  RSquared -> 0.999435, AdjustedRSquared -> 0.999293,

  EstimatedVariance -> 2.15692,

  ANOVATable ->

            DoF   SoS         MeanSS     FRatio     PValue}
   Model    2     30501.      15250.5    7070.48    0

   Error    8     17.2554     2.15692

   Total    10    30518.2

s100fit[x_] := -4.71636 + 380.306 x^0.55 + 273.983 x
```

```
CurveAA = Show[Plot[s100fit[x], {x, 0.001, 0.3},
AxesLabel -> {"exposure", "output level"}],
ListPlot[CCDS100]]
```

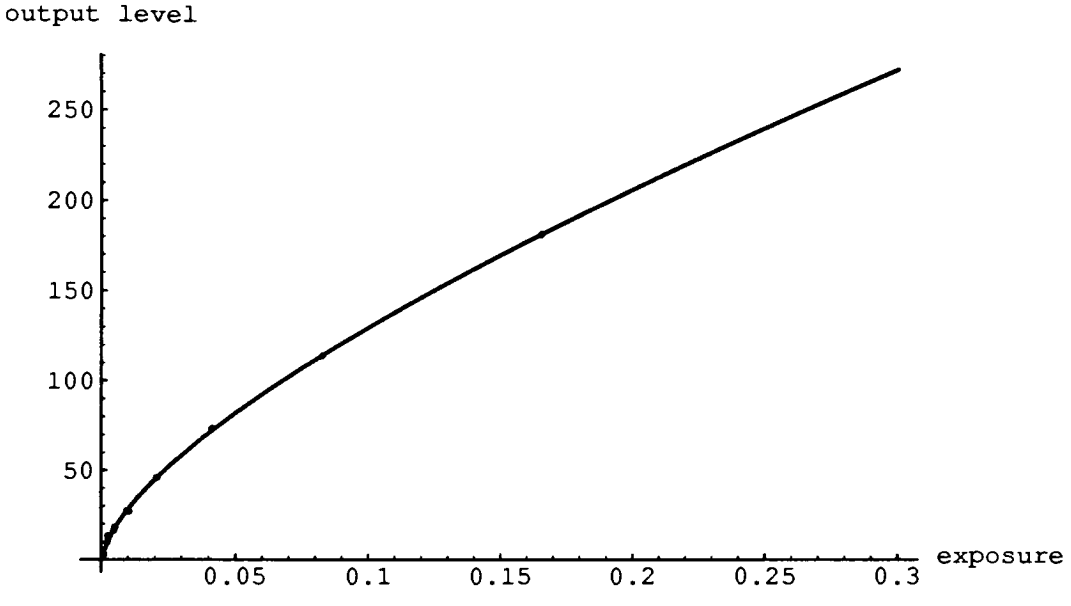

-Graphics-

```
Show[Plot[s100fit[x], {x, 0.001, 0.01},
AxesLabel -> {"exposure", "output level"}],
ListPlot[CCDS100]]
```

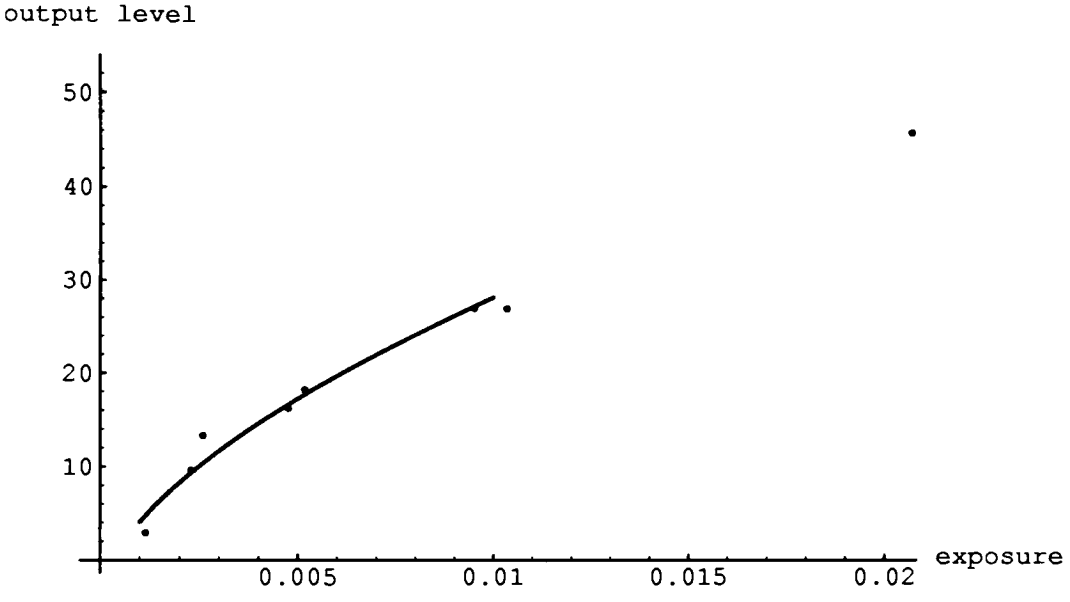


```
-Graphics-
```

```
<<Graphics`Graphics`
```

```
Show[LogLogListPlot[CCDS100,
AxesLabel -> {"exposure", "output level"}],
LogLogPlot[s100fit[x], {x, 0.001, 0.3}]]
```

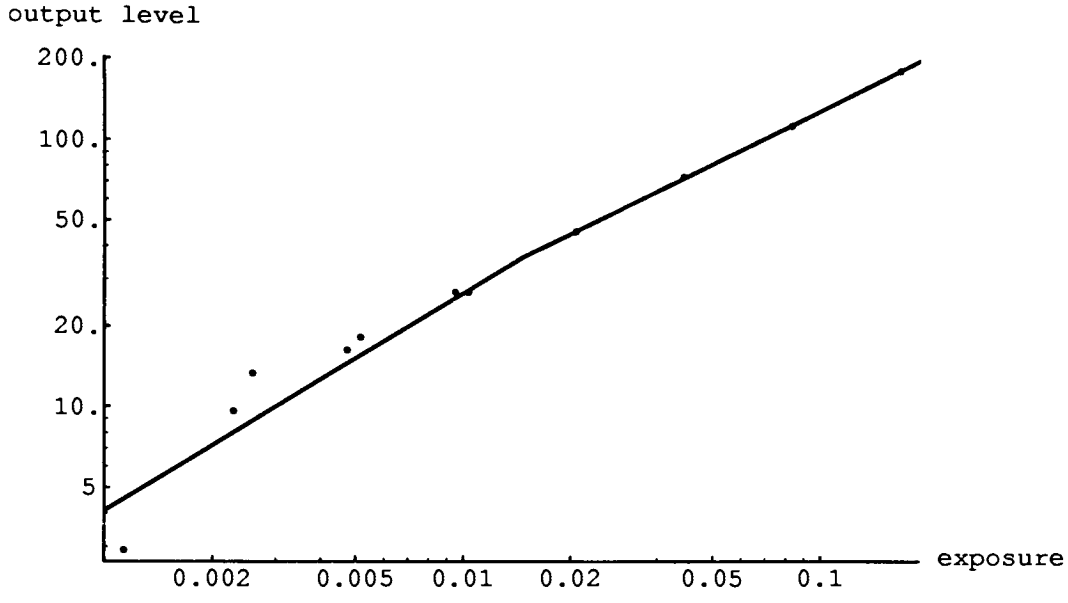


```
QS100 = {{1007, 2.92486},
         {2014, 9.60988},
         {2280, 13.3202},
         {4196, 16.2846},
         {4560, 18.2393},
         {8392, 27.077},
         {9119, 27.0167},
         {18239, 45.9052},
         {36477, 73.6219},
         {72955, 114.293},
         {145910, 182.109}};

Fit[QS100, {1, x^0.55, x}, x]
```

$$-4.71334 + 0.204325\, x^{0.55} + 0.000311047\, x$$

```
QFit100[x_] := -4.713335368046967635 +
               0.20432527013767169 84*x^0.55 +
               0.0003110466245226457792*x
```

```
D[QFit100[x],x]
```

$$0.00031104662452264577920 + \frac{0.112379}{x^{0.45}}$$

```
Gain100[x_] := 0.00031104662452264577920 +
               0.11237889857571943410/x^0.45

Plot[Gain100[x], {x, 3592, 285349}, AxesOrigin -> {0, 0},
AxesLabel -> {"exposure quanta", "gain"}]
```

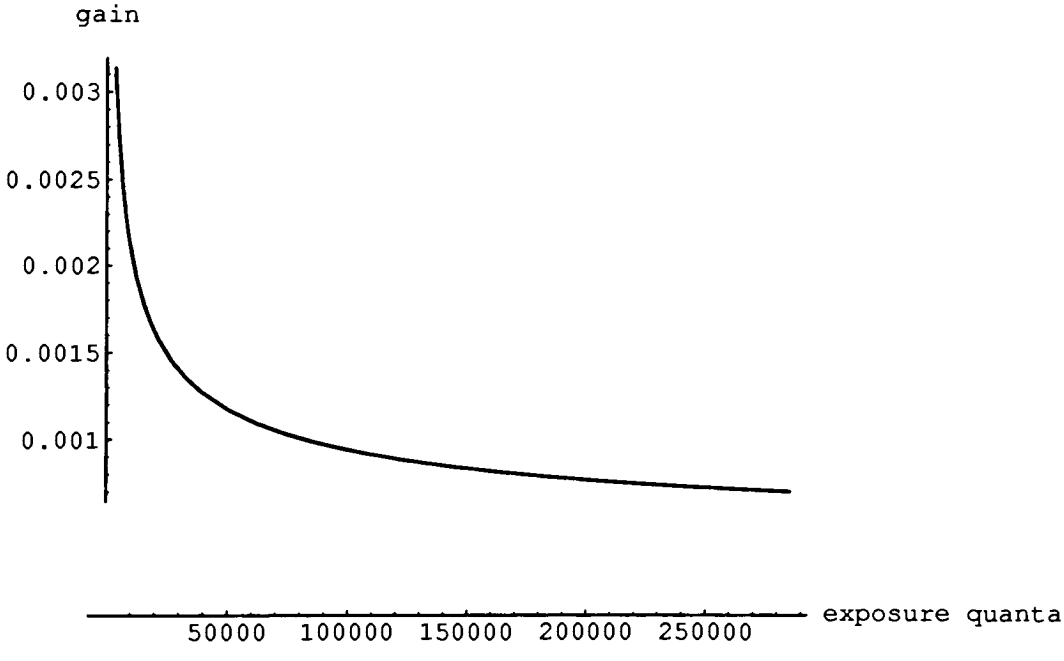

-Graphics-

```
CCDS200 = {{0.000571, 5.13516},
           {0.00114, 9.6834},
           {0.00229, 16.6442},
           {0.00259, 19.2363},
           {0.00476, 27.4443},
           {0.00518, 29.9266},
           {0.00952, 43.3152},
           {0.01035, 47.444},
           {0.0207, 73.1155},
           {0.0414, 110.953},
           {0.0828, 179.651}};

Regress[CCDS200, {1, x^0.55, x}, x]

{ParameterTable ->

            Estimate    SE          TStat       PValue       ,
   1        -3.6024     0.923794    -3.89957    0.00454741

    0.55
   x        547.52      22.1245     24.7472     0

   x        524.695     64.0972     8.18592     0.0000369982

  RSquared -> 0.999651, AdjustedRSquared -> 0.999563,

  EstimatedVariance -> 1.20945,

  ANOVATable ->

            DoF    SoS         MeanSS     FRatio     PValue}
   Model    2      27695.2     13847.6    11449.5    0

   Error    8      9.67561     1.20945

   Total    10     27704.9

s200fit[x_] := -3.6024 + 547.52 x^0.55 + 524.695 x
```

```
CurveBB = Show[Plot[s200fit[x], {x, 0.0005, 0.15},
AxesLabel -> {"exposure", "output level"}],
ListPlot[CCDS200]]
```

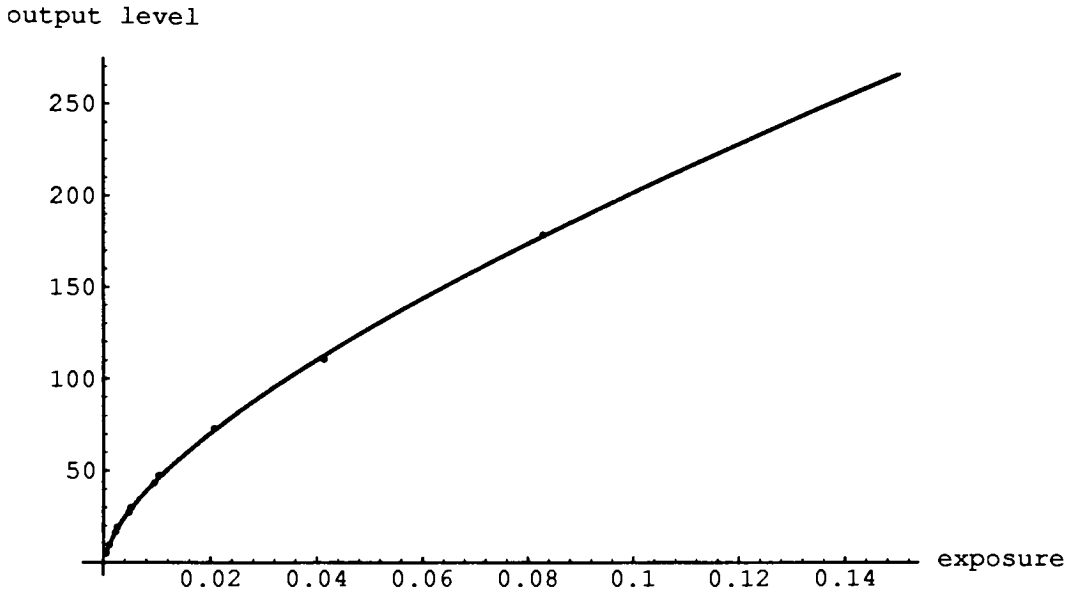

-Graphics-

```
<<Graphics`Graphics`
```

```
Show[LogLogListPlot[CCDS200,
AxesLabel -> {"exposure", "output level"}],
LogLogPlot[s200fit[x], {x, 0.0005, 0.15}]]
```

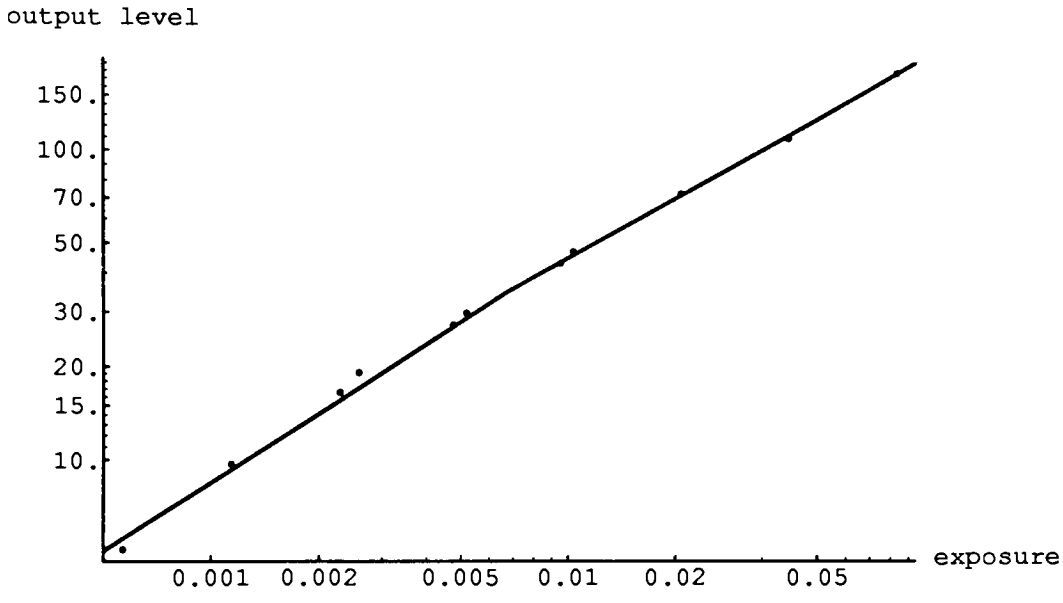


```
-Graphics-
```

```
QS200 = {{504, 5.13516},
         {1007, 9.6834},
         {2014, 16.6442},
         {2280, 19.2363},
         {4196, 27.4443},
         {4560, 29.9266},
         {8392, 43.3152},
         {9119, 47.444},
         {18239, 73.1155},
         {36477, 110.953},
         {72955, 179.651}};
```

```
Fit[QS200, {1, x^0.55, x}, x]
```

$$-3.60417 + 0.294223\ x^{0.55} + 0.000595337\ x$$

```
QFit200[x_] := -3.60416739726317803 +
               0.2942227374755486*x^0.55 +
               0.0005953370192514304066*x
```

```
D[QFit200[x],x]
```

$$0.000595337019251430406 6 + \frac{0.161823}{x^{0.45}}$$

```
Gain200[x_] := 0.0005953370192514304066 +
               0.16182250561155173/x^0.45

Plot[Gain200[x], {x, 1842, 146345}, AxesOrigin -> {0, 0},
AxesLabel -> {"exposure quanta", "gain"}]
```

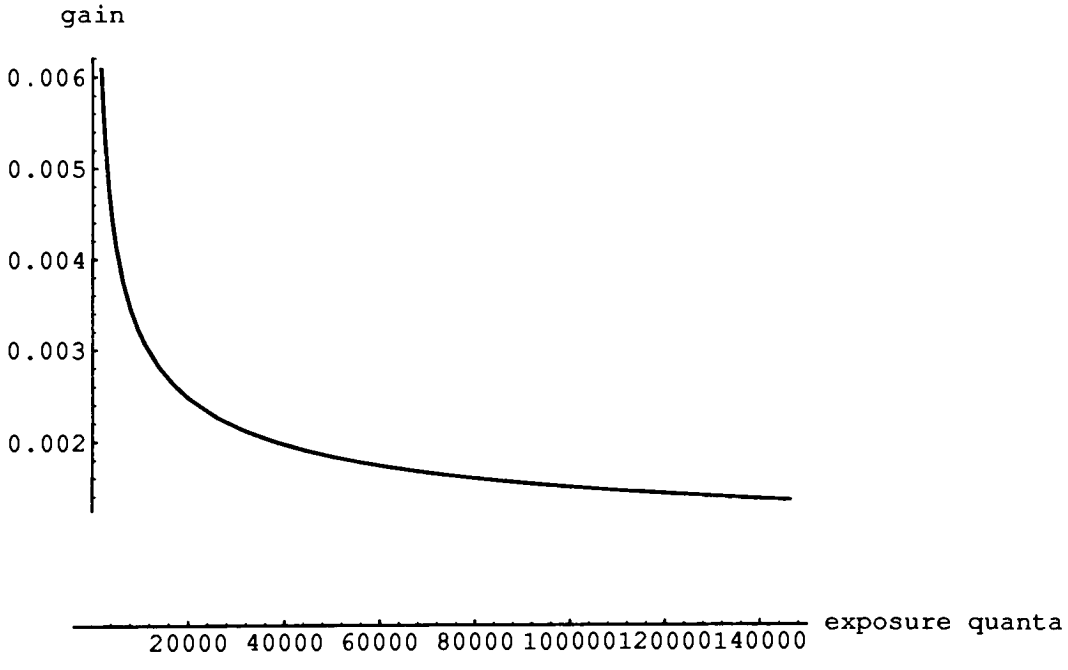

-Graphics-

```
CCDS400 = {{0.000286, 6.898},
           {0.000571, 11.397},
           {0.00114, 19.28},
           {0.00229, 29.927},
           {0.00259, 32.433},
           {0.00518, 51.273},
           {0.0207, 122.627},
           {0.0414, 195.938}};

Regress[CCDS400, {1, x^0.55, x}, x]

{ParameterTable ->

            Estimate    SE          TStat       PValue       ,
   1        -2.84723    0.512634    -5.55412    0.00260074

    0.55
   x        848.648     19.6162     43.2625     0

   x        1238.07     76.9171     16.0962     0.0000168615

  RSquared -> 0.999952, AdjustedRSquared -> 0.999933,

  EstimatedVariance -> 0.296111,

  ANOVATable ->

            DoF    SoS         MeanSS      FRatio     PValue}
   Model    2      30967.4     15483.7     52290.3    0

   Error    5      1.48055     0.296111

   Total    7      30968.9

s400fit[x_] := -2.84723 + 848.648 x^0.55 + 1238.07 x
```

```
CurveCC = Show[Plot[s400fit[x], {x, 0.00025, 0.075},
AxesLabel -> {"exposure", "output level"}],
ListPlot[CCDS400]]
```

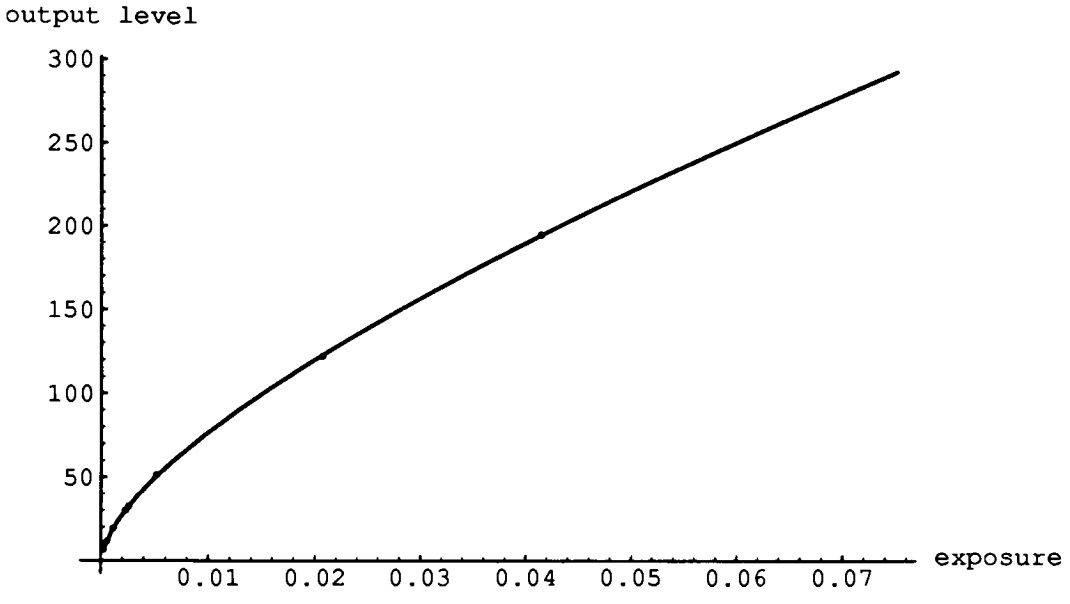


```
-Graphics-
```

```
<<Graphics`Graphics`
```

```
Show[LogLogListPlot[CCDS400,
AxesLabel -> {"exposure", "output level"}],
LogLogPlot[s400fit[x], {x, 0.00025, 0.075}]]
```

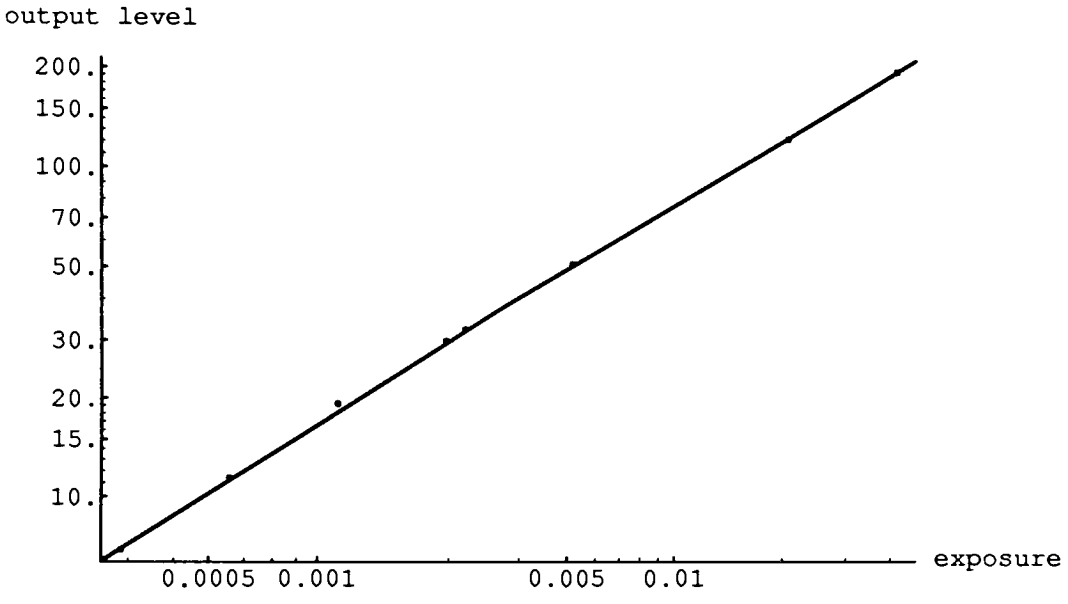

-Graphics-

```
QS400 = {{252, 6.898},
         {504, 11.397},
         {1007, 19.28},
         {2014, 29.927},
         {2280, 32.433},
         {4560, 51.273},
         {18239, 122.627},
         {36477, 195.938}};

Fit[QS400, {1, x^0.55, x}, x]
```

$$-2.86522 + 0.456529\ x^{0.55} + 0.00140079\ x$$

```
QFit400[x_] := -2.865221175173713015 +
               0.45652866909758122 25*x^0.55 +
               0.0014007864929044216 47*x
```

```
D[QFit400[x],x]
```

$$0.0014007864929044216 47 + \frac{0.251091}{x^{0.45}}$$

```
Gain400[x_] := 0.0014007864929044216 47 +
               0.25109076800366967 24/x^0.45

Plot[Gain400[x], {x, 786, 62428}, AxesOrigin -> {0, 0},
AxesLabel -> {"exposure quanta", "gain"}]
```

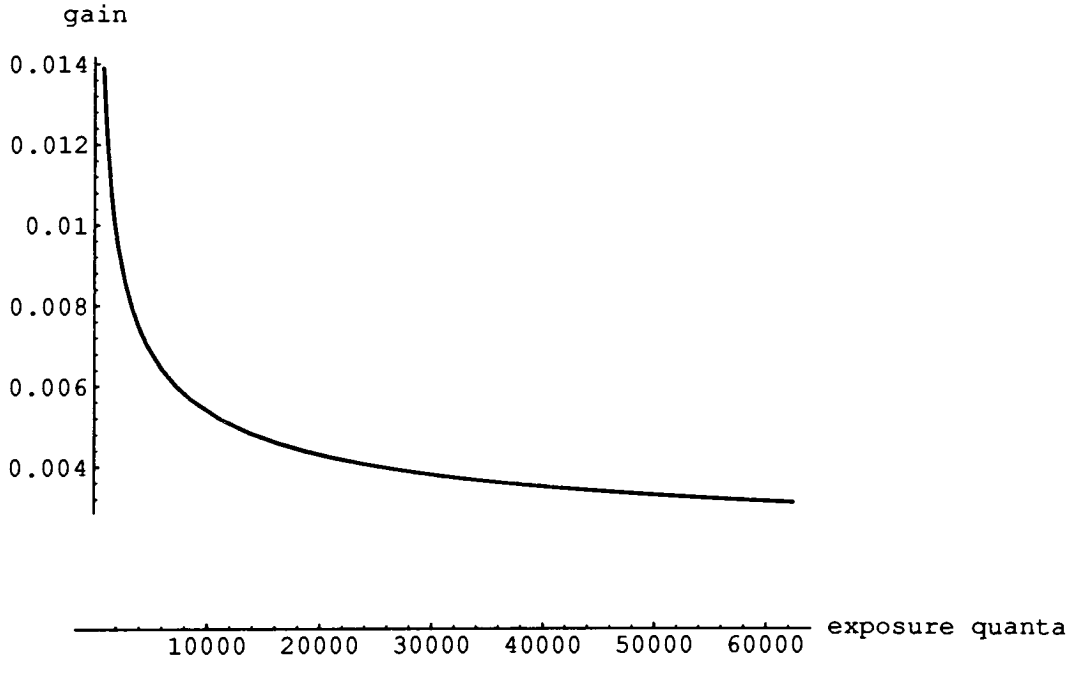

-Graphics-

```
CCDS800 = {{0.000143, 9.814},
           {0.000286, 13.508},
           {0.000571, 19.429},
           {0.00114, 26.317},
           {0.00259, 55.009},
           {0.00518, 82.631},
           {0.01035, 125.592},
           {0.0207, 198.061}};

Regress[CCDS800, {1, x^0.55, x}, x]

{ParameterTable ->

            Estimate    SE          TStat      PValue      ,
   1        -2.55545    2.48706     -1.0275    0.351302

    0.55
   x        1307.83     127.533     10.2548    0.000151495

   x        2207.89     692.003     3.19058    0.0242494

  RSquared -> 0.998727, AdjustedRSquared -> 0.998218,

  EstimatedVariance -> 7.9011,

  ANOVATable ->

            DoF    SoS         MeanSS     FRatio     PValue}
   Model    2      31004.4     15502.2    1962.03    0

   Error    5      39.5055     7.9011

   Total    7      31043.9

s800fit[x_] := -2.55545 + 1307.83 x^0.55 + 2207.89 x
```

```
CurveDD = Show[Plot[s800fit[x], {x, 0.000125, 0.0375},
AxesLabel -> {"exposure", "output level"}],
ListPlot[CCDS800]]
```

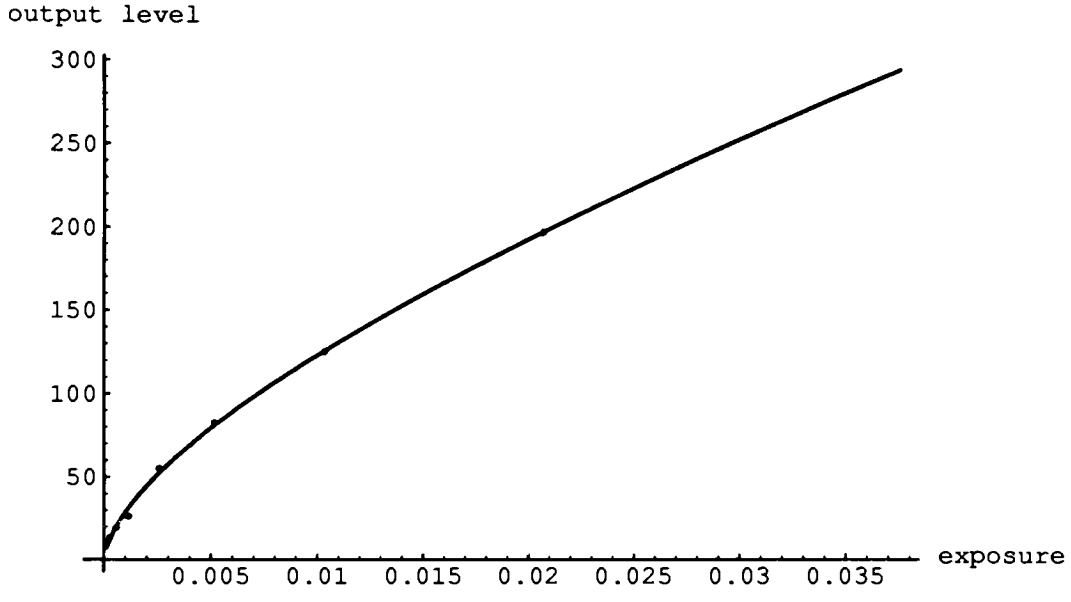

-Graphics-

```
<<Graphics`Graphics`
```

```
Show[LogLogListPlot[CCDS800,
AxesLabel -> {"exposure", "output level"}],
LogLogPlot[s800fit[x], {x, 0.000125, 0.0375}]]
```

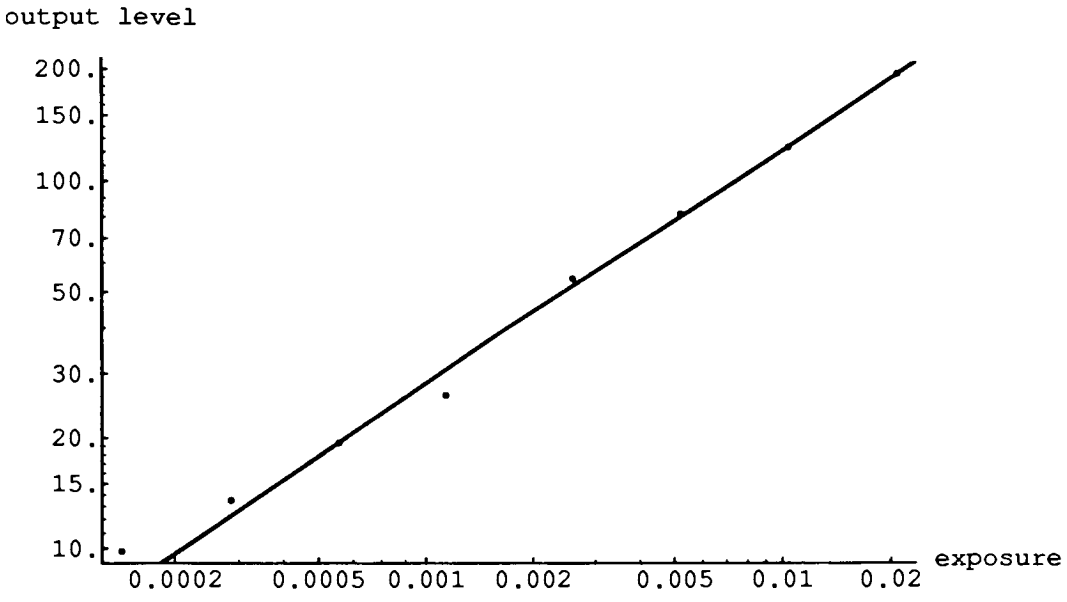

-Graphics-

```
QS800 = {{126, 9.814},
         {252, 13.508},
         {504, 19.429},
         {1007, 26.317},
         {2280, 55.009},
         {4560, 82.631},
         {9119, 125.592},
         {18239, 198.061}};

Fit[QS800, {1, x^0.55, x}, x]
```

$$-2.58095 + 0.703467\ x^{0.55} + 0.00249821\ x$$

```
QFit800[x_] := -2.580952214888372537 +
               0.7034668926381708431*x^0.55 +
               0.0024982088450960367 13*x
```

```
D[QFit800[x],x]
```

$$0.00249820884509603671 3 + \frac{0.386907}{x^{0.45}}$$

```
Gain800[x_] := 0.00249820884509603671 3 +
               0.3869067909509939637/x^0.45

Plot[Gain800[x], {x, 394, 31288}, AxesOrigin -> {0, 0},
AxesLabel -> {"exposure quanta", "gain"}]
```

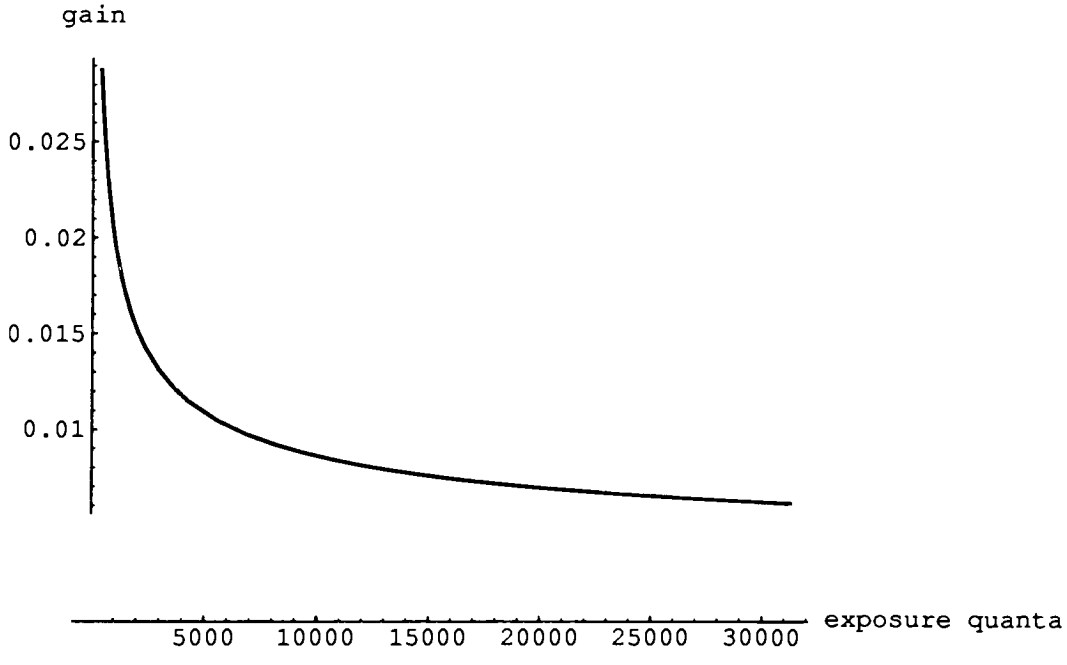

-Graphics-

```
Show[{CurveAA, CurveBB, CurveCC, CurveDD},
PlotRange -> {0, 255}]
```

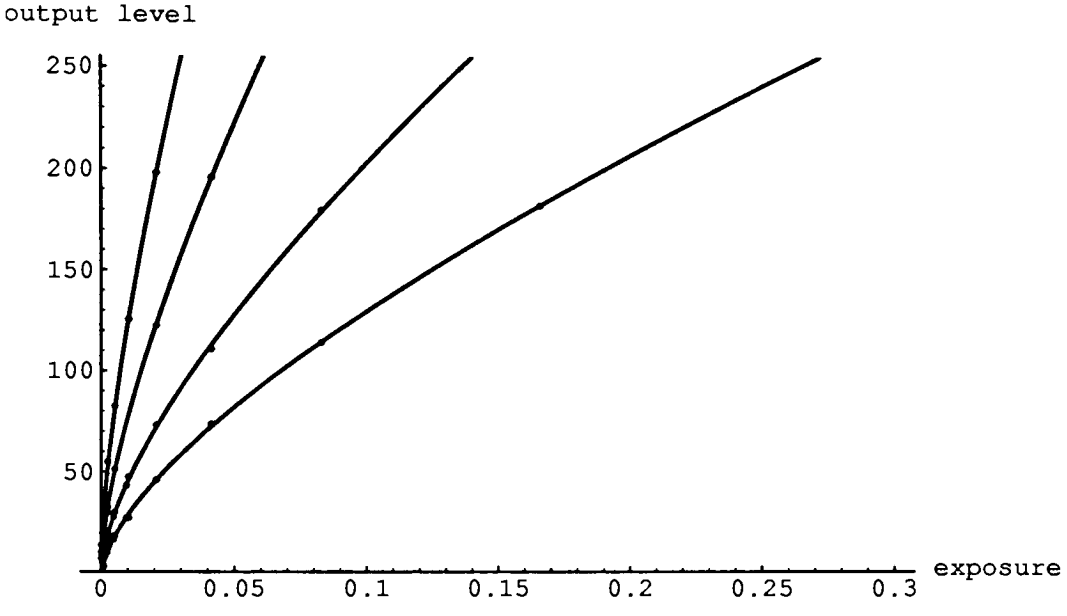

-Graphics-

Appendix F: DCS200mi/Microscope Flat Field.

```
ff37 = Round[Flatten[255 {
{0.5216, 0.5216, 0.5216, 0.5216, 0.5216, 0.5216, 0.5216, 0.521
0.5255, 0.5255, 0.5255, 0.5255, 0.5255, 0.5255, 0.5216, 0.521
0.5216, 0.5176, 0.5176, 0.5176, 0.5176, 0.5176, 0.5176, 0.517
0.5176, 0.5176, 0.5176, 0.5137, 0.5137, 0.5137, 0.5137, 0.513
0.5137, 0.5137, 0.5176, 0.5137, 0.5137, 0.5137, 0.5137, 0.509
0.5098, 0.5098, 0.5098, 0.5059, 0.5059, 0.5059, 0.5059, 0.505
0.5098, 0.5098, 0.5098, 0.5098, 0.5098},

{data edited to reduce length},

{0.5608, 0.5608, 0.5608, 0.5569, 0.5608, 0.5569, 0.5569, 0.560
0.5608, 0.5608, 0.5608, 0.5608, 0.5608, 0.5608, 0.5608, 0.560
0.5608, 0.5608, 0.5608, 0.5608, 0.5647, 0.5647, 0.5686, 0.568
0.5647, 0.5608, 0.5569, 0.5569, 0.5569, 0.5569, 0.5569, 0.556
0.5529, 0.5529, 0.5529, 0.5529, 0.5529, 0.5529, 0.5490, 0.549
0.5451, 0.5412, 0.5412, 0.5412, 0.5373, 0.5373, 0.5333, 0.533
0.5333, 0.5294, 0.5294, 0.5294, 0.5294}}]];
ff38 = Round[Flatten[255 {
{0.5569, 0.5569, 0.5569, 0.5569, 0.5569, 0.5569, 0.5569, 0.556
0.5608, 0.5608, 0.5608, 0.5608, 0.5608, 0.5608, 0.5608, 0.556
0.5569, 0.5569, 0.5569, 0.5569, 0.5569, 0.5569, 0.5569, 0.556
0.5569, 0.5529, 0.5529, 0.5529, 0.5529, 0.5529, 0.5490, 0.549
0.5529, 0.5529, 0.5529, 0.5529, 0.5529, 0.5490, 0.5490, 0.549
0.5451, 0.5451, 0.5412, 0.5412, 0.5412, 0.5412, 0.5412, 0.541
0.5451, 0.5451, 0.5451, 0.5451, 0.5451},

{data edited to reduce length},

{0.5765, 0.5765, 0.5765, 0.5725, 0.5725, 0.5725, 0.5725, 0.572
0.5765, 0.5765, 0.5765, 0.5765, 0.5765, 0.5765, 0.5765, 0.576
0.5765, 0.5765, 0.5765, 0.5765, 0.5804, 0.5804, 0.5843, 0.584
0.5804, 0.5765, 0.5725, 0.5725, 0.5725, 0.5725, 0.5725, 0.568
0.5647, 0.5647, 0.5647, 0.5647, 0.5647, 0.5608, 0.5608, 0.560
0.5569, 0.5569, 0.5569, 0.5529, 0.5529, 0.5490, 0.5490, 0.549
0.5451, 0.5451, 0.5451, 0.5451, 0.5451}}]];
```

```
ff39 = Round[Flatten[255 {
{0.5490, 0.5490, 0.5490, 0.5490, 0.5490, 0.5490, 0.5490, 0.549
0.5529, 0.5529, 0.5529, 0.5529, 0.5529, 0.5529, 0.5490, 0.549(
0.5490, 0.5490, 0.5490, 0.5451, 0.5451, 0.5451, 0.5451, 0.545(
0.5451, 0.5451, 0.5412, 0.5412, 0.5412, 0.5412, 0.5412, 0.541(
0.5412, 0.5412, 0.5451, 0.5451, 0.5412, 0.5412, 0.5412, 0.537(
0.5373, 0.5373, 0.5373, 0.5333, 0.5333, 0.5333, 0.5333, 0.533(
0.5373, 0.5373, 0.5373, 0.5373, 0.5373},

{data edited to reduce length},

{0.5608, 0.5608, 0.5608, 0.5569, 0.5569, 0.5569, 0.5569, 0.556
0.5608, 0.5608, 0.5608, 0.5608, 0.5608, 0.5608, 0.5608, 0.560
0.5608, 0.5608, 0.5608, 0.5608, 0.5647, 0.5647, 0.5647, 0.568
0.5647, 0.5608, 0.5569, 0.5569, 0.5569, 0.5569, 0.5569, 0.556
0.5529, 0.5529, 0.5529, 0.5490, 0.5490, 0.5490, 0.5490, 0.549(
0.5412, 0.5412, 0.5412, 0.5373, 0.5373, 0.5333, 0.5333, 0.533(
0.5333, 0.5294, 0.5294, 0.5294, 0.5294}}]];

ff40 = Round[Flatten[255 {
{0.6314, 0.6314, 0.6353, 0.6353, 0.6353, 0.6353, 0.6314, 0.631
0.6353, 0.6392, 0.6392, 0.6392, 0.6392, 0.6392, 0.6353, 0.635(
0.6314, 0.6314, 0.6314, 0.6314, 0.6314, 0.6314, 0.6314, 0.631(
0.6275, 0.6275, 0.6275, 0.6235, 0.6275, 0.6235, 0.6235, 0.623(
0.6275, 0.6275, 0.6275, 0.6275, 0.6235, 0.6235, 0.6235, 0.619(
0.6196, 0.6157, 0.6157, 0.6157, 0.6118, 0.6118, 0.6157, 0.615(
0.6157, 0.6157, 0.6157, 0.6157, 0.6157},

{data edited to reduce length},

{0.6510, 0.6510, 0.6510, 0.6471, 0.6471, 0.6510, 0.6471, 0.647
0.6510, 0.6510, 0.6549, 0.6510, 0.6510, 0.6510, 0.6510, 0.651(
0.6510, 0.6510, 0.6510, 0.6510, 0.6549, 0.6549, 0.6588, 0.658(
0.6549, 0.6510, 0.6471, 0.6471, 0.6471, 0.6471, 0.6471, 0.643(
0.6431, 0.6392, 0.6392, 0.6392, 0.6392, 0.6392, 0.6353, 0.631(
0.6275, 0.6275, 0.6235, 0.6235, 0.6196, 0.6196, 0.6157, 0.615(
0.6157, 0.6118, 0.6118, 0.6118, 0.6118}}]];
```

```
ff41 = Round[Flatten[255 {
{0.6078, 0.6078, 0.6078, 0.6078, 0.6078, 0.6078, 0.6078, 0.607
0.6078, 0.6118, 0.6118, 0.6118, 0.6118, 0.6118, 0.6078, 0.607
0.6078, 0.6078, 0.6078, 0.6039, 0.6039, 0.6039, 0.6078, 0.603
0.6039, 0.6039, 0.6039, 0.6000, 0.6000, 0.6000, 0.6000, 0.600
0.6039, 0.6039, 0.6039, 0.6039, 0.6000, 0.6000, 0.6000, 0.596
0.5961, 0.5961, 0.5922, 0.5922, 0.5922, 0.5922, 0.5922, 0.592
0.5922, 0.5922, 0.5961, 0.5961, 0.5961},

{data edited to reduce length},

{0.6392, 0.6392, 0.6392, 0.6353, 0.6353, 0.6353, 0.6353, 0.635
0.6392, 0.6392, 0.6392, 0.6392, 0.6392, 0.6392, 0.6392, 0.639
0.6392, 0.6392, 0.6392, 0.6392, 0.6431, 0.6431, 0.6471, 0.647
0.6431, 0.6392, 0.6353, 0.6353, 0.6353, 0.6353, 0.6314, 0.631
0.6275, 0.6275, 0.6275, 0.6235, 0.6235, 0.6235, 0.6235, 0.619
0.6157, 0.6118, 0.6118, 0.6118, 0.6078, 0.6078, 0.6078, 0.603
0.6039, 0.6000, 0.6000, 0.6000, 0.6000}}]];
ff42 = Round[Flatten[255 {
{0.5765, 0.5765, 0.5765, 0.5765, 0.5765, 0.5765, 0.5765, 0.576
0.5804, 0.5804, 0.5804, 0.5804, 0.5804, 0.5804, 0.5804, 0.576
0.5765, 0.5765, 0.5765, 0.5725, 0.5725, 0.5725, 0.5765, 0.572
0.5725, 0.5725, 0.5686, 0.5686, 0.5686, 0.5686, 0.5686, 0.568
0.5686, 0.5725, 0.5725, 0.5725, 0.5686, 0.5686, 0.5647, 0.564
0.5647, 0.5608, 0.5608, 0.5608, 0.5608, 0.5608, 0.5608, 0.560
0.5608, 0.5608, 0.5647, 0.5647, 0.5647},

{data edited to reduce length},

{0.5882, 0.5882, 0.5882, 0.5882, 0.5882, 0.5882, 0.5882, 0.588
0.5882, 0.5922, 0.5922, 0.5922, 0.5922, 0.5922, 0.5922, 0.588
0.5882, 0.5882, 0.5922, 0.5922, 0.5922, 0.5961, 0.5961, 0.596
0.5922, 0.5882, 0.5882, 0.5882, 0.5882, 0.5843, 0.5843, 0.584
0.5804, 0.5804, 0.5804, 0.5804, 0.5804, 0.5804, 0.5765, 0.576
0.5725, 0.5686, 0.5686, 0.5686, 0.5647, 0.5647, 0.5608, 0.560
0.5608, 0.5569, 0.5569, 0.5569, 0.5569}}]];
```

```
ff43 = Round[Flatten[255 {
{0.5569, 0.5569, 0.5569, 0.5569, 0.5569, 0.5569, 0.5569, 0.556
0.5608, 0.5608, 0.5608, 0.5608, 0.5608, 0.5608, 0.5569, 0.556
0.5569, 0.5569, 0.5569, 0.5569, 0.5569, 0.5569, 0.5569, 0.556
0.5529, 0.5529, 0.5529, 0.5529, 0.5529, 0.5529, 0.5490, 0.549
0.5529, 0.5529, 0.5529, 0.5529, 0.5529, 0.5490, 0.5490, 0.549
0.5451, 0.5412, 0.5412, 0.5412, 0.5373, 0.5412, 0.5412, 0.541
0.5412, 0.5412, 0.5451, 0.5451, 0.5451},

{data edited to reduce length},

{0.5686, 0.5686, 0.5725, 0.5686, 0.5686, 0.5686, 0.5686, 0.568
0.5686, 0.5725, 0.5725, 0.5725, 0.5725, 0.5725, 0.5725, 0.568
0.5725, 0.5686, 0.5725, 0.5725, 0.5725, 0.5765, 0.5765, 0.576
0.5725, 0.5686, 0.5686, 0.5647, 0.5647, 0.5647, 0.5647, 0.564
0.5608, 0.5608, 0.5608, 0.5569, 0.5569, 0.5569, 0.5569, 0.556
0.5529, 0.5490, 0.5490, 0.5490, 0.5451, 0.5451, 0.5412, 0.537
0.5373, 0.5373, 0.5373, 0.5373, 0.5373}}]];

ff44 = Round[Flatten[255 {
{0.5647, 0.5647, 0.5686, 0.5686, 0.5686, 0.5686, 0.5686, 0.564
0.5686, 0.5725, 0.5725, 0.5725, 0.5686, 0.5725, 0.5686, 0.568
0.5647, 0.5647, 0.5647, 0.5647, 0.5647, 0.5647, 0.5647, 0.564
0.5647, 0.5608, 0.5608, 0.5608, 0.5608, 0.5608, 0.5608, 0.560
0.5608, 0.5608, 0.5608, 0.5608, 0.5608, 0.5608, 0.5569, 0.556
0.5569, 0.5569, 0.5569, 0.5529, 0.5529, 0.5529, 0.5529, 0.552
0.5569, 0.5569, 0.5569, 0.5569, 0.5569},

{data edited to reduce length},

{0.6039, 0.6039, 0.6039, 0.6039, 0.6039, 0.6039, 0.6039, 0.603
0.6039, 0.6078, 0.6078, 0.6078, 0.6078, 0.6078, 0.6078, 0.603
0.6039, 0.6039, 0.6078, 0.6078, 0.6078, 0.6118, 0.6118, 0.611
0.6078, 0.6039, 0.6039, 0.6039, 0.6000, 0.6000, 0.6000, 0.600
0.5961, 0.5961, 0.5961, 0.5922, 0.5922, 0.5922, 0.5882, 0.588
0.5843, 0.5843, 0.5843, 0.5804, 0.5804, 0.5804, 0.5765, 0.576
0.5765, 0.5725, 0.5725, 0.5725, 0.5725}}]];
```

```
ff45 = Round[Flatten[255 {
{0.5765, 0.5765, 0.5765, 0.5765, 0.5765, 0.5765, 0.5765, 0.576
0.5804, 0.5804, 0.5804, 0.5804, 0.5804, 0.5804, 0.5765, 0.576
0.5765, 0.5765, 0.5765, 0.5725, 0.5725, 0.5725, 0.5725, 0.572
0.5725, 0.5686, 0.5686, 0.5686, 0.5686, 0.5686, 0.5686, 0.568
0.5686, 0.5686, 0.5725, 0.5686, 0.5686, 0.5686, 0.5647, 0.564
0.5647, 0.5608, 0.5608, 0.5608, 0.5608, 0.5608, 0.5608, 0.560
0.5608, 0.5608, 0.5608, 0.5647, 0.5647},

{data edited to reduce length},

{0.5882, 0.5882, 0.5882, 0.5882, 0.5882, 0.5882, 0.5882, 0.588
0.5882, 0.5922, 0.5922, 0.5922, 0.5922, 0.5922, 0.5922, 0.588
0.5882, 0.5882, 0.5882, 0.5922, 0.5961, 0.5961, 0.6000, 0.600
0.5922, 0.5882, 0.5882, 0.5882, 0.5843, 0.5843, 0.5843, 0.584
0.5804, 0.5804, 0.5804, 0.5804, 0.5765, 0.5765, 0.5765, 0.572
0.5686, 0.5686, 0.5647, 0.5647, 0.5647, 0.5608, 0.5608, 0.560
0.5569, 0.5569, 0.5569, 0.5569, 0.5569}}]];
ff46 = Round[Flatten[255 {
{0.5843, 0.5843, 0.5843, 0.5843, 0.5843, 0.5843, 0.5843, 0.584
0.5843, 0.5882, 0.5882, 0.5882, 0.5882, 0.5882, 0.5843, 0.584
0.5843, 0.5843, 0.5843, 0.5843, 0.5804, 0.5843, 0.5843, 0.580
0.5804, 0.5804, 0.5804, 0.5804, 0.5804, 0.5765, 0.5765, 0.576
0.5804, 0.5804, 0.5804, 0.5804, 0.5765, 0.5765, 0.5765, 0.572
0.5725, 0.5725, 0.5725, 0.5686, 0.5686, 0.5686, 0.5686, 0.568
0.5725, 0.5725, 0.5725, 0.5725, 0.5725},

{data edited to reduce length},

{0.6000, 0.6000, 0.6000, 0.6000, 0.6000, 0.6000, 0.6000, 0.600
0.6000, 0.6039, 0.6039, 0.6039, 0.6039, 0.6039, 0.6039, 0.603
0.6039, 0.6000, 0.6039, 0.6039, 0.6039, 0.6078, 0.6078, 0.607
0.6039, 0.6000, 0.5961, 0.5961, 0.5961, 0.5961, 0.5961, 0.592
0.5882, 0.5882, 0.5882, 0.5843, 0.5843, 0.5843, 0.5843, 0.584
0.5804, 0.5765, 0.5765, 0.5765, 0.5725, 0.5725, 0.5686, 0.568
0.5647, 0.5647, 0.5647, 0.5647, 0.5647}}]];
```

```
ff139 = Round[Flatten[255 {
{0.4588, 0.4588, 0.4588, 0.4549, 0.4549, 0.4549, 0.4549, 0.454
0.4549, 0.4549, 0.4549, 0.4549, 0.4510, 0.4510, 0.4471, 0.4471
0.4471, 0.4431, 0.4431, 0.4431, 0.4431, 0.4431, 0.4431, 0.4431
0.4392, 0.4392, 0.4392, 0.4392, 0.4392, 0.4353, 0.4353, 0.4353
0.4353, 0.4353, 0.4353, 0.4353, 0.4314, 0.4314, 0.4314, 0.4314
0.4314, 0.4314, 0.4314, 0.4314, 0.4275, 0.4314, 0.4314, 0.4275
0.4314, 0.4314, 0.4314, 0.4314, 0.4353},

{data edited to reduce length},

{0.4510, 0.4510, 0.4510, 0.4471, 0.4510, 0.4471, 0.4471, 0.447
0.4471, 0.4471, 0.4471, 0.4471, 0.4431, 0.4431, 0.4431, 0.4431
0.4431, 0.4431, 0.4431, 0.4431, 0.4431, 0.4431, 0.4392, 0.4392
0.4392, 0.4353, 0.4353, 0.4353, 0.4353, 0.4353, 0.4353, 0.4314
0.4314, 0.4314, 0.4314, 0.4275, 0.4275, 0.4314, 0.4275, 0.4275
0.4275, 0.4235, 0.4235, 0.4235, 0.4235, 0.4235, 0.4235, 0.4235
0.4235, 0.4235, 0.4235, 0.4235, 0.4275}}]];

ff140 = Round[Flatten[255 {
{0.7255, 0.7255, 0.7255, 0.7216, 0.7176, 0.7176, 0.7176, 0.717
0.7176, 0.7176, 0.7176, 0.7176, 0.7137, 0.7137, 0.7098, 0.7059
0.7059, 0.7020, 0.7020, 0.7020, 0.6980, 0.7020, 0.6980, 0.6980
0.6941, 0.6941, 0.6941, 0.6902, 0.6902, 0.6902, 0.6902, 0.6902
0.6863, 0.6863, 0.6863, 0.6863, 0.6863, 0.6824, 0.6824, 0.6824
0.6824, 0.6784, 0.6784, 0.6784, 0.6784, 0.6784, 0.6784, 0.6784
0.6824, 0.6824, 0.6824, 0.6824, 0.6824},

{data edited to reduce length},

{0.7216, 0.7176, 0.7216, 0.7176, 0.7176, 0.7176, 0.7137, 0.713
0.7137, 0.7137, 0.7137, 0.7098, 0.7098, 0.7098, 0.7098, 0.7059
0.7059, 0.7059, 0.7059, 0.7059, 0.7059, 0.7020, 0.7020, 0.7020
0.6980, 0.6980, 0.6941, 0.6941, 0.6941, 0.6941, 0.6902, 0.6902
0.6863, 0.6863, 0.6863, 0.6863, 0.6863, 0.6863, 0.6824, 0.6824
0.6784, 0.6784, 0.6784, 0.6784, 0.6745, 0.6745, 0.6745, 0.6745
0.6784, 0.6784, 0.6784, 0.6784, 0.6784}}]];
```

```
FlatField = N[(ff37 + ff38 + ff39 + ff40 + ff41 + ff42 +
            ff43 + ff44 + ff45 + ff46)/1464.97];

<<Statistics`DescriptiveStatistics`

Mean[FlatField]

1.

Variance[FlatField]

0.000435926

N[Mean[FlatField 146.497]]
N[Variance[FlatField 146.497]]

146.497

9.35557

N[Mean[ff37]]
N[Variance[ff37]]

136.388

15.367

N[Mean[ff38]]
N[Variance[ff38]]

142.523

8.63044

N[Mean[ff39]]
N[Variance[ff39]]

139.372

7.08948

N[Mean[ff40]]
N[Variance[ff40]]

160.93

11.375
```

```
N[Mean[ff41]]
N[Variance[ff41]]

155.231

11.9532

N[Mean[ff42]]
N[Variance[ff42]]

146.514

7.61862

N[Mean[ff43]]
N[Variance[ff43]]

141.412

8.21627

N[Mean[ff44]]
N[Variance[ff44]]

147.563

13.7287

N[Mean[ff45]]
N[Variance[ff45]]

146.335

7.76116

N[Mean[ff46]]
N[Variance[ff46]]

148.703

9.20707

N[Mean[ff37/FlatField]]
N[Variance[ff37/FlatField]]

136.371

2.83495
```

```
N[Mean[ff38/FlatField]]
N[Variance[ff38/FlatField]]

142.524

0.15443

N[Mean[ff39/FlatField]]
N[Variance[ff39/FlatField]]

139.379

0.405689

N[Mean[ff40/FlatField]]
N[Variance[ff40/FlatField]]

160.93

0.325669

N[Mean[ff41/FlatField]]
N[Variance[ff41/FlatField]]

155.228

0.563332

N[Mean[ff42/FlatField]]
N[Variance[ff42/FlatField]]

146.521

0.38656

N[Mean[ff43/FlatField]]
N[Variance[ff43/FlatField]]

141.415

0.40987

N[Mean[ff44/FlatField]]
N[Variance[ff44/FlatField]]

147.554

1.5607
```

```
N[Mean[ff45/FlatField]]
N[Variance[ff45/FlatField]]
```

```
146.342
```

```
0.425505
```

```
N[Mean[ff46/FlatField]]
N[Variance[ff46/FlatField]]
```

```
148.706
```

```
0.310815
```

```
N[Mean[ff139]]
N[Variance[ff139]]
```

```
110.025
```

```
6.18765
```

```
N[Mean[ff140]]
N[Variance[ff140]]
```

```
174.524
```

```
13.4426
```

```
N[Mean[ff139/FlatField]]
N[Variance[ff139/FlatField]]
```

```
110.04
```

```
4.39832
```

```
N[Mean[ff140/FlatField]]
N[Variance[ff140/FlatField]]
```

```
174.55
```

```
9.183
```

```
ListDensityPlot[Partition[FlatField, 59], Mesh -> False,
AspectRatio -> 0.666667]
```

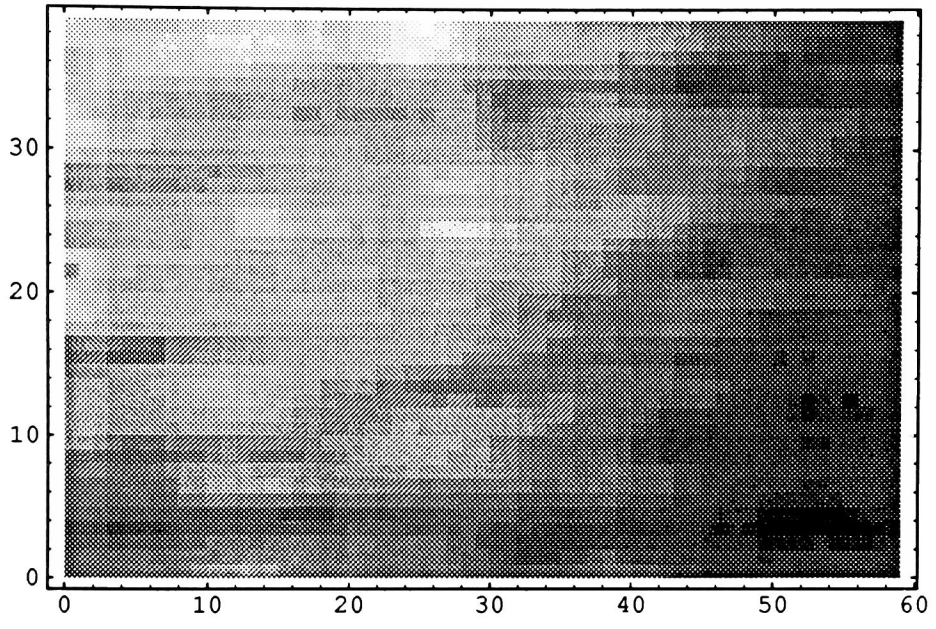


```
-DensityGraphics-
```

Image #	Mean	Variance	Variance w/ FF Sub.	Standard Deviation
37	136.388	15.367	2.83495	3.92007653
38	142.523	8.63044	0.15443	2.937761052
39	139.372	7.08948	0.405689	2.662607744
40	160.93	11.375	0.325669	3.372684391
41	155.231	11.9532	0.563332	3.457340018
42	146.514	7.61862	0.38656	2.760184776
43	141.412	8.21627	0.40987	2.86640367
44	147.563	13.7287	1.5607	3.705226039
45	146.335	7.76116	0.425505	2.785885856
46	148.703	9.20707	0.310815	3.034315409
Average	146.497	10.094694	0.737752	3.150248549
139	110.025	6.18765	4.39832	2.487498744
140	174.524	13.4426	9.183	3.666415143
Flat Field	146.497	9.35557		3.058687627
Norm. FF	1	0.000435926		0.020878841

S.D. w/ FF Sub.	Level/Noise	L/N w/ FF Sub.
1.683730976	34.792178	81.00343935
0.392975826	48.514157	362.6762526
0.636937203	52.344173	218.8159201
0.570674163	47.715701	281.9998004
0.750554462	44.898968	206.821767
0.621739495	53.081229	235.6517498
0.640210903	49.334294	220.883461
1.249279793	39.82564	118.1184558
0.652307443	52.527278	224.3344018
0.557507847	49.0071	266.728084
0.775591811	47.204072	221.7033332
2.097217204	44.231178	52.46237719
3.030346515	47.60072	57.59209356
	47.895378	
	47.895379	

Flat Field Variance

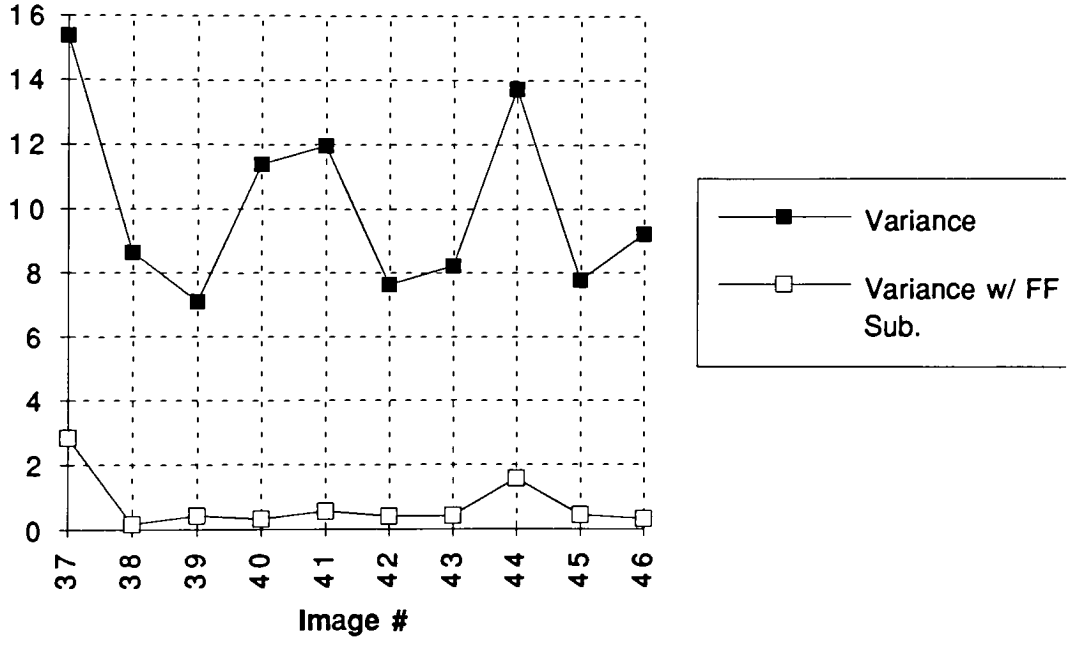

Flat Field Mean, Noise

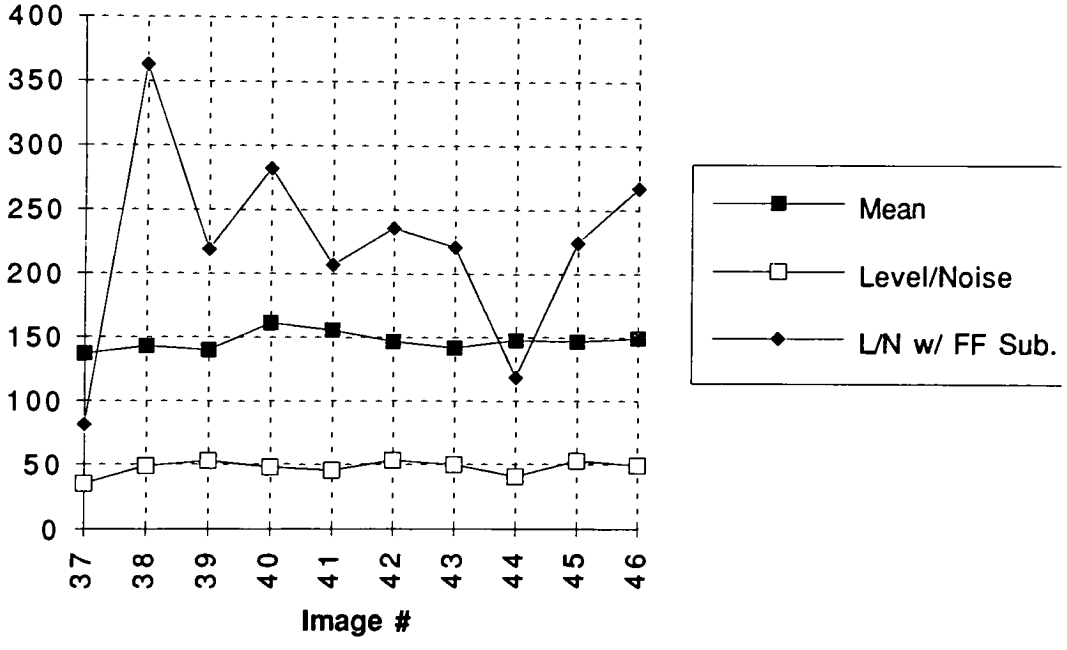

Appendix G: DCS200mi/Microscope MTF.

```
row1 = {0.0863, 0.0980, 0.0980, 0.0980, 0.0863, 0.0980, 0.086
0.0980, 0.0980, 0.0980, 0.0980, 0.0980, 0.1059, 0.0980, 0.098
0.1059, 0.0980, 0.1059, 0.1059, 0.1059, 0.0980, 0.1059, 0.105
0.1059, 0.0980, 0.1137, 0.1059, 0.1137, 0.1137, 0.1137, 0.113
0.1137, 0.1137, 0.1137, 0.1137, 0.1216, 0.1137, 0.1294, 0.180
0.2275, 0.3882, 0.6784, 0.7843, 0.7922, 0.7961, 0.8000, 0.796
0.8000, 0.7922, 0.7961, 0.8000, 0.8000, 0.8000, 0.8000, 0.796
0.8000, 0.7961, 0.8039, 0.8039, 0.8078, 0.8039, 0.8118, 0.815
0.8118, 0.8078, 0.8157, 0.8118, 0.8039, 0.8039, 0.8078, 0.803
0.8000, 0.8118, 0.8039, 0.8157, 0.8118, 0.8118, 0.8118, 0.807
0.8157, 0.8039, 0.8196, 0.8157, 0.8118, 0.8118, 0.8039, 0.811
0.8157, 0.8118, 0.8196, 0.8196, 0.8196, 0.8118, 0.8196, 0.815
0.8157, 0.8157, 0.8157, 0.8118, 0.7961};

ListPlot[row1, AspectRatio -> 0.25]
```

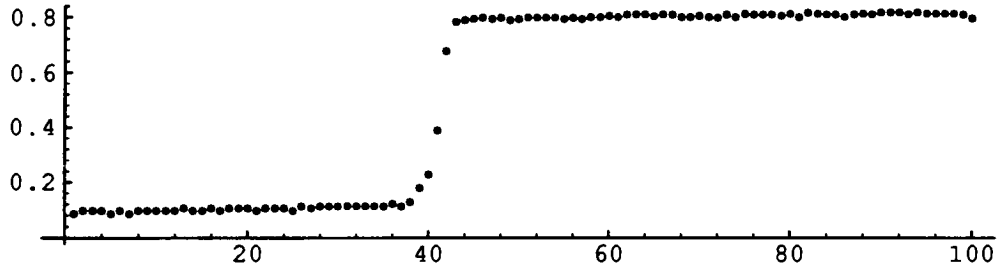


```
-Graphics-
```

```
pixel41 = 0.3882;
pixel42 = 0.6784;
MidtonePixelTop =
((0.5 - pixel41)/(pixel42 - pixel41)) + 41
```

```
41.3853
```

```
row1012 = {0.0784, 0.0863, 0.0784, 0.0784, 0.0863, 0.0784,
0.0784, 0.0784, 0.0784, 0.0784, 0.0784, 0.0784, 0.0863, 0.0784
0.0784, 0.0784, 0.0784, 0.0784, 0.0863, 0.0784, 0.0863, 0.0863
0.0784, 0.0863, 0.0863, 0.0863, 0.0863, 0.0863, 0.0863, 0.0863
0.0980, 0.0863, 0.0863, 0.0980, 0.0863, 0.0980, 0.0980, 0.0863
0.0863, 0.0980, 0.0863, 0.0980, 0.0863, 0.0863, 0.0980, 0.0980
0.0980, 0.0980, 0.0980, 0.1059, 0.0863, 0.1059, 0.0980, 0.0980
0.1059, 0.1059, 0.1059, 0.1059, 0.1137, 0.1137, 0.1137, 0.1059
0.1059, 0.1216, 0.1137, 0.1137, 0.1137, 0.1294, 0.1843, 0.2549
0.3686, 0.6157, 0.7412, 0.7725, 0.7843, 0.7922, 0.7961, 0.7922
0.7922, 0.7922, 0.7922, 0.8000, 0.8000, 0.8039, 0.7961, 0.7961
0.7882, 0.7922, 0.8039, 0.8039, 0.8000, 0.7922, 0.7922, 0.7922
0.8000, 0.8000, 0.7961, 0.8118, 0.8039, 0.7961};
```

```
ListPlot[row1012, AspectRatio -> 0.25]
```

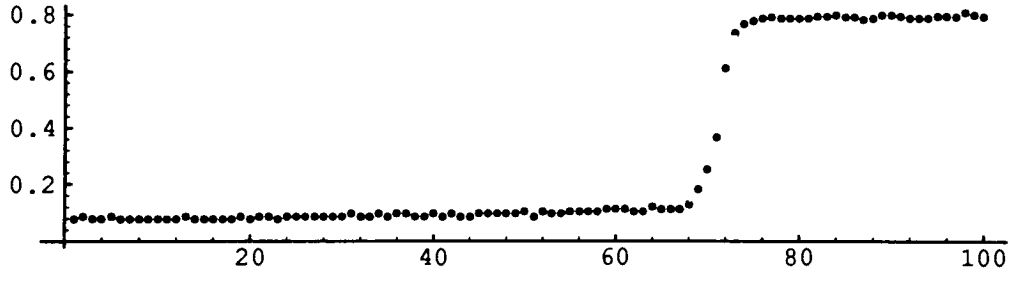


```
-Graphics-
```

```
pixel71 = 0.3686;
pixel72 = 0.6157;
MidtonePixelBottom =
((0.5 - pixel71)/(pixel72 - pixel71)) + 71
```

```
71.5318
```

```
Angle =
ArcTan[(MidtonePixelBottom - MidtonePixelTop)/1012]
```

```
0.0297802
```

```
BlockHeight = 1/Tan[Angle]
```

```
33.5694
```

```
TopCrop = Round[(Ceiling[MidtonePixelTop] -
MidtonePixelTop)/Tan[Angle]]
```

```
21
```

```
NumberBlocks = Floor[(1012 - TopCrop)/BlockHeight]
```

```
29
```

```
NumberRows = Round[NumberBlocks BlockHeight]
```

```
974
```

```
LargeBlocks =
NumberRows - NumberBlocks Floor[BlockHeight]
```

```
17
```

```
LargeBlockNumbers =
Table[Round[NumberBlocks/LargeBlocks x],
{x, 1, LargeBlocks}]
```

```
{2, 3, 5, 7, 9, 10, 12, 14, 15, 17, 19, 20, 22, 24, 26, 27,
  29}
```

```
BlockTopCenters = Table[Round[712 + MidtonePixelTop +
(BlockHeight (x - 1) + TopCrop) Tan[Angle]],
{x, 1, NumberBlocks}]
```

```
{754, 755, 756, 757, 758, 759, 760, 761, 762, 763, 764,
  765, 766, 767, 768, 769, 770, 771, 772, 773, 774, 775,
  776, 777, 778, 779, 780, 781, 782}
```

```
data = Flatten[Transpose[255 {
{0.0471, 0.0431, 0.0471, 0.0431, 0.0471, 0.0431, 0.0471, 0.047
0.0471, 0.0431, 0.0471, 0.0471, 0.0471, 0.0471, 0.0471, 0.051C
0.0471, 0.0510, 0.0510, 0.0471, 0.0510, 0.0510, 0.0510, 0.051C
0.0510, 0.0549, 0.0549, 0.0510, 0.0549, 0.0510, 0.0549, 0.054S
0.0510, 0.0510, 0.0549, 0.0549, 0.0588, 0.0549, 0.0549, 0.054S

{data edited to reduce length},

0.8039, 0.8078, 0.8118, 0.8078, 0.8078, 0.8078, 0.8078, 0.807E
0.8078, 0.8039, 0.8039, 0.8039, 0.8039, 0.8039, 0.8039, 0.807E
0.8039, 0.8078, 0.8078, 0.8039, 0.8039, 0.8078, 0.8078, 0.800C
0.8039, 0.8039, 0.8039, 0.8078, 0.8039, 0.8078, 0.8078, 0.803S
0.8078, 0.8039, 0.8118, 0.8039, 0.8078, 0.8039, 0.8078, 0.807E
0.8039, 0.8078}}]];
```

```
SmoothingFactor = 10
```

```
10
```

```
DataPoints = Length[data]
```

```
6600
```

```
smooth[i_] := N[Sum[data[[j]],
{j, i + 1 - SmoothingFactor/2, i + SmoothingFactor/2}]]
```

```
smoothdata = Table[smooth[i],
{i, SmoothingFactor/2,
DataPoints - SmoothingFactor/2,
SmoothingFactor}];
```

```
ListPlot[smoothdata, AspectRatio -> 0.25]
```

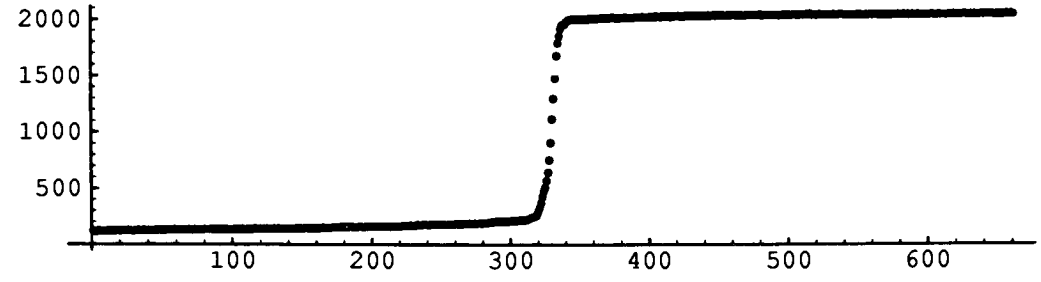


```
-Graphics-
```

```
SmoothPoints = DataPoints/SmoothingFactor
```

```
660
```

```
ChopData = 249
```

```
249
```

```
lnsf = Table[(smoothdata[[i+1]] - smoothdata[[i]]),
{i, ChopData + 1, SmoothPoints - ChopData - 2}];
```

```
ListPlot[lnsf, AspectRatio -> 0.25, PlotRange -> All]
```

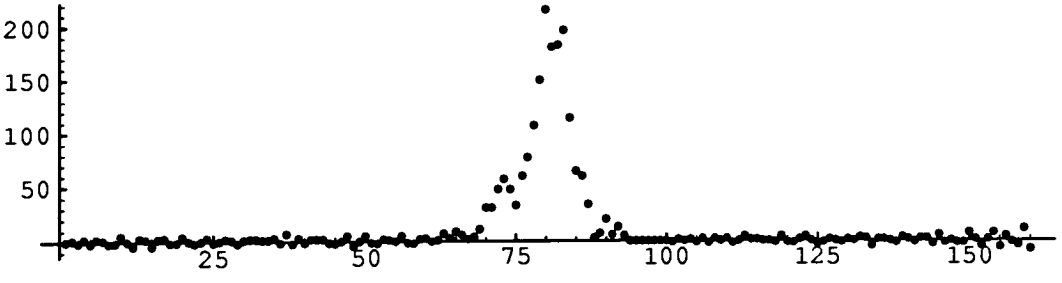


```
-Graphics-
```

```
OffsetError = 1
```

```
1
```

```
symlsf = Table[(lnsf[[i]] +
lnsf[[SmoothPoints - 2 (ChopData + 1) - i]]),
{i, OffsetError + 1, SmoothPoints - 2 ChopData - 3}];
```

```
ListPlot[symlsf, AspectRatio -> 0.25, PlotRange -> All]
```

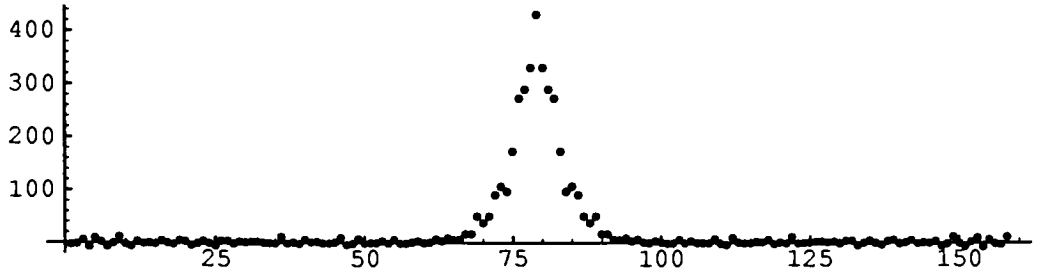


```
-Graphics-
```

```
n = Length[symlsf]
```

```
158
```

```
redft = 1/(n^0.5) Re[Fourier[symlsf]];
imdft = 1/(n^0.5) Im[Fourier[symlsf]];
cbd[x_] := (-1)^x
checkerboard = DiagonalMatrix[N[Table[cbd[x],
    {x, 0, (n-1)}]]];
recbdft = checkerboard.redft;
imcbdft = checkerboard.imdft;
repardft = Partition[recbdft, (n/2)];
impardft = Partition[imcbdft, (n/2)];
realdft = Flatten[{repardft[[2]], repardft[[1]]}];
imagdft = Flatten[{impardft[[2]], impardft[[1]]}];
ftrans = Table[(realdft[[i]] + I imagdft[[i]]),
    {i, 1, n}];

modulation = Abs[ftrans];
```

PercentModulation = 100/(modulation[[1+n/2]]) modulation

```
{2.09824, 2.32664, 3.91364, 0.406224, 0.517719, 0.637164,
  2.80455, 0.217635, 1.36784, 0.0831988, 0.341099, 1.26535,
  0.853343, 4.55173, 1.25928, 2.81407, 3.08132, 3.26262,
  0.958916, 1.75937, 0.016738, 3.22079, 0.433799, 3.72463,
  0.490045, 6.25894, 4.38049, 8.10824, 5.54824, 6.43626,
  5.48752, 10.7993, 9.11627, 5.08971, 8.80627, 2.76939,
  6.0499, 2.78452, 1.51541, 1.16942, 0.767533, 0.218747,
  0.67195, 0.761802, 5.39762, 0.307241, 0.701846,
  0.0784422, 1.88467, 0.0623484, 0.469489, 0.315578,
  0.172883, 0.486413, 1.57542, 1.45993, 2.34356, 3.9074,
  4.99015, 7.15039, 8.29976, 10.2676, 10.1384, 12.3433,
  14.1531, 15.2198, 18.0544, 20.4422, 23.9989, 28.1785,
  32.5701, 39.3681, 46.6436, 54.6015, 63.8691, 73.7869,
  82.1261, 88.6932, 94.1142, 100., 94.1142, 88.6932,
  82.1261, 73.7869, 63.8691, 54.6015, 46.6436, 39.3681,
  32.5701, 28.1785, 23.9989, 20.4422, 18.0544, 15.2198,
  14.1531, 12.3433, 10.1384, 10.2676, 8.29976, 7.15039,
  4.99015, 3.9074, 2.34356, 1.45993, 1.57542, 0.486413,
  0.172883, 0.315578, 0.469489, 0.0623484, 1.88467,
  0.0784422, 0.701846, 0.307241, 5.39762, 0.761802,
  0.67195, 0.218747, 0.767533, 1.16942, 1.51541, 2.78452,
  6.0499, 2.76939, 8.80627, 5.08971, 9.11627, 10.7993,
  5.48752, 6.43626, 5.54824, 8.10824, 4.38049, 6.25894,
  0.490045, 3.72463, 0.433799, 3.22079, 0.016738, 1.75937,
  0.958916, 3.26262, 3.08132, 2.81407, 1.25928, 4.55173,
  0.853343, 1.26535, 0.341099, 0.0831988, 1.36784,
  0.217635, 2.80455, 0.637164, 0.517719, 0.406224, 3.91364,
  2.32664}
```

PixelSize = 0.009

```
0.009
```

Oversampling = Floor[BlockHeight]

```
33
```

MagnificationFactor = 26

```
26
```

```
Frequencies = Table[i (Oversampling MagnificationFactor)/
(n PixelSize SmoothingFactor), {i, -n/2, n/2-1}]
```

```
{-4766.67, -4706.33, -4645.99, -4585.65, -4525.32,
  -4464.98, -4404.64, -4344.3, -4283.97, -4223.63,
  -4163.29, -4102.95, -4042.62, -3982.28, -3921.94,
  -3861.6, -3801.27, -3740.93, -3680.59, -3620.25,
  -3559.92, -3499.58, -3439.24, -3378.9, -3318.57,
  -3258.23, -3197.89, -3137.55, -3077.22, -3016.88,
  -2956.54, -2896.2, -2835.86, -2775.53, -2715.19,
  -2654.85, -2594.51, -2534.18, -2473.84, -2413.5,
  -2353.16, -2292.83, -2232.49, -2172.15, -2111.81,
  -2051.48, -1991.14, -1930.8, -1870.46, -1810.13,
  -1749.79, -1689.45, -1629.11, -1568.78, -1508.44,
  -1448.1, -1387.76, -1327.43, -1267.09, -1206.75,
  -1146.41, -1086.08, -1025.74, -965.401, -905.063,
  -844.726, -784.388, -724.051, -663.713, -603.376,
  -543.038, -482.7, -422.363, -362.025, -301.688, -241.35,
  -181.013, -120.675, -60.3376, 0, 60.3376, 120.675,
  181.013, 241.35, 301.688, 362.025, 422.363, 482.7,
  543.038, 603.376, 663.713, 724.051, 784.388, 844.726,
  905.063, 965.401, 1025.74, 1086.08, 1146.41, 1206.75,
  1267.09, 1327.43, 1387.76, 1448.1, 1508.44, 1568.78,
  1629.11, 1689.45, 1749.79, 1810.13, 1870.46, 1930.8,
  1991.14, 2051.48, 2111.81, 2172.15, 2232.49, 2292.83,
  2353.16, 2413.5, 2473.84, 2534.18, 2594.51, 2654.85,
  2715.19, 2775.53, 2835.86, 2896.2, 2956.54, 3016.88,
  3077.22, 3137.55, 3197.89, 3258.23, 3318.57, 3378.9,
  3439.24, 3499.58, 3559.92, 3620.25, 3680.59, 3740.93,
  3801.27, 3861.6, 3921.94, 3982.28, 4042.62, 4102.95,
  4163.29, 4223.63, 4283.97, 4344.3, 4404.64, 4464.98,
  4525.32, 4585.65, 4645.99, 4706.33}
```

```
MTF = Table[
{Frequencies[[i]], PercentModulation[[i]]}, {i, n/2+1,
(n/2 + (n SmoothingFactor)/(2 Oversampling) + 2)}];
```

```
ListPlot[MTF, PlotJoined -> True, PlotRange -> All,
AxesLabel -> {"frequency (cy./mm.)", "% modulation"},
AxesOrigin -> {0, 0}]
```

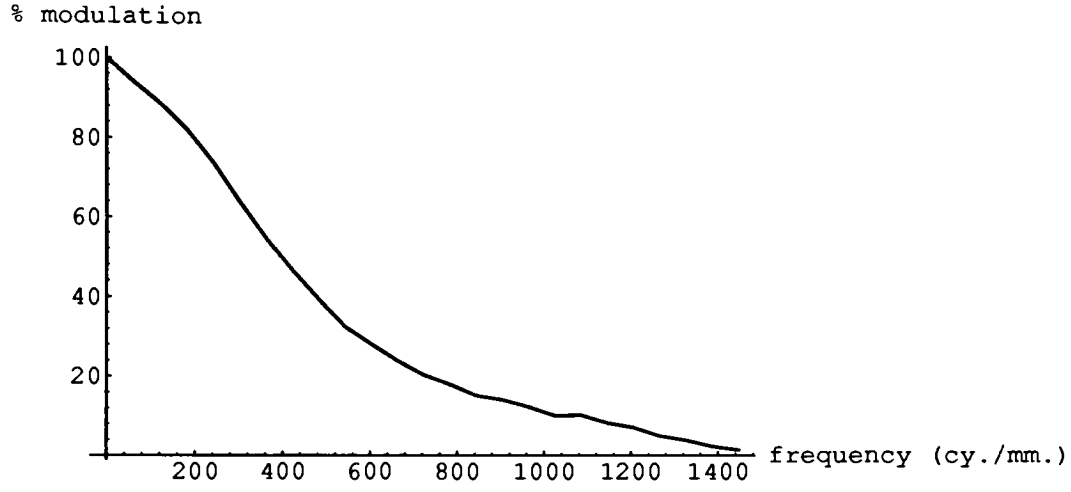

-Graphics-

Appendix H: Granularity vs. Aperture Area.

Reduced Image Size	Aperture Area (μm^2)	Mean Sample Trans.	Mean Output
12 x 8	1976	0.132	127
17 x 11	984	0.132	127
24 x 16	494	0.132	127
34 x 23	246	0.132	127
48 x 32	123.5	0.132	127
68 x 45	61.5	0.132	127
96 x 64	30.9	0.132	127
136 x 90	15.38	0.132	127
192 x 127	7.72	0.132	127
		from:	
	Step Tablet Noise Contribution		
		Appendix C	

Mean CCD Exposure	Variance	CCD Variance	Film Variance	Std. Dev.
0.09446	24.6411	6.42	18.4211	4.292
0.09446	28.9932	6.35	22.7732	4.772
0.09446	36.2513	6.1	30.0313	5.480
0.09446	55.5379	6.16	49.3179	7.023
0.09446	83.5118	6.19	77.2918	8.792
0.09446	148.639	6.18	142.419	11.934
0.09446	269.227	6.18	263.007	16.217
0.09446	459.585	6.19	453.365	21.292
0.09446	739.74	6.21	733.52	27.084
		Mean:		
		6.22		

Minus 1 S.D. Exp.	Plus 1 S.D. Exp.	Minus 1 S.D. Trans.	Plus 1 S.D. Trans.
0.089629594	0.099409268	0.125243929	0.138909558
0.08909554	0.099969272	0.124497669	0.13969208
0.088310609	0.100797481	0.123400845	0.140849378
0.086610645	0.102612447	0.121025401	0.143385521
0.08467874	0.104711155	0.118325852	0.14631815
0.081292822	0.108485411	0.11359454	0.151592109
0.076772114	0.11372516	0.107277526	0.158913872
0.071557855	0.120074481	0.099991382	0.167786097
0.06579521	0.127507629	0.091938948	0.178172808

Minus 1 S.D. Density	Plus 1 S.D. Density	Density Variance	Granularity (G)
0.902	0.857	0.00051	0.999
0.905	0.855	0.00063	0.615
0.909	0.851	0.00082	0.407
0.917	0.843	0.00136	0.333
0.927	0.835	0.00213	0.263
0.945	0.819	0.00393	0.241
0.969	0.799	0.00728	0.225
1.000	0.775	0.01263	0.194
1.037	0.749	0.02064	0.159

Reduced Image Size	Aperture Area (µm^2)	Mean Sample Trans.	Mean Output
24 x 36	82	0.132	117
24 x 36	82	0.132	114
24 x 36	82	0.132	116
24 x 36	82	0.132	114
24 x 36	82	0.132	121
24 x 36	82	0.132	121
24 x 36	82	0.132	119
24 x 36	82	0.132	119
24 x 36	82	0.132	116
24 x 36	82	0.132	114
24 x 36	82	0.141	119
24 x 36	82	0.141	125
24 x 36	82	0.141	120
24 x 36	82	0.141	124
24 x 36	82	0.141	121
24 x 36	82	0.141	121
24 x 36	82	0.141	122
24 x 36	82	0.141	123
24 x 36	82	0.141	123
24 x 36	82	0.141	121
39 x 59	31	0.132	117
39 x 59	31	0.132	114
39 x 59	31	0.132	116
39 x 59	31	0.132	114
39 x 59	31	0.132	121
39 x 59	31	0.132	121
39 x 59	31	0.132	119
39 x 59	31	0.132	119
39 x 59	31	0.132	116
39 x 59	31	0.132	114
39 x 59	31	0.141	119
39 x 59	31	0.141	125
39 x 59	31	0.141	120
39 x 59	31	0.141	124
39 x 59	31	0.141	121
39 x 59	31	0.141	121
39 x 59	31	0.141	122
39 x 59	31	0.141	123
39 x 59	31	0.141	123
39 x 59	31	0.141	121
39 x 59	82	0.132	127
39 x 59	82	0.132	124
39 x 59	82	0.132	125

Mean CCD Exposure	Variance	Std. Dev.	Minus 1 S.D. Exp.	Plus 1 S.D. Exp.
0.08337	93	9.644	0.073235014	0.094058902
0.08016	84	9.165	0.070676579	0.090139327
0.08229	91	9.539	0.072321811	0.092806806
0.08016	84	9.165	0.070676579	0.090139327
0.08774	92	9.592	0.077425766	0.098594938
0.08774	94	9.695	0.077317297	0.098715332
0.08554	90	9.487	0.075453508	0.096165044
0.08554	89	9.434	0.075508219	0.09610437
0.08229	91	9.539	0.072321811	0.092806806
0.08016	82	9.055	0.070787164	0.090016817
0.08554	72	8.485	0.07649313	0.095018092
0.09220	84	9.165	0.082115759	0.102780802
0.08664	77	8.775	0.077234073	0.096496113
0.09107	80	8.944	0.08128179	0.101342141
0.08774	80	8.944	0.078104398	0.097844753
0.08774	72	8.485	0.078587052	0.097314397
0.08884	78	8.832	0.079276432	0.098873794
0.08996	78	8.832	0.080336234	0.10003892
0.08996	77	8.775	0.080396606	0.099972585
0.08774	78	8.832	0.078222593	0.097714632
0.08337	225	15.000	0.067845478	0.100235525
0.08016	208	14.422	0.065464438	0.096090853
0.08229	221	14.866	0.06699011	0.098913669
0.08016	208	14.422	0.065464438	0.096090853
0.08774	225	15.000	0.071854086	0.104959667
0.08774	229	15.133	0.071719524	0.105118081
0.08554	228	15.100	0.069738002	0.102703413
0.08554	226	15.033	0.069804492	0.102624998
0.08229	230	15.166	0.066695172	0.099262271
0.08016	211	14.526	0.065363346	0.096209834
0.08554	202	14.213	0.070628728	0.101657655
0.09220	221	14.866	0.076097164	0.109616298
0.08664	213	14.595	0.071252251	0.103288873
0.09107	212	14.560	0.075377566	0.108033452
0.08774	213	14.595	0.072265765	0.104476435
0.08774	201	14.177	0.072690236	0.103980411
0.08884	215	14.663	0.073215362	0.105751765
0.08996	215	14.663	0.074240394	0.106951661
0.08996	216	14.697	0.074205383	0.106992634
0.08774	216	14.697	0.072161688	0.104598401
0.09446	106	10.296	0.083050767	0.106510309
0.09107	85	9.220	0.080988004	0.101665741
0.09220	88	9.381	0.081884533	0.103035879

Minus 1 S.D. Trans.	Plus 1 S.D. Trans.	Minus 1 S.D. Density	Plus 1 S.D. Density
0.115953676	0.14892433	0.936	0.827
0.116387195	0.148437622	0.934	0.828
0.116005964	0.1488644	0.936	0.827
0.116387195	0.148437622	0.934	0.828
0.116488028	0.148337311	0.934	0.829
0.116324836	0.148518445	0.934	0.828
0.116433859	0.148394257	0.934	0.829
0.116518285	0.148300629	0.934	0.829
0.116005964	0.1488644	0.936	0.827
0.116569301	0.148235877	0.933	0.829
0.126086176	0.156621487	0.899	0.805
0.125581267	0.157184729	0.901	0.804
0.125699061	0.157048183	0.901	0.804
0.125840537	0.15689799	0.900	0.804
0.125521018	0.157245601	0.901	0.803
0.126296688	0.15639327	0.899	0.806
0.12581781	0.156920335	0.900	0.804
0.125923021	0.156805995	0.900	0.805
0.126017651	0.156702018	0.900	0.805
0.125710969	0.157036485	0.901	0.804
0.107420373	0.158703835	0.969	0.799
0.107804061	0.158238344	0.967	0.801
0.107453784	0.158659958	0.969	0.800
0.107804061	0.158238344	0.967	0.801
0.108105367	0.157913126	0.966	0.802
0.107902916	0.15815146	0.967	0.801
0.107614146	0.158483748	0.968	0.800
0.107716746	0.158362745	0.968	0.800
0.106980697	0.159219126	0.971	0.798
0.107637586	0.158434276	0.968	0.800
0.116419687	0.1675657	0.934	0.776
0.116376909	0.16763839	0.934	0.776
0.115963599	0.168103454	0.936	0.774
0.116699613	0.167257483	0.933	0.777
0.116137793	0.167903331	0.935	0.775
0.116819958	0.167106173	0.932	0.777
0.116198424	0.167836205	0.935	0.775
0.116368098	0.16764137	0.934	0.776
0.11631322	0.167705594	0.934	0.775
0.115970532	0.16809934	0.936	0.774
0.116051004	0.148832198	0.935	0.827
0.117382355	0.147352243	0.930	0.832
0.117234395	0.147516856	0.931	0.831

Density Variance	Granularity (G)
0.00295	0.242
0.00279	0.229
0.00293	0.240
0.00279	0.229
0.00275	0.226
0.00281	0.231
0.00277	0.227
0.00274	0.225
0.00293	0.240
0.00272	0.223
0.00222	0.182
0.00238	0.195
0.00234	0.192
0.00229	0.188
0.00239	0.196
0.00215	0.177
0.00230	0.189
0.00227	0.186
0.00224	0.184
0.00233	0.191
0.00718	0.223
0.00695	0.215
0.00716	0.222
0.00695	0.215
0.00677	0.210
0.00689	0.214
0.00707	0.219
0.00700	0.217
0.00746	0.231
0.00705	0.218
0.00625	0.194
0.00628	0.195
0.00650	0.202
0.00611	0.189
0.00641	0.199
0.00604	0.187
0.00637	0.198
0.00628	0.195
0.00631	0.196
0.00650	0.201
0.00292	0.239
0.00244	0.200
0.00249	0.204

Aperture Area (μm^2)	Variance	Std. Dev.	Density S.D. (ΔD=1.05)	Density Variance	"Granularity"
1335640	6.42061	2.5339	0.010392917	0.000108013	144.266128
665510	6.3492	2.5198	0.010334961	0.000106811	71.0840659
333911	6.10441	2.4707	0.010133773	0.000102693	34.2904424
166378	6.16357	2.4827	0.01018276	0.000103689	17.2515015
83478	6.1925	2.4885	0.010206629	0.000104175	8.69634415
41594	6.18174	2.4863	0.010197758	0.000103994	4.32553758
20869	6.18334	2.4866	0.010199078	0.000104021	2.1708181
10399	6.19407	2.4888	0.010207923	0.000104202	1.08359341
5217	6.21056	2.4921	0.010221502	0.000104479	0.54506747
The above samples were obtained from the entire CCD frame (averaged down).					
The following values were obtained from cropped CCD frames (114 x 76 pixels in final image).					
10399	5.02728	2.2422	0.009196358	8.4573E-05	0.87947464
5217	2.54263	1.5946	0.006540198	4.27742E-05	0.22315297
2600	1.53431	1.2387	0.005080493	2.58114E-05	0.06710967
1304	1.09754	1.0476	0.004296942	1.84637E-05	0.02407668
652	0.766985	0.8758	0.003592053	1.29028E-05	0.00841266
326	1.2036	1.0971	0.004499771	2.02479E-05	0.00660083
163	1.02486	1.0124	0.004152232	1.7241E-05	0.00281029
82.8	1.12539	1.0608	0.004351118	1.89322E-05	0.00156759
		Assumes linear density relationship.			

```
FilmGranularityData = {{1976, 0.999},
                       {984, 0.615},
                       {494, 0.407},
                       {246, 0.333},
                       {123.5, 0.263},
                       {61.5, 0.241},
                       {30.9, 0.225},
                       {15.38, 0.194},
                       {7.72, 0.159}};

<<Graphics`Graphics`
```

```
LogLogListPlot[FilmGranularityData,
AxesLabel -> {"aperture area", "granularity"}]
```

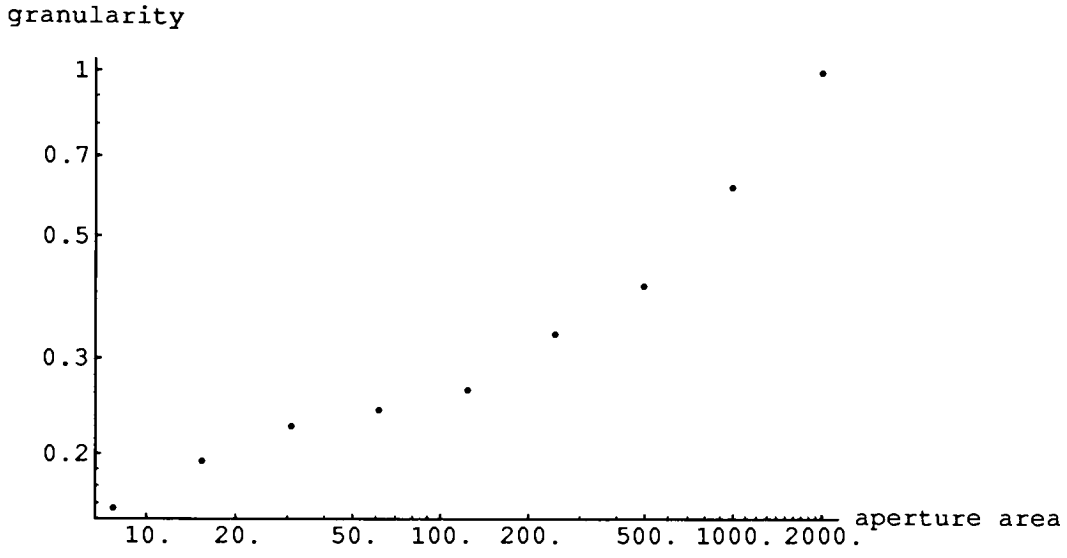


```
-Graphics-
```

```
FilmDataTwo =
{{31, 0.223}, {31, 0.215}, {31, 0.222}, {31, 0.215}, {31, 0
 {31, 0.214}, {31, 0.219}, {31, 0.217}, {31, 0.231}, {31, 0
 {31, 0.194}, {31, 0.195}, {31, 0.202}, {31, 0.189}, {31, 0
 {31, 0.187}, {31, 0.198}, {31, 0.195}, {31, 0.196}, {31, 0
 {82, 0.242}, {82, 0.229}, {82, 0.240}, {82, 0.229}, {82, 0
 {82, 0.231}, {82, 0.227}, {82, 0.225}, {82, 0.240}, {82, 0
 {82, 0.182}, {82, 0.195}, {82, 0.192}, {82, 0.188}, {82, 0
 {82, 0.195}, {82, 0.177}, {82, 0.189}, {82, 0.186}, {82, 0
 {82, 0.239}, {82, 0.200}, {82, 0.204}};
```

```
<<Statistics`LinearRegression`
```

```
Regress[FilmDataTwo, {1, x}, x]

{ParameterTable ->

        Estimate        SE              TStat       PValue   ,
   1    0.204939        0.00705322      29.056      0

   x    0.0000664962    0.000110919     0.599501    0.552138

  RSquared -> 0.00868971, AdjustedRSquared -> -0.0154886,

  EstimatedVariance -> 0.000342329,

  ANOVATable ->

   Model

   Error

   Total

      DoF   SoS             MeanSS          FRatio      PValue
      1     0.000123033     0.000123033     0.359401    0.552138

      41    0.0140355       0.000342329

      42    0.0141585
}
GranFit[x_] := 0.204939 + 0.0000664962 x
```

```
Show[LogLogPlot[GranFit[x], {x, 20, 100}, PlotRange -> {0.1,
AxesLabel -> {"aperture area", "granularity"}],
LogLogListPlot[FilmDataTwo]]
```

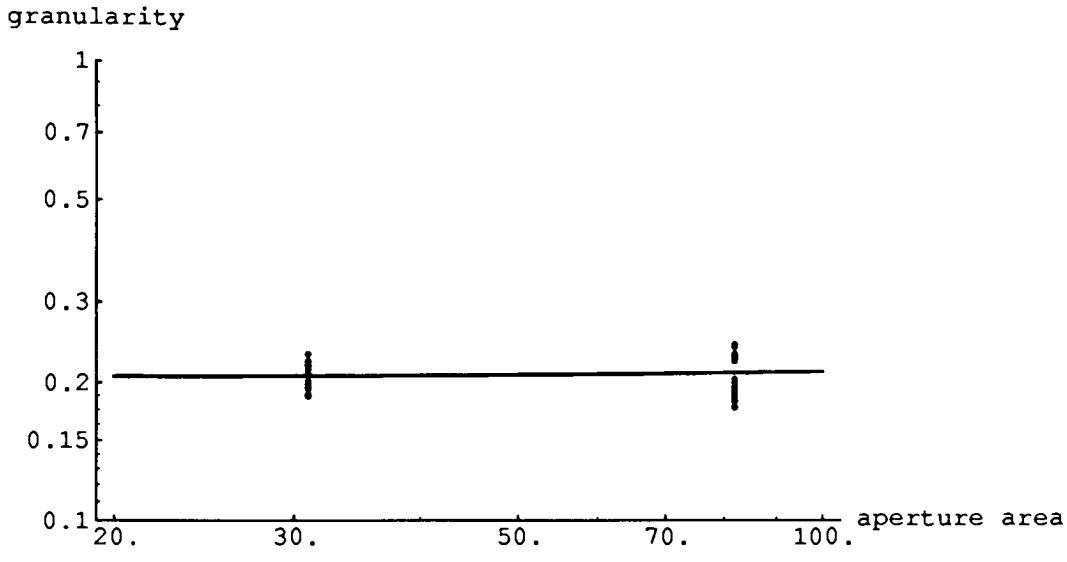


```
-Graphics-
```

```
CCDData = {{1335640, 144}, {665510, 71}, {333911, 34.3},
           {166378, 17.25}, {83478, 8.696}, {41594, 4.3255},
           {20869, 2.1708}, {10399, 1.0836}, {10399, 0.87947
           {5217, 0.54507}, {5217, 0.22315}, {2600, 0.067110
           {1304, 0.24077}, {652, 0.0084127}, {326, 0.006601
           {163, 0.00281029}, {82.8, 0.00156759}};
```

```
LogLogListPlot[CCDData,
AxesLabel -> {"aperture area", "granularity"}]
```

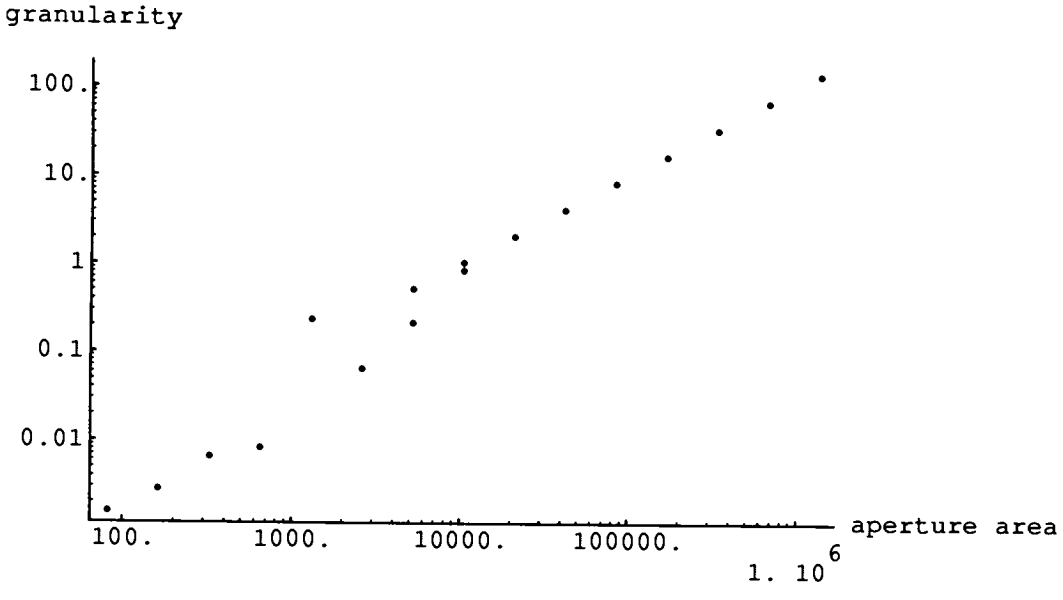


```
-Graphics-
```

Appendix I: Image Log.

Image Log

DCS200mI Camera Data

Monochrome camera with 80 Mb internal hard drive, serial # K376-9026.
1524 x 1012 pixel CCD; 13.85 x 9.23 mm. => pixel size = 9.1 µm. sq.

Microscope Data

Nikon Optiphot Microscope with:

60X 1.40 N.A. objective, 2.5X eyepiece => 158X on CCD; 1 pixel = 0.056 µm.
40X 0.95 N.A. objective, 2.5X eyepiece => 105X on CCD; 1 pixel = 0.087 µm.
20X 0.75 N.A. objective, 2.5X eyepiece => 53X on CCD; 1 pixel = 0.17 µm.
10X 0.45 N.A. objective, 2.5X eyepiece => 26X on CCD; 1 pixel = 0.35 µm.
10X 0.45 N.A. objective, 4.0X eyepiece => 42X on CCD; 1 pixel = 0.22 µm.

FIlm Data

Image Set #1:

Obtained on 10/3 and 10/4 1992.

Data recorded at E.I. 100 setting of DCS200mi, manual metering, 1/4000 sec., lamp voltage adjusted to keep exposure constant according to light meter, 10X 0.45 objective, apo condenser set on 0.30 N.A., 2.5X eyepiece.

Sample 1: Technical Pan 35mm roll film, processed in Technidol for 9 min. @ 68°F.

step	logH	density	lamp volt.	color temp.	image #
4	-1.86	0.20			
5	-1.69	0.23	5.8	2960	47, 83, 84, 85
6	-1.55	0.28	6.0	2980	48, 49, 80, 81, 82
7	-1.40	0.34	6.5	3070	50, 78, 79
8	-1.27	0.43	7.0	3210	51, 52, 77
9	-1.12	0.53	7.5	3280	53, 54, 55
10	-0.97	0.63	8.0	3370	56, 57, 58
11	-0.83	0.72	9.0	3570	59, 60, 61
12	-0.66	0.82	9.5	3610	62, 63, 64
13	-0.49	0.91	10.6	3730	65, 66, 67, 68, 69
14	-0.34	1.01	11.5	3840	70, 71, 72, 73
15	-0.17	1.09	11.5	3880	74, 75, 76
16	-0.02	1.19			
B+F	N/A	0.16	5.5	2930	86, 87, 88

Sample 2: T-Max 100 35mm roll film, processed in T-Max dev. (1:4) for 8 min. @ 68°F.

step	logH	density	lamp volt.	color temp.	image #
3	-2.46	0.26			
4	-2.31	0.30	6.0	3030	119
5	-2.14	0.35	6.7	3120	120
6	-2.00	0.40	6.9	3150	121
7	-1.85	0.47	7.2	3230	122
8	-1.72	0.56	8.0	3370	123, 124
9	-1.57	0.65	8.0	3370	125
10	-1.42	0.73	9.0	3530	126
11	-1.28	0.82	9.9	3620	127
12	-1.11	0.91	11.0	3780	128
13	-0.94	1.00	11.4	3780	129, 130, 131
14	-0.79	1.11	11.5	3800	132
15	-0.62	1.21			
B+F	N/A	0.23	5.9	2930	133

Sample 3: T-Max 400 4x5 sheet film, processed in D-76 for 6.75 min. @ 70°F.

step	logH	density	lamp volt.	color temp.	image #
5	-2.56	0.15			
6	-2.41	0.20	5.7	2920	31, 32, 33
7	-2.26	0.25	5.8	2940	28, 29, 30
8	-2.11	0.30	6.0	2990	25, 26, 27
9	-1.96	0.36	6.3	3050	22, 23, 24
10	-1.81	0.43	6.8	3150	19, 20, 21
11	-1.66	0.50	7.1	3210	16, 17, 18
12	-1.51	0.57	7.5	3270	13, 14, 15
13	-1.36	0.64	8.0	3360	10, 11, 12
14	-1.21	0.72	8.5	3440	7, 8, 9
15	-1.06	0.80	9.5	3610	4, 5, 6
16	-0.91	0.88	10	3660	1, 2, 3
17	-0.76	0.97			
B+F	N/A	0.10	5.5	2890	34, 35, 36
Flat field (no film)		0.00	5.0	2770	37, 38, 39, 40, 41, 42, 43, 44, 45, 46

Sample 4: T-Max P3200 35mm roll film, processed in T-Max dev. (1:4), 9 min. @ 68°F.

step	logH	density(A)	lamp volt.	color temp.	image #
4	-3.32	0.32			
5	-3.17	0.36	6.8	3120	89, 90, 91
6	-3.02	0.42	7.0	3180	92, 93, 94
7	-2.87	0.49	7.2	3230	95, 96, 97
8	-2.72	0.58	7.7	3330	98, 99, 100
9	-2.57	0.67	8.5	3480	101, 102, 103
10	-2.42	0.76	9.2	3610	104, 105, 106
11	-2.27	0.84	9.5	3610	107, 108, 109
12	-2.12	0.93	10.8	3770	110
13	-1.97	1.04	11.5	3860	111, 112
14	-1.82	1.14	11.5	3840	113
15	-1.67	1.25	11.5	3810	114
16	-1.52	1.36			
B+F	N/A	0.28	6.2	3050	115, 116, 117, 118

Image Set #2:

Obtained on 2/7/93.

Data recorded at E.I. 100 setting of DCS200mi, manual metering, 1/2000 sec. exposure with film samples, 1/4000 sec. exposure for flat fields, lamp voltage adjusted to keep exposure constant according to light meter, 10X 0.45 objective, apo condenser set on 0.30 N.A., 4.0X eyepiece.

Sample 5: T-Max 400 4x5 sheet film, exposed in a camera to a gray scale and processed in D-76 for 6.75 min. @ 70°F (with sample #6).

density	lamp volt	image #'s
0.85	10.8	203, 204, 205, 206, 207, 208, 209, 210, 211, 212 (A4)

Sample 6: T-Max 400 4x5 sheet film, exposed in a sensitometer and processed in D-76 for 6.75 min. @ 70°F (same as step 16 of sample #3).

logH	density	lamp volt	image #'s
-0.91	0.88	11	213, 214, 215, 216, 217, 218, 219, 220, 221, 222 (A5)

Flat Field Exposures:

lamp volt	image #'s
6	223, 224, 225, 226, 227, 228, 229, 230, 231, 232 (A6)

Camera Calibration

Light Meter Calibration:

5681 lux on an 18% gray card @ 2770°K produced a light meter reading of 1/60 @ f/5.6 for E.I. 100. The calculated E.I. for this illuminance is 71. The meter overexposes by 1/2 stop for 18% mean reflectance, but this calibration is within the specified range of 10% to 18% for mean reflectance (12.8% reflectance gives E.I. 100).

CCD Photometric Calibration:

Enlarger height: 88, bulb 148 cm. from baseboard, CCD ~ 4 cm. above baseboard;
distance from CCD to bulb = 144 cm.
Illuminance on CCD: 20.7 lux w/o N.D. filter.
Color temperature: 3100°K (with #301 infrared cutoff filter).
Measured value, 2.0 N.D. filter: 1.86

DCS200ml Images

Obtained on 10/4/92.

ISO 100	image #
1/8000	134 (A2/1)
1/4000	135 (A2/2)
1/2000	136 (A2/3)
1/1000	137 (A2/4)
1/500	138 (A2/5)
1/250	139 (A2/6)
1/125	140 (A2/7)
1/60	141 (A2/8)
1/30	142 (A2/9)
1/15	143 (A2/10)
1/8	144 (A2/11)

ISO 100 +2.0 N.D.	image #
1/8000	145 (A2/12)
1/4000	146 (A2/13)
1/2000	147 (A2/14)
1/1000	148 (A2/15)
1/500	149 (A2/16)
1/250	150 (A2/17)
1/125	151 (A2/18)
1/60	152 (A2/19)
1/30	153 (A2/20)

ISO 200	image #
1/8000	154 (A2/21)
1/4000	155 (A2/22)
1/2000	156 (A2/23)
1/1000	157 (A2/24)
1/500	158 (A2/25)
1/250	159 (A2/26)
1/125	160 (A2/27)
1/60	161 (A2/28)
1/30	162 (A2/29)
1/15	163 (A2/30)

ISO 200 +2.0 N.D.	image #
1/8000	164 (A2/31)
1/4000	165 (A2/32)
1/2000	166 (A2/33)
1/1000	167 (A2/34)
1/500	168 (A2/35)
1/250	169 (A2/36)
1/125	170 (A2/37)
1/60	171 (A2/38)
1/30	172 (A2/39)

ISO 400	image #
1/8000	173 (A3/1)
1/4000	174 (A3/2)
1/2000	(no image)
1/1000	175 (A3/3)
1/500	176 (A3/4)
1/250	177 (A3/5)
1/125	178 (A3/6)
1/60	179 (A3/7)
1/30	180 (A3/8)

ISO 400 +2.0 N.D.	image #
1/8000	181 (A3/9)
1/4000	182 (A3/10)
1/2000	183 (A3/11)
1/1000	184 (A3/12)
1/500	185 (A3/13)
1/250	186 (A3/14)
1/125	187 (A3/15)

ISO 100	image #
1/8000	188 (A3/16)
1/4000	189 (A3/17)
1/2000	190, 191 (A3/18, 19)
1/1000	192 (A3/20)
1/500	193 (A3/21)
1/250	194 (A3/22)
1/125	195 (A3/23)
1/60	196 (A3/24)

ISO 100 +2.0 N.D.	image #
1/8000	197 (A3/25)
1/4000	198 (A3/26)
1/2000	199 (A3/27)
1/1000	200 (A3/28)
1/500	201 (A3/29)
1/250	202 (A3/30)

MTF Knife Edge Images

Images obtained on 6/24/93 using the DCS200mi/Microscope setup to image the edge of a microtome blade.

Image #	Data
233	2.5X eyepiece, 1/4000 sec. E.I. 100 Quantization Setting
234	2.5X eyepiece, 1/4000 sec. E.I. 100 Quantization Setting
235	2.5X eyepiece, 1/4000 sec. E.I. 100 Quantization Setting
236	4X eyepiece, 1/2000 sec. E.I. 100 Quantization Setting

Miscellaneous Data

Color temperatures measured with Minolta Color Meter II, serial # 124649.
Illuminances measured with United Detector Technology Model 61 photometer.

Reduced Image Sizes

Image Set #1 Film images averaged down to 39 x 59 pixels for the determination of film noise, "aperture" area 82.1 μm^2.

Image Set #2 Film images averaged down to 39 x 59 pixels, "aperture" area 31 μm^2, and also averaged down to 24 x 36 pixels, "aperture" area 82 μm^2. These images were used for the determination of the granularity vs. aperture area relationship. Images #1, 2, and 3 from image set #1 were also used for this purpose, except in this case the 24 x 36 pixel images corresponded to an aperture area of 219 μm^2.

CCD images cropped down to 114 x 76 pixels (from top left corner), "aperture" area 82.81 μm^2

Image Index

All the images used in this work are contained on five 128 Mb magneto-optical disks labeled DCS Images 1 through DCS Images 5. The locations of various images on the disks are as follows:

DCS Images 1: Images **1-80** (film images); PICT Format. (119.1 Mb)

DCS Images 2: Images **81-133** (film images); PICT Format.
Misc. & Resolution Tests (pictorial & resolution target); DCS200mi Archive Format (18 images, not used due to overexposure clipping). (107.5 Mb)

DCS Images 3: DCS200mi E.I. 100 & 200 (contains images **134-172**); DCS200mi Archive Format (**A2**).
DCS200mi E.I. 400 & 800 (contains images **173-202**); DCS200mi Archive Format (**A3**). (109.6 Mb)

DCS Images 4: Shutter Speed Test Images (a TV screen at various shutter speeds); DCS200mi Archive Format (27 images, not used - this shutter speed test method is not that precise, and other data indicated that the DCS200mi camera shutter speeds were accurate).
Color DCS MTF Images (ISO test chart and knife edges taken with the Kodak DCS200ci, some with the microscope and some with a 28mm lens); DCS200mi Archive Format (18 images, not used as the DCS200ci was not used for data acquisition; for future reference).

Step Tablet Gran. Test (folder)
Gray Scale, D = 0.85 (contains images **203-212**); DCS200mi Archive Format (**A4**).
Sensi. Strip, D = 0.88 (contains images **213-222**); DCS200mi Archive Format (**A5**).
Flat Field Two (contains images **223-232**); DCS200mi Archive Format (**A6**). (119.1 Mb)

DCS Images 5: DCS200mi RGB Composite; PICT Format (not used; filter wheel composite for future reference).

50mm lens ISO Chart Images (folder)
12 images; PICT Format (not used in Thesis; for ISO test).

50mm lens Knife Edge Images (folder)
12 images; PICT Format (not used in Thesis; for ISO test).

Microscope Knife Edge Images (folder)
Images **233-236**; PICT Format.

28mm lens ISO Chart Images (folder)
3 Images; PICT Format (not used; for future reference).

DCS200mi Pictorial Series (folder)
18 images; PICT Format (not used; for future use in a subjective study).

DCS200ci Images (folder)
2 images; PICT Format (not used; examples of DCS200ci output).

Printer Noise Test Images (folder)
One computer constructed gray scale and color balance file.
One composite DCS200mi noise image file.
(Both for use in a future printer noise analysis test.) (72.1 Mb)

Other Means of Data Acquisition

28mm lens MTF curve obtained using the Imaging Science MTF bench with the lens set at f/8.

Data:

Spatial Frequency (cy./mm.)	Percent Modulation
0	100
15.6	71.5
31.3	52.8
46.9	40.2
62.5	31.8
78.1	25.7
93.8	20.9
109	17.2
125	14.2
141	11.2
156	8.3
172	5.4
188	2.9
203	1.3

Appendix J: Film Data & Analysis.

Image #'s	Log Exposure (lux-sec)	Quanta/82.1 µm^2	Density
	-0.02	1497533	1.19
74, 75, 76	-0.17	1060172	1.09
70, 71, 72	-0.34	716765	1.01
65, 66, 67	-0.49	507430	0.91
62, 63, 64	-0.66	343065	0.82
59, 60, 61	-0.83	231940	0.72
56, 57, 58	-0.97	168026	0.63
53, 54, 55	-1.12	118953	0.53
51, 52, 77	-1.27	84212	0.43
50, 78, 79	-1.4	62428	0.34
48, 49, 80	-1.55	44195	0.28
47, 83, 84	-1.69	32017	0.23
	-1.86	21646	0.2
86, 87, 88	B+F	0	0.16
*specify	*	1568110*(10^B)	*

Mean Transmittance	Gain	Mean #1	Mean #2	Mean #3	Mean CCD Resp.
0.0646					
0.0813	2.31E-07	111	109	107	109
0.0977	3.55E-07	124	127	129	127
0.1230	5.13E-07	125	125	128	126
0.1514	7.24E-07	129	132	131	131
0.1905	1.15E-06	135	137	134	135
0.2344	1.72E-06	129	128	133	130
0.2951	2.46E-06	133	129	129	130
0.3715	3.50E-06	143	137	137	139
0.4571	3.71E-06	128	140	146	138
0.5248	3.70E-06	131	137	148	139
0.5888	3.50E-06	140	133	135	136
0.6310					
0.6918		151	150	147	149
1/(10^D)		*	*	*	AVERAGE(F:H)
((D1-D2)/(C1-C2)+(D2-D3)/(C2-C3))/2					

Mean CCD Exp.	Variance #1	Variance #2	Variance #3	Variance (mean, levels)
0.0749	44.1662	42.8413	41.1168	42.7081
0.0941	43.5528	45.5643	47.1126	45.4099
0.0933	42.0125	41.2693	42.3116	41.86446667
0.0987	38.0061	37.4609	36.5426	37.33653333
0.1042	34.7688	37.1226	34.3378	35.40973333
0.0979	27.5212	29.6137	29.6171	28.91733333
0.0983	27.9935	23.3645	23.54	24.966
0.1086	21.9033	21.6404	22.7276	22.09043333
0.1074	15.8813	17.2423	19.7336	17.61906667
0.1082	11.5997	11.7005	15.2121	12.83743333
0.1050	10.1947	9.43181	9.25681	9.627773333
0.1214	4.00703	5.29692	5.02072	4.77489
-2.14E-03	*	*	*	AVERAGE(K:M)
3.82E-4*I				
2.98E-6*I^2				

Std. Dev. (levels)	Minus 1 S.D. Exp.	Plus 1 S.D. Exp.	Minus 1 S.D. Trans.
6.5351	0.0683	0.0818	0.07410
6.7387	0.0866	0.1019	0.08990
6.4703	0.0861	0.1008	0.11352
6.1104	0.0917	0.1059	0.14064
5.9506	0.0972	0.1113	0.17780
5.3775	0.0918	0.1042	0.21973
4.9966	0.0926	0.1042	0.27795
4.7000	0.1029	0.1143	0.35228
4.1975	0.1024	0.1125	0.43578
3.5829	0.1039	0.1125	0.50398
3.1029	0.1013	0.1087	0.56824
2.1852	0.1186	0.1242	0.67607
N^0.5			E*P/J

Plus 1 S.D. Trans.	Minus 1 S.D. Den.	Plus 1 S.D. Den.	Density S.D.	Density Variance
0.08874	1.13015	1.05189	0.03913	0.00153126
0.10582	1.04622	0.97541	0.03540	0.001253448
0.13286	0.94491	0.87661	0.03415	0.001166085
0.16241	0.85188	0.78939	0.03124	0.000976175
0.20368	0.75008	0.69105	0.02951	0.000871066
0.24953	0.65811	0.60288	0.02761	0.000762588
0.31273	0.55603	0.50482	0.02560	0.000655384
0.39124	0.45311	0.40756	0.02277	0.000518608
0.47884	0.36073	0.31981	0.02046	0.00041879
0.54601	0.29759	0.26280	0.01739	0.000302557
0.60977	0.24547	0.21483	0.01532	0.000234652
0.70776	0.17001	0.15012	0.00995	9.89614E-05
E*Q/J	LOG10(1/R)	LOG10(1/S)	(T-U)/2	V^2

Granularity	DQE (%)	NEQ	log NEQ
0.126	0.004	39	1.59
0.103	0.007	52	1.71
0.096	0.011	58	1.76
0.080	0.018	63	1.80
0.071	0.035	82	1.92
0.063	0.065	110	2.04
0.054	0.110	130	2.12
0.043	0.199	168	2.23
0.034	0.205	128	2.11
0.025	0.200	88	1.95
0.019	0.167	53	1.73
0.008			
82*X	100*C*(F^2)/X	C*Z/100	LOG10(AA)

Image #'s	Log Exposure (lux-sec)	Quanta/82.1 µm^2	Density
	-0.62	376163	1.21
132	-0.79	254318	1.11
129, 130, 131	-0.94	180043	1
128	-1.11	121724	0.91
127	-1.28	82296	0.82
126	-1.42	59618	0.73
125	-1.57	42206	0.65
123, 124	-1.72	29880	0.56
122	-1.85	22150	0.47
121	-2	15681	0.4
120	-2.14	11360	0.35
119	-2.31	7680	0.3
	-2.46	5437	0.26
133	B+F	0	0.23
*specify	*	1568110*(10^B)	*

Mean Transmittance	Gain	Mean #1	Mean #2	Mean #3	Mean CCD Resp.
0.0617					
0.0776	1.15E-06	104			104
0.1000	1.51E-06	124	124	122	123
0.1230	1.91E-06	135			135
0.1514	3.13E-06	131			131
0.1862	4.28E-06	136			136
0.2239	5.95E-06	124			124
0.2754	9.47E-06	146	142		144
0.3388	1.12E-05	136			136
0.3981	1.12E-05	134			134
0.4467	1.26E-05	151			151
0.5012	1.57E-05	136			136
0.5495					
0.5888		129			129
1/(10^D)		*	*	*	AVERAGE(F:H)
((D1-D2)/(C1-C2)+(D2-D3)/(C2-C3))/2					

Mean CCD Exp.	Variance #1	Variance #2	Variance #3	Variance (mean, levels)
0.0698	55.3057			55.3057
0.0903	73.2163	74.5273	71.559	73.10086667
0.1038	86.9581			86.9581
0.0991	70.8892			70.8892
0.1050	94.7904			94.7904
0.0911	63.4691			63.4691
0.1147	67.547	75.299		71.423
0.1050	59.46			59.46
0.1026	51.2764			51.2764
0.1235	56.2823			56.2823
0.1050	42.9891			42.9891
0.0968	17.4727			17.4727
-2.14E-03	*	*	*	AVERAGE(K:M)
3.82E-4*I				
2.98E-6*I^2				

Std. Dev. (levels)	Minus 1 S.D. Exp.	Plus 1 S.D. Exp.	Minus 1 S.D. Trans.
7.4368	0.0625	0.0775	0.06952
8.5499	0.0810	0.1001	0.08966
9.3251	0.0930	0.1151	0.11021
8.4196	0.0895	0.1091	0.13672
9.7360	0.0936	0.1169	0.16610
7.9667	0.0823	0.1002	0.20238
8.4512	0.1044	0.1254	0.25076
7.7110	0.0959	0.1143	0.30972
7.1608	0.0943	0.1112	0.36588
7.5022	0.1141	0.1333	0.41250
6.5566	0.0973	0.1129	0.46445
4.1800	0.0920	0.1016	0.55987
N^0.5			E*P/J

Plus 1 S.D. Trans.	Minus 1 S.D. Den.	Plus 1 S.D. Den.	Density S.D.	Density Variance
0.08609	1.15786	1.06504	0.04641	0.002154139
0.11082	1.04738	0.95539	0.04600	0.002115645
0.13646	0.95777	0.86500	0.04639	0.002151615
0.16664	0.86418	0.77822	0.04298	0.001847214
0.20732	0.77962	0.68337	0.04813	0.002316062
0.24630	0.69384	0.60854	0.04265	0.001819105
0.30111	0.60075	0.52127	0.03974	0.001579211
0.36911	0.50903	0.43284	0.03810	0.001451307
0.43152	0.43666	0.36500	0.03583	0.001283846
0.48208	0.38458	0.31688	0.03385	0.001145664
0.53915	0.33306	0.26829	0.03238	0.001048775
0.61845	0.25191	0.20870	0.02161	0.000466819
E*Q/J	LOG10(1/R)	LOG10(1/S)	(T-U)/2	V^2

Granularity	DQE (%)	NEQ	log NEQ
0.177	0.016	40	1.60
0.173	0.019	35	1.54
0.176	0.021	25	1.40
0.151	0.044	36	1.55
0.190	0.047	28	1.45
0.149	0.082	35	1.54
0.129	0.170	51	1.71
0.119	0.193	43	1.63
0.105	0.153	24	1.38
0.094	0.157	18	1.25
0.086	0.181	14	1.14
0.038			
82*X	100*C*(F^2)/X	C*Z/100	LOG10(AA)

Image #'s	Log Exposure (lux-sec)	Quanta/82.1 μm^2	Density
	-0.76	272506	0.97
1, 2, 3	-0.91	192920	0.88
4, 5, 6	-1.06	136577	0.8
7, 8, 9	-1.21	96689	0.72
10, 11, 12	-1.36	68450	0.64
13, 14, 15	-1.51	48459	0.57
16, 17, 18	-1.66	34307	0.5
19, 20, 21	-1.81	24287	0.43
22, 23, 24	-1.96	17194	0.36
25, 26, 27	-2.11	12172	0.3
28, 29, 30	-2.26	8617	0.25
31, 32, 33	-2.41	6101	0.2
	-2.56	4319	0.15
34, 35, 36	B+F	0	0.1
*specify	*	1568110*(10^B)	*

Mean Transmittance	Gain	Mean #1	Mean #2	Mean #3	Mean CCD Resp.
0.1072					
0.1318	1.28E-06	127	124	125	125
0.1585	1.71E-06	133	131	127	130
0.1905	2.42E-06	128	126	127	127
0.2291	3.17E-06	132	129	128	130
0.2692	4.22E-06	125	138	132	132
0.3162	5.97E-06	130	129	127	129
0.3715	8.43E-06	131	140	135	135
0.4365	1.09E-05	141	141	150	144
0.5012	1.30E-05	138	138	141	139
0.5623	1.70E-05	133	132	140	135
0.6310	2.40E-05	140	146	140	142
0.7079					
0.7943		163	151	151	155
1/(10^D)		*	*	*	AVERAGE(F:H)
((D1-D2)/(C1-C2)+(D2-D3)/(C2-C3))/2					

Mean CCD Exp.	Variance #1	Variance #2	Variance #3	Variance (mean, levels)
0.0926	106.32	85.5826	87.9224	93.275
0.0983	88.9341	91.7907	88.5185	89.74776667
0.0945	101.494	88.9442	80.6206	90.35293333
0.0975	84.4981	86.1644	85.389	85.3505
0.0998	84.2563	105.983	89.4799	93.23973333
0.0964	92.7708	97.1456	90.0152	93.31053333
0.1042	91.7125	101.408	93.6428	95.58776667
0.1147	101.569	101.569	111.791	104.9763333
0.1086	102.928	103.261	100.195	102.128
0.1038	91.0842	85.2229	90.1397	88.8156
0.1122	97.5987	103.827	97.5074	99.64436667
0.1287	93.1394	81.6844	80.6751	85.1663
-2.14E-03	*	*	*	AVERAGE(K:M)
3.82E-4*I				
2.98E-6*I^2				

Std. Dev. (levels)	Minus 1 S.D. Exp.	Plus 1 S.D. Exp.	Minus 1 S.D. Trans.
9.6579	0.0819	0.1038	0.11669
9.4735	0.0876	0.1095	0.14121
9.5054	0.0839	0.1056	0.16925
9.2385	0.0871	0.1085	0.20461
9.6561	0.0889	0.1114	0.23952
9.6597	0.0855	0.1078	0.28071
9.7769	0.0928	0.1161	0.33109
10.2458	0.1023	0.1277	0.38933
10.1058	0.0966	0.1211	0.44610
9.4242	0.0928	0.1152	0.50316
9.9822	0.1003	0.1248	0.56367
9.2286	0.1169	0.1410	0.72149
N^0.5			E*P/J

Plus 1 S.D. Trans.	Minus 1 S.D. Den.	Plus 1 S.D. Den.	Density S.D.	Density Variance
0.14775	0.93297	0.83046	0.05125	0.002626839
0.17663	0.85012	0.75294	0.04859	0.002360886
0.21293	0.77148	0.67176	0.04986	0.002486443
0.25475	0.68906	0.59388	0.04759	0.002265004
0.30028	0.62065	0.52247	0.04909	0.002409979
0.35357	0.55174	0.45153	0.05010	0.002510476
0.41401	0.48005	0.38298	0.04853	0.002355632
0.48609	0.40968	0.31329	0.04820	0.002323134
0.55908	0.35056	0.25252	0.04902	0.002403013
0.62440	0.29830	0.20454	0.04688	0.002197697
0.70159	0.24898	0.15392	0.04753	0.002259042
0.87030	0.14177	0.06033	0.04072	0.001657858
E*Q/J	LOG10(1/R)	LOG10(1/S)	(T-U)/2	V^2

Granularity	DQE (%)	NEQ	log NEQ
0.215	0.012	23	1.36
0.194	0.017	23	1.37
0.204	0.023	22	1.34
0.186	0.030	21	1.32
0.198	0.036	17	1.24
0.206	0.049	17	1.22
0.193	0.073	18	1.25
0.190	0.088	15	1.18
0.197	0.086	10	1.02
0.180	0.113	10	0.99
0.185	0.155	9	0.98
82*X	100*C*(F^2)/X	C*Z/100	LOG10(AA)

Image #'s	Log Exposure (lux-sec)	Quanta/82.1 µm^2	Density
	-1.52	47356	1.36
114	-1.67	33526	1.25
113	-1.82	23734	1.14
111, 112	-1.97	16803	1.04
110	-2.12	11895	0.93
107, 108, 109	-2.27	8421	0.84
104, 105, 106	-2.42	5962	0.76
101, 102, 103	-2.57	4221	0.67
98, 99, 100	-2.72	2988	0.58
95, 96, 97	-2.87	2115	0.49
92, 93, 94	-3.02	1498	0.42
89, 90, 91	-3.17	1060	0.36
	-3.32	751	0.32
115, 116, 117	B+F	0	0.28
*specify	*	1568110*(10^B)	*

Mean Transmittance	Gain	Mean #1	Mean #2	Mean #3	Mean CCD Resp.
0.0437					
0.0562	9.59E-06	75			75
0.0724	1.28E-05	91			91
0.0912	1.84E-05	115	112		114
0.1175	2.42E-05	112			112
0.1445	2.92E-05	111	112	115	113
0.1738	4.21E-05	123	119	121	121
0.2138	6.24E-05	121	126	123	123
0.2630	8.81E-05	121	123	119	121
0.3236	1.08E-04	120	128	125	124
0.3802	1.25E-04	136	137	140	138
0.4365	1.33E-04	142	135	135	137
0.4786					
0.5248		144	156	155	152
1/(10^D)		*	*	*	AVERAGE(F:H)
((D1-D2)/(C1-C2)+(D2-D3)/(C2-C3))/2					

Mean CCD Exp.	Variance #1	Variance #2	Variance #3	Variance (mean, levels)
0.0433	171.53			171.53
0.0573	216.638			216.638
0.0796	303.327	333.965		318.646
0.0780	282.981			282.981
0.0787	264.812	280.307	287.809	277.6426667
0.0877	316.271	278.888	290.301	295.1533333
0.0903	276.685	297.256	297.17	290.3703333
0.0877	315.001	324.947	311.361	317.103
0.0914	328.4	359.027	345.465	344.2973333
0.1070	443.457	444.203	468.491	452.0503333
0.1066	443.123	404.095	399.462	415.56
0.1244	352.963	406.923	414.691	391.5256667
-2.14E-03	*	*	*	AVERAGE(K:M)
3.82E-4*I				
2.98E-6*I^2				

Std. Dev. (levels)	Minus 1 S.D. Exp.	Plus 1 S.D. Exp.	Minus 1 S.D. Trans.
13.0969	0.0329	0.0547	0.04279
14.7186	0.0444	0.0716	0.05606
17.8507	0.0617	0.0995	0.07064
16.8220	0.0612	0.0966	0.09217
16.6626	0.0620	0.0971	0.11383
17.1800	0.0697	0.1076	0.13797
17.0403	0.0722	0.1102	0.17078
17.8074	0.0690	0.1083	0.20695
18.5553	0.0716	0.1133	0.25346
21.2615	0.0827	0.1339	0.29407
20.3853	0.0833	0.1323	0.34130
19.7870	0.1001	0.1510	0.42234
N^0.5			E*P/J

Plus 1 S.D. Trans.	Minus 1 S.D. Den.	Plus 1 S.D. Den.	Density S.D.	Density Variance
0.07101	1.36867	1.14869	0.10999	0.012098342
0.09046	1.25136	1.04353	0.10391	0.01079821
0.11394	1.15094	0.94334	0.10380	0.010774573
0.14535	1.03539	0.83760	0.09890	0.009780931
0.17829	0.94374	0.74886	0.09744	0.009493989
0.21307	0.86021	0.67147	0.09437	0.008905821
0.26091	0.76757	0.58350	0.09204	0.008470514
0.32477	0.68414	0.48842	0.09786	0.009576159
0.40099	0.59608	0.39687	0.09961	0.009921406
0.47589	0.53155	0.32249	0.10453	0.010926337
0.54188	0.46686	0.26610	0.10038	0.010076481
0.63713	0.37434	0.19577	0.08929	0.007971892
E*Q/J	LOG10(1/R)	LOG10(1/S)	(T-U)/2	V^2

Granularity	DQE (%)	NEQ	log NEQ
0.992	0.026	9	0.93
0.885	0.036	9	0.93
0.884	0.053	9	0.95
0.802	0.071	8	0.93
0.779	0.076	6	0.80
0.730	0.119	7	0.85
0.695	0.194	8	0.91
0.785	0.242	7	0.86
0.814	0.250	5	0.72
0.896	0.215	3	0.51
0.826	0.187	2	0.30
0.654			
82*X	100*C*(F^2)/X	C*Z/100	LOG10(AA)

Appendix K: Wiener Spectrum Calculations.

```
<<Statistics`DescriptiveStatistics`

deltas = Table[
data[[i]] - Mean[data[[i]]], {i, 1, 128}];

npower = Flatten[Partition[
N[Sum[Abs[Fourier[deltas[[i]]]]^2, {i, 1, 128}] (1/128)], 65

{0., 7.33111, 4.99282, 2.27812, 3.6636, 2.09144, 1.97295,
  1.77394, 2.208, 1.59305, 1.79948, 1.61534, 2.93755,
  1.43371, 1.34341, 1.7951, 2.34727, 1.70903, 1.33892,
  1.48648, 1.7875, 1.5626, 1.74087, 1.72788, 2.08795,
  1.9077, 2.10283, 2.07949, 1.77433, 1.92782, 1.63841,
  1.76879, 2.42462, 2.09697, 1.616, 1.9248, 1.73564,
  1.65142, 1.76332, 1.75455, 1.99422, 1.48153, 1.59797,
  1.73308, 1.62836, 1.3021, 1.59275, 1.59445, 1.33132,
  1.36587, 1.41116, 1.23492, 1.49461, 1.23072, 1.23507,
  1.44609, 1.3214, 1.22577, 1.13956, 1.25805, 1.30214,
  1.60753, 1.34241, 1.24299, 1.38983}

frequencies = N[Table[55 - 0.859 (64-x), {x, 0, 64}]]

{0.024, 0.883, 1.742, 2.601, 3.46, 4.319, 5.178, 6.037,
  6.896, 7.755, 8.614, 9.473, 10.332, 11.191, 12.05,
  12.909, 13.768, 14.627, 15.486, 16.345, 17.204, 18.063,
  18.922, 19.781, 20.64, 21.499, 22.358, 23.217, 24.076,
  24.935, 25.794, 26.653, 27.512, 28.371, 29.23, 30.089,
  30.948, 31.807, 32.666, 33.525, 34.384, 35.243, 36.102,
  36.961, 37.82, 38.679, 39.538, 40.397, 41.256, 42.115,
  42.974, 43.833, 44.692, 45.551, 46.41, 47.269, 48.128,
  48.987, 49.846, 50.705, 51.564, 52.423, 53.282, 54.141,
  55.}
```

```
ListPlot[Transpose[{frequencies, npower}],
AxesLabel -> {"frequency (cy./mm.)", "noise power"},
PlotRange -> {0, 3}]
```

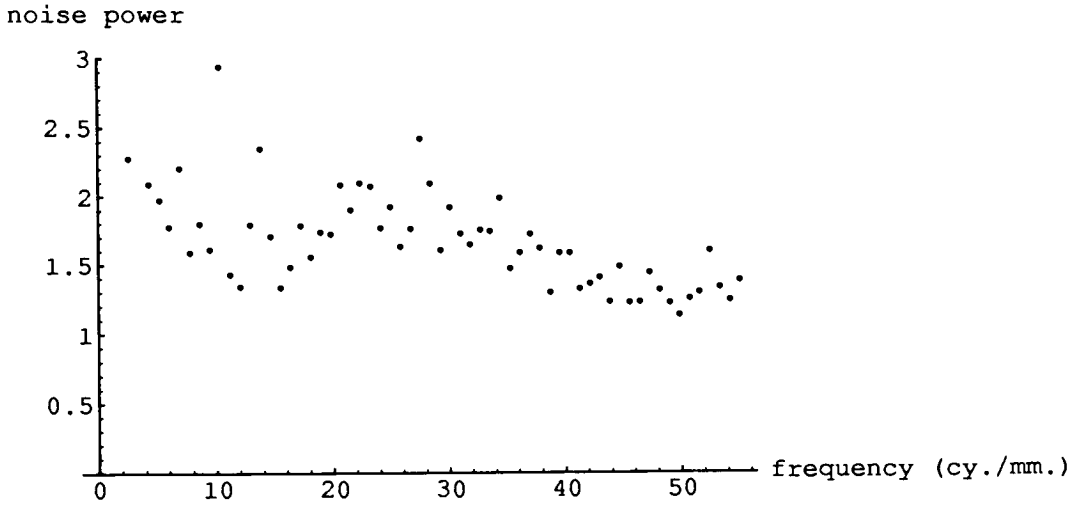

-Graphics-

```
<<Statistics`DescriptiveStatistics`

deltas = Table[
data[[i]] - Mean[data[[i]]], {i, 1, 128}];

npower = Flatten[Partition[
N[Sum[Abs[Fourier[deltas[[i]]]]^2, {i, 1, 128}] (1/128)], 65]]

{0., 37.4928, 11.9741, 10.5446, 4.3912, 3.45201, 1.92006,
  2.1583, 2.71074, 2.18285, 1.75084, 1.5083, 1.8405,
  2.16402, 1.5908, 1.56903, 1.75068, 1.90748, 1.84658,
  1.55852, 1.93019, 1.97073, 1.73737, 1.9156, 2.19408,
  1.99813, 2.02117, 1.67804, 1.76259, 1.74552, 1.76858,
  1.56371, 1.46466, 1.49751, 1.60823, 1.53888, 1.38315,
  1.5556, 1.48898, 1.72744, 1.63077, 1.58031, 1.48928,
  1.48462, 1.35329, 1.68455, 1.5128, 1.63063, 1.5468,
  1.46954, 1.58336, 1.99126, 1.45905, 1.38234, 1.38489,
  1.46972, 1.7425, 1.44896, 1.51325, 1.54851, 1.43326,
  1.43123, 1.80291, 1.62391, 1.64276}

frequencies = N[Table[55 - 0.859 (64-x), {x, 0, 64}]]

{0.024, 0.883, 1.742, 2.601, 3.46, 4.319, 5.178, 6.037,
  6.896, 7.755, 8.614, 9.473, 10.332, 11.191, 12.05,
  12.909, 13.768, 14.627, 15.486, 16.345, 17.204, 18.063,
  18.922, 19.781, 20.64, 21.499, 22.358, 23.217, 24.076,
  24.935, 25.794, 26.653, 27.512, 28.371, 29.23, 30.089,
  30.948, 31.807, 32.666, 33.525, 34.384, 35.243, 36.102,
  36.961, 37.82, 38.679, 39.538, 40.397, 41.256, 42.115,
  42.974, 43.833, 44.692, 45.551, 46.41, 47.269, 48.128,
  48.987, 49.846, 50.705, 51.564, 52.423, 53.282, 54.141,
  55.}
```

```
ListPlot[Transpose[{frequencies, npower}],
AxesLabel -> {"frequency (cy./mm.)", "noise power"},
PlotRange -> {0, 3}]
```

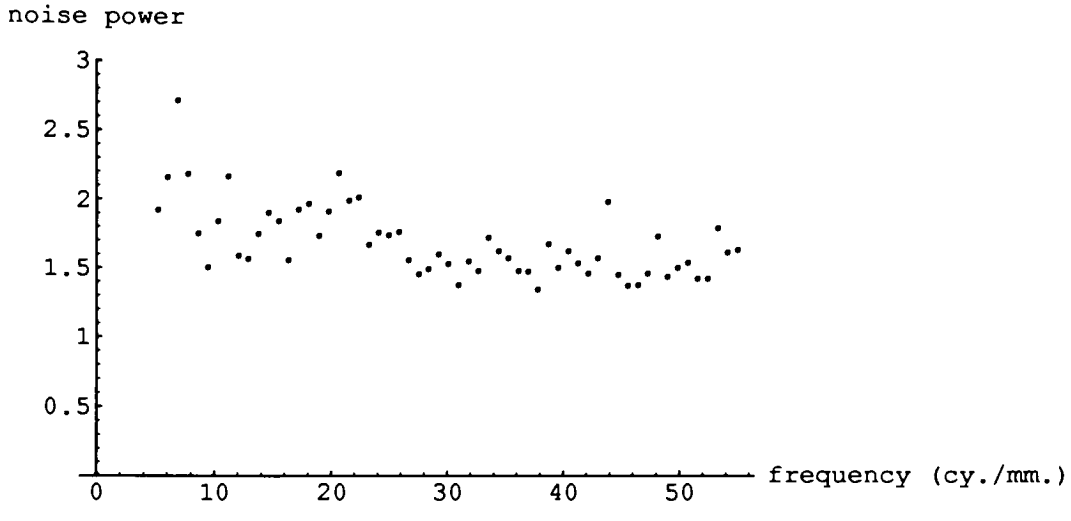

-Graphics-

```
<<Statistics`DescriptiveStatistics`

deltas = Table[
data[[i]] - Mean[data[[i]]], {i, 1, 128}];

npower = Flatten[Partition[
N[Sum[Abs[Fourier[deltas[[i]]]]^2, {i, 1, 128}] (1/128)], 65]]

{0., 42.8206, 23.3476, 13.4134, 15.3089, 11.2717, 12.1898,
  10.9017, 11.6653, 10.7541, 10.4673, 12.2779, 13.3814,
  12.9931, 11.7386, 11.9576, 12.3331, 13.9681, 14.6962,
  16.3759, 15.6154, 16.1206, 18.8312, 22.2901, 23.2866,
  23.8606, 24.8979, 27.2912, 27.8286, 27.2997, 23.0209,
  27.6729, 24.5858, 25.9714, 29.5225, 25.7318, 21.8681,
  22.7, 21.8955, 19.4151, 20.0526, 19.3615, 18.9597,
  21.0128, 17.9793, 17.2363, 15.7434, 14.5753, 14.5629,
  15.3093, 13.6452, 16.947, 16.519, 13.8417, 14.9437,
  15.8617, 12.5374, 12.4213, 12.912, 15.3881, 13.0667,
  16.4118, 13.7862, 12.831, 13.1727}

frequencies = N[Table[55 - 0.859 (64-x), {x, 0, 64}]]

{0.024, 0.883, 1.742, 2.601, 3.46, 4.319, 5.178, 6.037,
  6.896, 7.755, 8.614, 9.473, 10.332, 11.191, 12.05,
  12.909, 13.768, 14.627, 15.486, 16.345, 17.204, 18.063,
  18.922, 19.781, 20.64, 21.499, 22.358, 23.217, 24.076,
  24.935, 25.794, 26.653, 27.512, 28.371, 29.23, 30.089,
  30.948, 31.807, 32.666, 33.525, 34.384, 35.243, 36.102,
  36.961, 37.82, 38.679, 39.538, 40.397, 41.256, 42.115,
  42.974, 43.833, 44.692, 45.551, 46.41, 47.269, 48.128,
  48.987, 49.846, 50.705, 51.564, 52.423, 53.282, 54.141,
  55.}
```

```
ListPlot[Transpose[{frequencies, npower}],
AxesLabel -> {"frequency (cy./mm.)", "noise power"},
PlotRange -> {0, 48}]
```

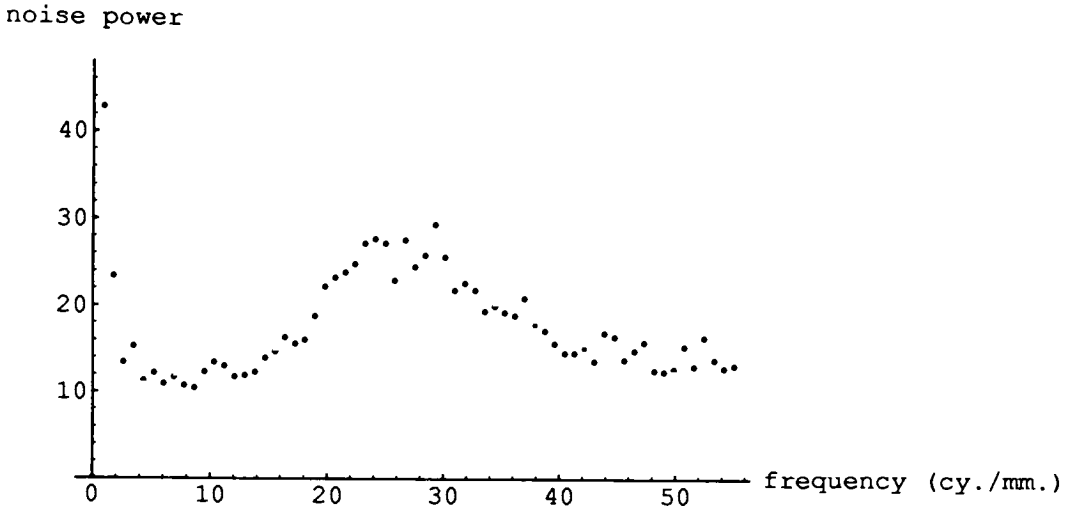

-Graphics-

```
<<Statistics`DescriptiveStatistics`

deltas = Table[
data[[i]] - Mean[data[[i]]], {i, 1, 128}];

npower = Flatten[Partition[
N[Sum[Abs[Fourier[deltas[[i]]]]^2, {i, 1, 128}] (1/128)], 65]]

{0., 22.8801, 15.7603, 16.2482, 17.0781, 18.6443, 16.2055,
  16.6472, 14.2942, 17.3898, 18.9604, 15.6474, 17.4108,
  17.2449, 19.3081, 17.1518, 17.0414, 18.3333, 16.5151,
  17.136, 18.0436, 18.2005, 16.2683, 15.556, 12.8859,
  17.2408, 14.9085, 16.6805, 17.4095, 14.6698, 16.2656,
  18.4877, 17.1128, 13.6911, 17.1179, 19.0221, 16.0286,
  15.5269, 15.6613, 18.1745, 15.6227, 16.6482, 13.9489,
  19.1026, 13.6096, 15.8189, 15.2588, 17.6179, 16.6048,
  17.8458, 18.252, 18.962, 16.0725, 18.4918, 15.1739,
  17.765, 15.6089, 18.5016, 17.6382, 15.6349, 16.149,
  17.3743, 14.5189, 16.758, 14.9825}

frequencies = N[Table[55 - 0.859 (64-x), {x, 0, 64}]]

{0.024, 0.883, 1.742, 2.601, 3.46, 4.319, 5.178, 6.037,
  6.896, 7.755, 8.614, 9.473, 10.332, 11.191, 12.05,
  12.909, 13.768, 14.627, 15.486, 16.345, 17.204, 18.063,
  18.922, 19.781, 20.64, 21.499, 22.358, 23.217, 24.076,
  24.935, 25.794, 26.653, 27.512, 28.371, 29.23, 30.089,
  30.948, 31.807, 32.666, 33.525, 34.384, 35.243, 36.102,
  36.961, 37.82, 38.679, 39.538, 40.397, 41.256, 42.115,
  42.974, 43.833, 44.692, 45.551, 46.41, 47.269, 48.128,
  48.987, 49.846, 50.705, 51.564, 52.423, 53.282, 54.141,
  55.}
```

```
ListPlot[Transpose[{frequencies, npower}],
AxesLabel -> {"frequency (cy./mm.)", "noise power"},
PlotRange -> {0, 48}]
```

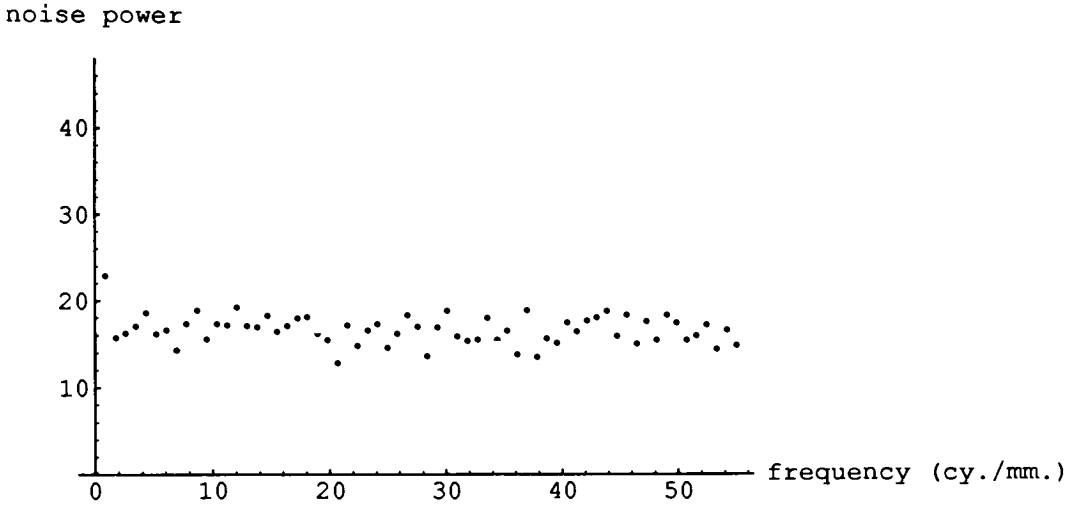

-Graphics-

Appendix L: DCS200mi Data & Analysis.

E w/o N.D. (lux)	N.D. Filter	1/Exp. Time	Exposure (lux-sec.)	Log Exposure	Exposure (quanta/pixel)
20.7	1.86	8000	3.57174E-05	-4.45	31
20.7	1.86	4000	7.14349E-05	-4.15	63
20.7	1.86	2000	0.00014287	-3.85	126
20.7	1.86	1000	0.00028574	-3.54	252
20.7	1.86	500	0.000571479	-3.24	504
20.7	1.86	250	0.001142958	-2.94	1007
20.7	1.86	125	0.002285916	-2.64	2014
20.7	1.86	60	0.004762326	-2.32	4196
20.7	1.86	30	0.009524651	-2.02	8392
20.7	0	8000	0.0025875	-2.59	2280
20.7	0	4000	0.005175	-2.29	4560
20.7	0	2000	0.01035	-1.99	9119
20.7	0	1000	0.0207	-1.68	18239
20.7	0	500	0.0414	-1.38	36477
20.7	0	250	0.0828	-1.08	72955
20.7	0	125	0.1656	-0.78	145910
20.7	0	60	0.345	-0.46	303979
*specify	*	*	(A/C)/(10^B)	LOG10(D)	D*881098

S=100 Im. #	S=100 Mean	S=100 Var.	S=100 Gain	S=100 DQE	S=100 NEQ	S=100 log NEQ
145	1.0374	6.1863				
146	0.0428	0.2979				
147	3.4381	12.2781				
148						
149	6.12038	6.00894	0.007148	0.0043	2	0.334
150	2.92486	11.9663	0.005316	0.0024	2	0.379
151	9.60988	3.80946	0.003975	0.0084	17	1.226
152	16.2846	2.04388	0.002944	0.0178	75	1.873
153	27.077	1.06518	0.002239	0.0395	331	2.520
134	13.3202	1.84669	0.003776	0.0176	40	1.603
135	18.2393	2.34365	0.002848	0.0158	72	1.857
136	27.0167	1.0512	0.002168	0.0408	372	2.570
137	45.9052	0.852961	0.001670	0.0597	1088	3.037
138	73.6219	0.701984	0.001306	0.0886	3233	3.510
139	114.293	1.12539	0.001039	0.0700	5110	3.708
140	182.109	2.81653	0.000844	0.0369	5388	3.731
141	254	0	0.000694			
*	*	*		(L^2)*F/K	F*M	LOG10(M)
		0.000311+0.1124/(F^0.45)				

S=200 Im. #	S=200 Mean	S=200 Var.	S=200 Gain	S=200 DQE	S=200 NEQ	S=200 log NEQ
164	5.0953	15.3496				
165	1.8044	9.881				
166	1.7851	9.8028				
167	2.40501	11.8723	0.014039	0.0042	1	0.022
168	5.13516	14.6837	0.010437	0.0037	2	0.274
169	9.6834	10.8053	0.007800	0.0057	6	0.757
170	16.6442	5.43206	0.005869	0.0128	26	1.410
171	27.4443	3.7157	0.004386	0.0217	91	1.960
172	43.3152	3.39722	0.003370	0.0281	235	2.372
154	19.2363	5.29555	0.005583	0.0134	31	1.486
155	29.9266	2.60525	0.004246	0.0316	144	2.158
156	47.444	2.14439	0.003268	0.0454	414	2.617
157	73.1155	3.5308	0.002552	0.0336	613	2.788
158	110.953	2.07525	0.002027	0.0722	2635	3.421
159	179.651	2.63102	0.001644	0.0749	5465	3.738
160	254	0				
*	*	*		(Q^2)*F/P	F*R	LOG10(T)
		0.000595+0.1618/(F^0.45)				

S=400 Im. #	S=400 Mean	S=400 Var.	S=400 Gain	S=400 DQE	S=400 NEQ	S=400 log NEQ
181	3.57825	22.9762	0.054584	0.0041	0	-0.891
182	5.92705	30.6734	0.040333	0.0033	0	-0.678
183	7.40536	33.6344	0.029901	0.0033	0	-0.375
184	6.89831	34.4093	0.022264	0.0036	1	-0.039
185	11.3965	37.5169	0.016674	0.0037	2	0.274
186	19.2804	19.5701	0.012581	0.0081	8	0.914
187	29.9267	19.6189	0.009585	0.0094	19	1.279
173	32.4333	13.535	0.009141	0.0141	32	1.506
174	51.2725	10.3481	0.007067	0.0220	100	2.002
175	122.627	7.4541	0.004437	0.0482	879	2.944
176	195.938	5.66365	0.003624	0.0846	3085	3.489
177	254	0	0.003028			
*	*	*		(X^2)*F/W	F*Y	LOG10(AA)
		0.0014008+0.25109/(F^0.45)				

S=800 Im. #	S=800 Mean	S=800 Var.	S=800 Gain	S=800 DQE	S=800 NEQ	S=800 log NEQ
197	9.69979	80.7836	0.084447	0.0028	0	-1.058
198	7.80921	65.6523	0.062488	0.0037	0	-0.628
199	9.81429	73.0359	0.046413	0.0037	0	-0.330
200	13.5083	74.4688	0.034646	0.0041	1	0.009
201	19.4288	63.0047	0.026032	0.0054	3	0.436
202	26.3168	65.7261	0.019726	0.0060	6	0.778
188	55.0091	34.0797	0.014425	0.0139	32	1.502
189	82.6308	21.3529	0.011229	0.0269	123	2.089
190	125.592	19.4297	0.008890	0.0371	338	2.529
192	198.061	17.8041	0.007177	0.0528	962	2.983
193	255	0				
*	*	*		(AE^2)*F/AD	F*AF	LOG10(AH)
		0.0024982+0.3869/(F^0.45)				

Log Exposure	S=100 log NEQ	S=200 log NEQ	S=400 log NEQ	S=800 log NEQ	Mean log NEQ
-3.54				0.009	0.009
-3.24			0.274	0.436	0.355
-2.94		0.757	0.914	0.778	0.816
-2.64	1.226	1.41	1.279		1.305
-2.59	1.603	1.486	1.506	1.502	1.524
-2.32	1.873	1.96			1.917
-2.29	1.857	2.158	2.002	2.089	2.027
-2.02	2.52	2.372			2.446
-1.99	2.57	2.617		2.529	2.572
-1.68	3.037	2.788	2.944	2.983	2.938
-1.38	3.51	3.421	3.489		3.473
-1.08	3.708	3.738			3.723
-0.78	3.731				3.731

Appendix M: General Analyses.

```
TPan = {{-1.86, 0.2}, {-1.69, 0.23}, {-1.55, 0.28},
{-1.4, 0.34}, {-1.27, 0.43}, {-1.12, 0.53}, {-0.97, 0.63},
{-0.83, 0.72}, {-0.66, 0.82}, {-0.49, 0.91}, {-0.34, 1.01},
{-0.17, 1.09}, {-0.02, 1.19}};

TMX100 = {{-2.46, 0.26}, {-2.31, 0.3}, {-2.14, 0.35},
{-2, 0.4}, {-1.85, 0.47}, {-1.72, 0.56}, {-1.57, 0.65},
{-1.42, 0.73}, {-1.28, 0.82}, {-1.11, 0.91}, {-0.94, 1},
{-0.79, 1.11}, {-0.62, 1.21}};

TMY400 = {{-2.56, 0.15}, {-2.41, 0.2}, {-2.26, 0.25},
{-2.11, 0.3}, {-1.96, 0.36}, {-1.81, 0.43}, {-1.66, 0.5},
{-1.51, 0.57}, {-1.36, 0.64}, {-1.21, 0.72}, {-1.06, 0.8},
{-0.91, 0.88}, {-0.76, 0.97}};

TMP3200 = {{-3.32, 0.32}, {-3.17, 0.36}, {-3.02, 0.42},
{-2.87, 0.49}, {-2.72, 0.58}, {-2.57, 0.67}, {-2.42, 0.76},
{-2.27, 0.84}, {-2.12, 0.93}, {-1.97, 1.04}, {-1.82, 1.14},
{-1.67, 1.25}, {-1.52, 1.36}};
```

```
Show[ListPlot[TPan, PlotJoined -> True,
AxesOrigin -> {-3.4, 0},
AxesLabel -> {"log exposure", "density"}],
ListPlot[TMX100, PlotJoined -> True],
ListPlot[TMY400, PlotJoined -> True],
ListPlot[TMP3200, PlotJoined -> True]]
```

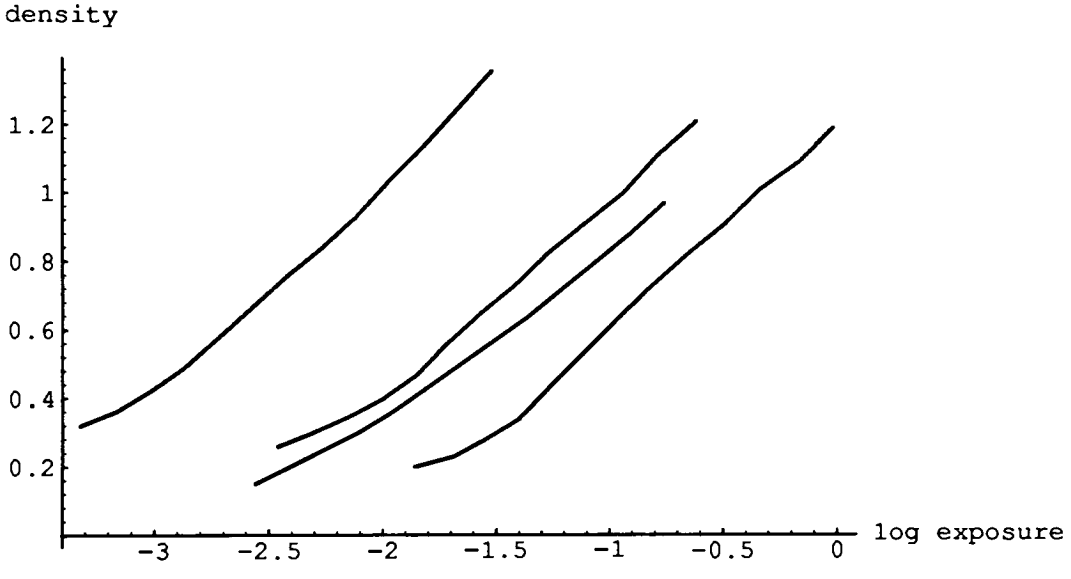

-Graphics-

```
S100 = {{-2.64, 9.61}, {-2.59, 13.32}, {-2.32, 16.28},
{-2.29, 18.24}, {-2.02, 27.1}, {-1.99, 27.0}, {-1.68, 45.9},
{-1.38, 73.6}, {-1.08, 114.3}, {-0.78, 182.1}, {-0.54, 255},
{-0.34, 255}};

S200 = {{-2.94, 9.68}, {-2.64, 16.64}, {-2.59, 19.24},
{-2.32, 27.4}, {-2.29, 29.9}, {-2.02, 43.3}, {-1.99, 47.4},
{-1.68, 73.1}, {-1.38, 111.0}, {-1.08, 180.0},
{-0.83, 255}, {-0.53, 255}};

S400 = {{-3.24, 11.40}, {-2.94, 19.28}, {-2.64, 29.9},
{-2.59, 32.4}, {-2.29, 51.3}, {-1.68, 122.6},
{-1.38, 195.9}, {-1.20, 255}, {-0.90, 255}};

S800 = {{-3.54, 13.51}, {-3.24, 19.43}, {-2.94, 26.3},
{-2.59, 55.0}, {-2.29, 82.6}, {-1.99, 125.6},
{-1.68, 198.1}, {-1.50, 255}, {-1.20, 255}};

Show[ListPlot[S100, PlotJoined -> True,
AxesOrigin -> {-3.6, 0},
AxesLabel -> {"log exposure", "output level"}],
ListPlot[S200, PlotJoined -> True],
ListPlot[S400, PlotJoined -> True],
ListPlot[S800, PlotJoined -> True]]
```

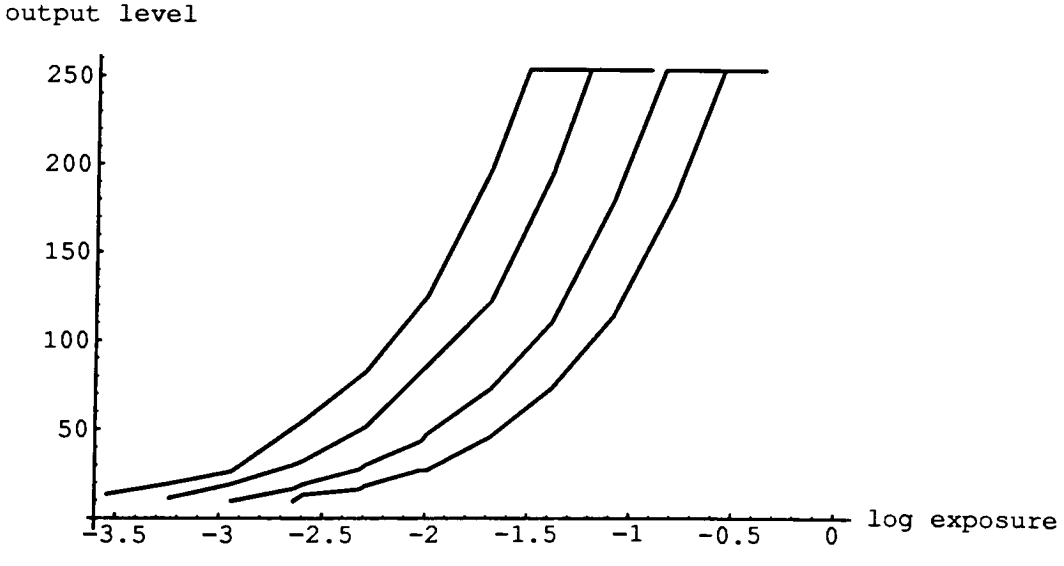


```
-Graphics-
```

```
TechPan = Transpose[{{-0.17, -0.34, -0.49, -0.66, -0.83,
-0.97, -1.12, -1.27, -1.4, -1.55, -1.69}, {1.59, 1.71,
1.76, 1.8, 1.92, 2.04, 2.12, 2.23, 2.11, 1.95, 1.73}}];

Fit[TechPan, {1, x, x^6}, x]

1.44536 - 0.657955 x - 0.0353188 x^6

TechPanFit[x_] := 1.445359551359099602 -
0.6579553478666173146*x - 0.035318822226863568556*x^6

AA = Show[ListPlot[TechPan, AxesOrigin -> {-3.2, 0},
AxesLabel -> {"log exposure", "log NEQ"}],
Plot[TechPanFit[x], {x, -1.61, 0.29}]]

-Graphics-

Table[TechPanFit[x], {x, -1.51, 0.29, 0.3}]

{2.02021, 2.13064, 2.02404, 1.84489, 1.64929, 1.45194,
  1.25453}

TMax100 = Transpose[{{-0.79, -0.94, -1.11, -1.28, -1.42,
-1.57, -1.72, -1.85, -2, -2.14, -2.31}, {1.60, 1.54,
1.40, 1.55, 1.45, 1.54, 1.71, 1.63, 1.38, 1.25, 1.14}}];

Fit[TMax100, {1, x, x^6}, x]

1.35994 - 0.172112 x - 0.0042062 x^6

TMax100Fit[x_] := 1.359936887868766501 -
0.17211161906393621444*x - 0.00420619956162045201*x^6

BB = Show[ListPlot[TMax100, AxesOrigin -> {-3.2, 0},
AxesLabel -> {"log exposure", "log NEQ"}],
Plot[TMax100Fit[x], {x, -2.2, -0.3}]]

-Graphics-

Table[TMax100Fit[x], {x, -2.1, -0.3, 0.3}]

{1.36062, 1.52668, 1.57019, 1.55391, 1.5126, 1.46301,
  1.41157}

TMY = Transpose[{{-0.91, -1.06, -1.21, -1.36, -1.51,
-1.66, -1.81, -1.96, -2.11, -2.26, -2.41}, {1.36, 1.37,
1.34, 1.32, 1.24, 1.22, 1.25, 1.18, 1.02, 0.99, 0.98}}];
```

```
Fit[TMY, {1, x, x^6}, x]
```

$$1.55195 + 0.181559\,x - 0.000878304\,x^6$$

```
TMYFit[x_] := 1.551947527785802234 +
0.1815594210367065 31*x - 0.0008783036798671381 69*x^6

CC = Show[ListPlot[TMY, AxesOrigin -> {-3.2, 0},
AxesLabel -> {"log exposure", "log NEQ"}],
Plot[TMYFit[x], {x, -2.41, -0.51}]]
```

-Graphics-

```
Table[TMYFit[x], {x, -2.31, -0.51, 0.3}]
```

```
{0.999096, 1.12909, 1.21952, 1.28905, 1.34877, 1.40464,
  1.45934}
```

```
TMaxP3200 = Transpose[{{-1.67, -1.82, -1.97, -2.12, -2.27,
-2.42, -2.57, -2.72, -2.87, -3.02, -3.17}, {0.93, 0.93,
0.95, 0.93, 0.80, 0.85, 0.91, 0.86, 0.72, 0.51, 0.30}}];

Fit[TMaxP3200, {1, x, x^6}, x]
```

$$0.551102 - 0.220252\,x - 0.000906153\,x^6$$

```
TMaxP3200Fit[x_] := 0.5511024464538081142 -
0.2202517339040842509*x - 0.0009061530101617013846*x^6

DD = Show[ListPlot[TMaxP3200, AxesOrigin -> {-3.2, 0},
AxesLabel -> {"log exposure", "log NEQ"}],
Plot[TMaxP3200Fit[x], {x, -3.12, -1.22}]]
```

-Graphics-

```
Table[TMaxP3200Fit[x], {x, -3.02, -1.22, 0.3}]
```

```
{0.528809, 0.78323, 0.902102, 0.935771, 0.919028, 0.87471,
  0.816822}
```

```
Show[AA, BB, CC, DD]
```

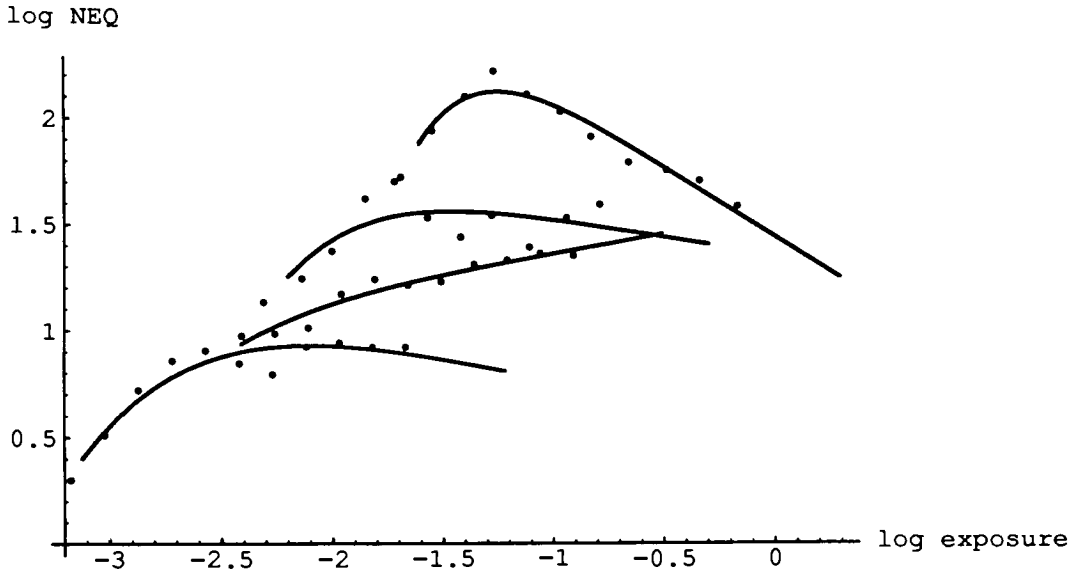


```
-Graphics-
```

```
DCS200 = {{-3.54, 0.009}, {-3.24, 0.355},
          {-2.94, 0.816}, {-2.64, 1.305}, {-2.59, 1.524},
          {-2.32, 1.917}, {-2.29, 2.027}, {-2.02, 2.446},
          {-1.99, 2.572}, {-1.68, 2.938}, {-1.38, 3.473},
          {-1.08, 3.723}, {-0.78, 3.731}};
```

```
Fit[{{-3.24, 0.355}, {-2.94, 0.816}, {-2.64, 1.305},
     {-2.59, 1.524}, {-2.32, 1.917}, {-2.29, 2.027},
     {-2.02, 2.446}, {-1.99, 2.572}, {-1.68, 2.938},
     {-1.38, 3.473}}, {1, x}, x]
```

```
5.8524 + 1.69558 x
```

```
DCS200Fit[x_] :=
5.85239635044808464 + 1.6955809226713229 28*x
```

```
EE = Show[ListPlot[DCS200, AxesOrigin -> {-4, 0},
AxesLabel -> {"log exposure", "log NEQ"}],
Plot[DCS200Fit[x], {x, -3.3, -1.4}]]
```

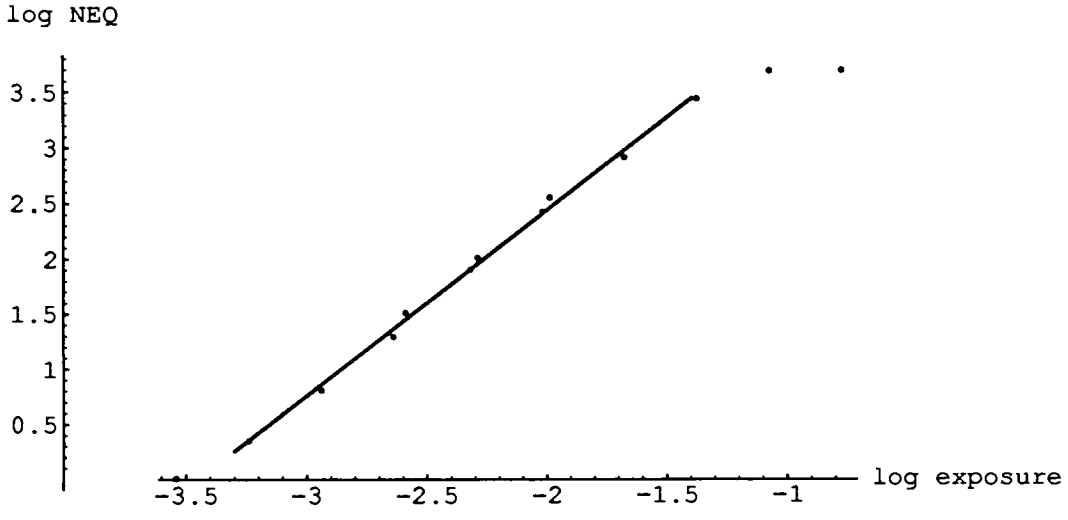

-Graphics-

```
Show[AA, BB, CC, DD, EE, AxesOrigin -> {-4, 0}]
```

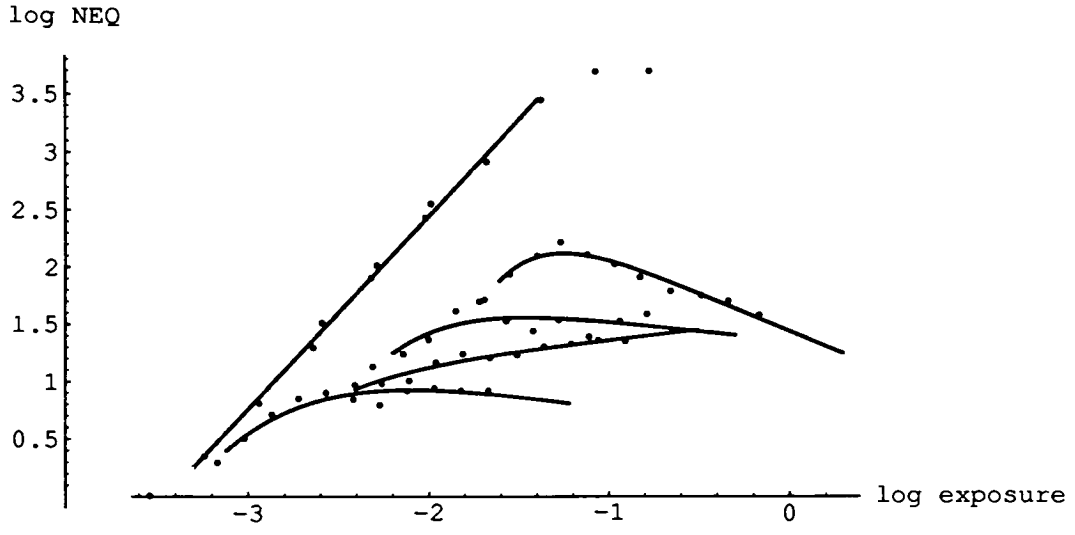

-Graphics-

```
DCSdataAA = {{-2.64, 1.23}, {-2.59, 1.60}, {-2.32, 1.87},
{-2.29, 1.86}, {-2.02, 2.52}, {-1.99, 2.57}, {-1.68, 3.04},
{-1.38, 3.51}, {-1.08, 3.71}, {-0.78, 3.73}};

DCSdataBB = {{-2.94, 0.76}, {-2.64, 1.41}, {-2.59, 1.49},
{-2.32, 1.96}, {-2.29, 2.16}, {-2.02, 2.37}, {-1.99, 2.62},
{-1.68, 2.79}, {-1.38, 3.42}, {-1.08, 3.74}};

DCSdataCC = {{-3.24, 0.27}, {-2.94, 0.91}, {-2.64, 1.28},
{-2.59, 1.51}, {-2.29, 2}, {-1.68, 2.94}, {-1.38, 3.49}};

DCSdataDD = {{-3.54, 0.01}, {-3.24, 0.44}, {-2.94, 0.78},
{-2.59, 1.5}, {-2.29, 2.09}, {-1.99, 2.53}, {-1.68, 2.98}};
```

```
Show[ListPlot[DCSdataAA, AxesOrigin -> {-3.6, 0},
AxesLabel -> {"log exposure", "log NEQ"}],
ListPlot[DCSdataBB], ListPlot[DCSdataCC],
ListPlot[DCSdataDD],
Plot[DCS200Fit[x], {x, -3.3, -1.4}]]
```

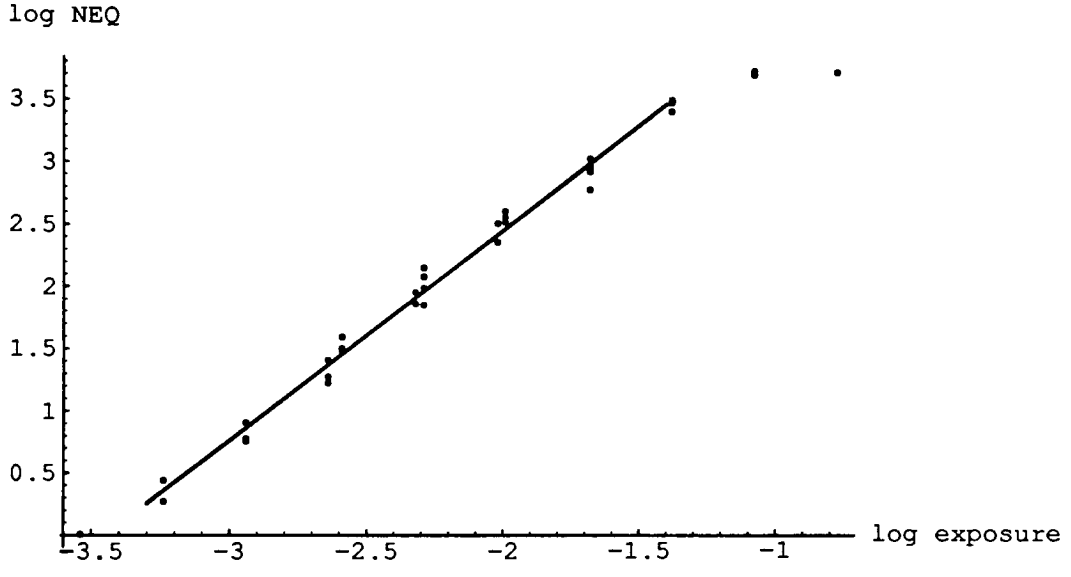

-Graphics-

Film	Receiver Size (V, mm)	by (H) (mm)	Speed Point logH	Speed
Technical Pan	24	36	-1.61	33
T-Max 100	24	36	-2.20	127
T-Max 400	24	36	-2.41	206
T-Max P3200	24	36	-3.12	1055
DCS 200 (100)	9.23	13.85	-0.54	347
DCS 200 (200)	9.23	13.85	-0.83	676
DCS 200 (400)	9.23	13.85	-1.20	1585
DCS 200 (800)	9.23	13.85	-1.50	3162
*specify	*	*	*	0.8/(10^D)
				100/(10^D)

Shadow logH	Highlight logH	Shadow Q	Highlight Q	Z2 log NEQ	Z3 log NEQ	Z4 log NEQ
-1.61	0.29	38493	3057571	2.02	2.13	2.02
-2.20	-0.3	9894	785917	1.36	1.53	1.57
-2.41	-0.51	6101	484592	1	1.13	1.22
-3.12	-1.22	1190	94488	0.53	0.78	0.9
-2.64	-0.74	3592	285349	1.545627	2.054301	2.562975
-2.93	-1.03	1842	146345	1.053909	1.562583	2.071257
-3.30	-1.40	786	62428	0.426544	0.935218	1.443892
-3.60	-1.70	394	31288	0	0.426544	0.935218
D	D+1.9					
D-2.1	D-0.2					

Z5 log NEQ	Z6 log NEQ	Z7 log NEQ	Z8 log NEQ	EIQ (18X enl.)	18X Print Size (H)
1.84	1.65	1.45	1.25	1.71	17.01
1.55	1.51	1.46	1.41	1.50	17.01
1.29	1.35	1.4	1.46	1.31	17.01
0.94	0.92	0.87	0.82	0.87	17.01
3.071649	3.580323	3.73	3.73	3.19	6.54
2.579931	3.088605	3.597279	3.73	2.82	6.54
1.952566	2.46124	2.969914	3.478588	2.22	6.54
1.443892	1.952566	2.46124	2.969914	1.71	6.54
					18*B/25.4
		(3*G+5*H+8*I+11*J+16*K+16*L+4*M)/63			

by (V) (inches)	EIQ (6x9 print)	Equiv. Enl.	Print Size (V)	by (H) (mm.)
25.51	2.610	0.72	12.18	18.26
25.51	2.400	0.56	9.56	14.35
25.51	2.209	0.45	7.67	11.51
25.51	1.772	0.27	4.64	6.96
9.81	3.262	3.94	25.80	38.71
9.81	2.893	2.58	16.86	25.30
9.81	2.289	1.29	8.42	12.63
9.81	1.784	0.72	4.71	7.06
18*C/25.4	N+0.9		18*R*B/25.4	18*R*C/25.4
	N+0.07			
	(10^(N-2))^0.5			

IX. References

General References:

A. J.C. Dainty & R. Shaw, *Image Science*, Academic Press (1974).

B. T.H. James, ed., *The Theory of the Photographic Process*, Kodak (1977).

C. L. Stroebel, J. Compton, I. Current, & R. Zakia, *Photographic Materials and Processes*, Focal Press (1986).

D. J. Sturge, ed., *Imaging Processes and Materials*, Van Nostrand Reinhold (1989).

Specific References:

Tone Reproduction:

1. L.A. Jones & H.R. Condit, "The Brightness Scale of Exterior Scenes and the Computation of Correct Photographic Exposure," *J. Opt. Soc. Amer.*, **31**, p. 651 - 678 (1941).

2. L.A. Jones & C.N. Nelson, "The Control of Photographic Printing by Measured Characteristics of the Negative," *J. Opt. Soc. Amer.*, **32**, p.558 - 619 (1942).

3. R.J. Ross, *Television Film Engineering*, Wiley (1966).

4. A. Adams, *The Camera*, Little, Brown & Co. (1980).

5. A. Adams, *The Negative*, Little, Brown & Co. (1981).

6. A. Adams, *The Print*, Little, Brown & Co. (1983).

7. J. Holm, "A System for Exposure Determination and Tone Reproduction Control," *Kodak Tech Bits*, issue #3, p. 23-28 (1990).

8. *Photography (Sensitometry) - Black and White Continuous Tone Papers - Determination of ISO Speed and Range for Printing,* American National Standards Institute PH2.2 - 1984 (Reaffirmed 1989).

9. *Method for Determining Speed of Photographic Negative Materials (Monochrome, Continuous Tone),* American National Standards Institute PH2.5 - 1979 (Reaffirmed 1986).

10. *Photography (Sensitometry) - Color Reversal Camera Films - Determination of ISO Speed,* American National Standards Institute PH2.21 - 1983 (Reaffirmed 1989).

11. *Photography - Colour Negative Films for Still Photography - Determination of ISO Speed,* American National Standards Institute PH2.27 - 1988.

12. *Photography (Sensitometry) - Direct Positive Colour Print Camera Materials - Determination of ISO Speed,* American National Standards Institute PH2.47 - 1984 (Reaffirmed 1991).

13. *Photography - General Purpose Photographic Exposure Meters (Photoelectric Type) - Guide to Product Specification,* American National Standards Institute PH3.49 - 1974 (Reaffirmed 1987).

Color Reproduction:

14. R.W.G. Hunt, *The Reproduction of Colour,* 3rd ed., Morgan & Morgan (1975).

15. Y. Miyake, K. Seidel, & F. Tomamichel, "Colour and Tone Corrections of Digitized Colour Pictures," *J. Phot. Sci.,* **29,** p. 111 - 118 (1981).

16. G. Wyszecki & W.S. Stiles, *Color Science: Concepts and Methods, Quantitative Data and Formulæ,* 2nd ed.,Wiley (1982).

17. K.R. Hailey, "The Mark II Colour Product Simulator," *Proceedings of the Symposium on Photographic and Electronic Image Quality,* p. 161 - 165, Cambridge (1984).

Detail Reproduction:

18. H. Frieser, "Spread Function and Contrast Transfer Function of Photographic Layers," *Phot. Sci. & Engr.*, 4:6, p. 324 - 329 (1960).

19. F. Scott, R.M. Scott, & R.V. Shack, "The Use of Edge Gradients in Determining Modulation Transfer Functions," *Phot. Sci. & Engr.*, 7:6, p. 345 - 349 (1963).

20. W.N. Charman, "Spatial Frequency Spectra and Other Properties of Conventional Resolution Targets," *Phot. Sci. & Engr.*, 8:5, p. 253 - 259 (1964).

21. M. DeBelder, J. Jespers, & R. Verbrugghe, "On the Evaluation of the Modulation Transfer Function of Photographic Materials," *Phot. Sci. & Engr.*, 9:5, p. 314 - 318 (1965).

22. R.L. Lamberts & C.M. Straub, "Equipment for Routine Evaluation of the Modulation Transfer Function of Photographic Emulsions. I. The Camera," *Phot. Sci. & Engr.*, 9:5, p. 331 - 334 (1965).

23. R.L. Lamberts & C.M. Straub, "Equipment for Routine Evaluation of the Modulation Transfer Function of Photographic Emulsions. II. The Microdensitometer," *Phot. Sci. & Engr.*, 9:5, p. 335 - 339 (1965).

24. R.L. Lamberts & W.F. Garbe, "Equipment for Routine Evaluation of the Modulation Transfer Function of Photographic Emulsions. III. Evaluating and Plotting Instrument," *Phot. Sci. & Engr.*, 9:5, p. 340 - 342 (1965).

25. R.A. Jones, "The Effect of Slit Misalignment on the Microdensitometer Modulation Transfer Function," *Phot. Sci. & Engr.*, 9:6, p. 355 - 359 (1965).

26. F. Scott, "Three-Bar Target Modulation Detectability," *Phot. Sci. & Engr.*, **10**:1, p. 49 - 52 (1966).

27. F. Scott, "A New Objective Characterization of Film Image Structure," *Phot. Sci. & Engr.*, **11**:1, p. 7 - 10 (1967).

28. R.A. Jones, "An Automated Technique for Deriving MTF's from Edge Traces," *Phot. Sci. & Engr.*, **11**:2, p. 102 - 106 (1967).

29. G.C. Brock, "Discussion and Evaluation: Reflections on Thirty Years of Image Evaluation," *Phot. Sci. & Engr.*, **11**:5, p. 356 - 362 (1967).

30. E.S. Blackman, "Effects of Noise on the Determination of Photographic System Modulation Transfer Functions," *Phot. Sci. & Engr.*, **12**:5, p. 244 - 250 (1968).

31. M.C. Goddard & R.G. Gendron, "An MTF Meter for Film," *Phot. Sci. & Engr.*, **13**:3, p. 150 - 155 (1969).

32. R. Williams, "A Re-examination of Resolution Prediction from Lens MTF's and Emulsion Thresholds," *Phot. Sci. & Engr.*, **13**:5, p. 251 - 261 (1969).

33. E.C. Yeadon, R.A. Jones, & J.T. Kelly, "Confidence Limits for Individual Modulation Transfer Function Measurements Based upon the Phase Transfer Function," *Phot. Sci. & Engr.*, **14**:2, p. 153 - 156 (1970).

34. C.B. Johnson, "A Method for Characterizing Electro-Optical Device Modulation Transfer Functions," *Phot. Sci. & Engr.*, **14**:6, p. 413 - 415 (1970).

35. C.N. Nelson, "Prediction of Densities in Fine Detail in Photographic Images," *Phot. Sci. & Engr.*, **15**:1, p. 82 - 97 (1971).

36. R. Arguello & H. Sellner, "Optimal Processing Bandwidth for Optical Transfer Function Compensation," *Phot. Sci. & Engr.*, **15**:4, p. 329 - 330 (1971).

37. R.A. Jones, "Use of the Modulation Transfer Function to Diagnose Camera Faults," *Phot. Sci. & Engr.*, **15**:5, p. 437 - 441 (1971).

38. J.J. DePalma & J. Gasper, "Determining the optical properties of photographic emulsions by the Monte Carlo method," *Phot. Sci. & Engr.*, **16**:3, p. 181 - 191 (1972).

39. H.T. Buschmann, "Fast Method of Determining the MTF of Photographic Materials," *Phot. Sci. & Engr.*, **18**:1, p. 29 - 32 (1974).

40. M.A. Kriss, C.N. Nelson, & F.C. Eisen, "Modulation Transfer Function in Photographic Systems Containing Development Adjacency Effects," *Phot. Sci. & Engr.*, **18**:2, p. 131 - 138 (1974).

41. S. Johansson & K. Biedermann, "On the Compensation for the Transfer Function of the Microdensitometer in Measurements of MTF of Photographic Emulsions," *Phot. Sci. & Engr.*, **18**:2, p. 151 - 155 (1974).

42. K. Biedermann & S. Johansson, "A universal instrument for the evaluation of the MTF and other recording parameters of photographic materials," *Journal of Physics E: Scientific Instruments*, **8**, p. 751 - 757 (1975).

43. R.L. Lamberts & F.C. Eisen, "A System for Automated Evaluation of Modulation Transfer Functions of Photographic Materials," *J. Appl. Phot. Engr.*, **6**:1, p. 1 - 8 (1980).

44. J. Gasper, "A Monte Carlo Study of Emulsion Optics," *Proceedings of the Symposium on Photographic and Electronic Image Quality*, p. 1 - 9, Cambridge (1984).

45. J.R. Jarvis, "The Calculation of Sharpness Parameters for Colour Negative Materials Incorporating DIR Coupler," *Proceedings of the Symposium on Photographic and Electronic Image Quality*, p. 10 - 20, Cambridge (1984).

46. A.B. Keen & J.R. Jarvis, "The Calculation of Photographic Chemical Spread Functions," *Proceedings of the Symposium on Photographic and Electronic Image Quality*, p. 167 - 171, Cambridge (1984).

47. G. Boreman, "Method for measuring modulation transfer function of charge-coupled devices using laser speckle," *Optical Engineering*, **25**:1, p. 148 - 150 (1986).

48. R. VanMetter, "Measurement of MTF by Noise Power Analysis of One-Dimensional White Noise Patterns," *J. Phot. Sci.*, **38**, p. 144 - 147 (1990).

49. S. Johansson, Y.A. Lebedinsky, K.G. Predko, "Experimental MTF Measurements of CCD using an Interferometrically Generated Test Pattern," *J. Imaging Sci.*, **35**:5, p. 320 - 325 (1991).

50. S.E. Reichenbach, S.K. Park, & R. Narayanswamy, "Characterizing digital image acquisition devices," *Optical Engineering*, **30**:2, p. 170 - 177 (1991).

51. Hon-Sum Wong, "Effect of knife edge skew on modulation transfer function measurements of charge-coupled device imagers employing a scanning knife edge," *Optical Engineering*, **30**:9, p. 1394 - 1398 (1991).

52. M. Sensiper, G.D. Boreman, A.D. Ducharme, & D.R. Snyder, "Modulation transfer function testing of detector arrays using narrow band laser speckle," 50. *Optical Engineering*, **32**:2, p. 395 - 400 (1993).

53. *Photography (Materials) - Determination of ISO Resolving Power*, American National Standards Institute PH2.33 - 1983 (Reaffirmed 1990).

54. *Method for Measuring the Photographic Modulation Transfer Function of Continuous-Tone, Black-and White Photographic Films*, American National Standards Institute PH2.39 - 1976 (Reaffirmed 1990).

55. G.D. Boreman, "Modulation transfer function and number of equivalent elements for SPRITE detectors," manuscript.

Signal-to-Noise Characteristics:

56. P.G. Nutting, "On the Absorption of Light in Heterogeneous Media," *Phil. Mag.*, **26**, p. 423 - 426 (1913).

57. N. Wiener, "Generalized Harmonic Analysis," *Acta Math.*, **55**, p. 117 - 258 (1930).

58. E.W.H. Selwyn, "A Theory of Graininess," *Photogr. J.*, **75**, p. 571 - 580 (1935).

59. H. Siedentopf, "Über Körnigkeit, Dichteschwankungen und Vergrößerungsfähigkeit photographischer Negative," *Physik Zeit*, **38**, p. 454 - 459 (1937).

60. L.A. Jones & G.C. Higgins, "The Relationship Between the Granularity and Graininess of Developed Photographic Materials," *J. Opt. Soc. Amer.*, **35**, p. 435 - 475 (1945).

61. L.A. Jones & G.C. Higgins, "Photographic Granularity and Graininess, Part II. The Effects of Various Instrumental and Analytical Techniques," *J. Opt. Soc. Amer.*, **36**, p. 203 - 227 (1946).

62. L.A. Jones & G.C. Higgins, "Photographic Granularity and Graininess, Part III. Some Characteristics of the Visual System of Importance in the Evaluation of Graininess and Granularity," *J. Opt. Soc. Amer.*, **37**, p. 217 - 262 (1947).

63. L.A. Jones & G.C. Higgins, "Photographic Granularity and Graininess, Part IV. Visual Acuity Thresholds; Dynamic *versus* Static Assumptions," *J. Opt. Soc. Amer.*, **38**, p. 398 - 405 (1948).

64. L.A. Jones & G.C. Higgins, "Photographic Granularity and Graininess, Part V. A Variable-Magnification Instrument for Measuring Graininess," *J. Opt. Soc. Amer.*, **41**, p. 41 - 52 (1951).

65. L.A. Jones & G.C. Higgins, "Photographic Granularity and Graininess, Part VI. Performance Characteristics of the Variable-Magnification Graininess Instrument," *J. Opt. Soc. Amer.*, **41**, p. 64 - 75 (1951).

66. L.A. Jones & G.C. Higgins, "Photographic Granularity and Graininess, Part VII. A Microphotometer for the Measurement of Granularity," *J. Opt. Soc. Amer.*, **41**, p. 192 - 200 (1951).

67. O.H. Schade, "Image Gradation, Graininess, and Sharpness in Television and Motion Picture Systems. Part II. The Grain Structure of Motion Picture Images - an Analysis of Deviations and Fluctuations of the Sample Number," *J. Soc. Motion Pict. Tel. Engrs.*, **58**, p. 181 - 222 (1952).

68. O.H. Schade, "Image Gradation, Graininess, and Sharpness in Television and Motion Picture Systems. Part III. The Grain Structure of Television Images," *J. Soc. Motion Pict. Tel. Engrs.*, **61**, p. 97 - 164 (1953).

69. P.B. Felgett, "Concerning Photographic Grain, Signal-to-Noise Ratio, and Information," *J. Opt. Soc. Amer.*, **43**:4, p. 271 - 282 (1953).

70. L.A. Jones, G.C. Higgins, & K.F. Stultz, "Photographic Granularity and Graininess. VIII. A Method of Measuring Granularity in Terms of the Scanning Area Giving a Threshold Luminance Gradient," *J. Opt. Soc. Amer.*, **45**:2 p. 107-112 (1955)

71. R.C. Jones, "On the Minimum Energy Detectable by Photographic Negatives," *Phot. Sci. & Tech*, **2**, p. 56 - 65 (1955).

72. R.C. Jones, "New Method for Describing and Measuring the Granularity of Photographic Materials," *J. Opt. Soc. Amer.*, **45**:10, p. 799 - 808 (1955).

73. H.J. Zweig, "Autocorrelation and Granularity. Part I. Theory," *J. Opt. Soc. Amer.*, **46**:10, p. 805 - 811 (1956).

74. H.J. Zweig, "Autocorrelation and Granularity. Part II. Results on Flashed Black-and-White Emulsions," *J. Opt. Soc. Amer.*, **46**:10, p. 812 - 820 (1956).

75. A. Marriage & E. Pitts, "Relation between Granularity and Autocorrelation," *J. Opt. Soc. Amer.*, **46**:12, p. 1019 - 1027 (1956).

76. E. Pitts & A. Marriage, "Relation between Granularity and Autocorrelation. II," *J. Opt. Soc. Amer.*, **47**:4, p. 321 - 326 (1957).

77. R.B. Blackman & J.W. Tukey, *The Measurement of Power Spectra*, Dover Publications (1958).

78. R.C. Jones, "On the Minimum Energy Detectable by Photographic Materials. Part II. Results for Four Current Kodak Films,' *Phot. Sci. & Engr.*, **2**:4, p. 191 - 197 (1958).

79. R.C. Jones, "On the Minimum Energy Detectable by Photographic Materials. Part III. Energy Incident on a Microscopic Area of the Film,' *Phot. Sci. & Engr.*, **2**:4, p. 198 - 204 (1958).

80. H.J. Zweig, "Autocorrelation and Granularity. Part III. Spatial Frequency Response of the Scanning System and Granularity Correlation Effects beyond the Aperture," *J. Opt. Soc. Amer.*, **49**:3, p. 238 - 244 (1959).

81. H. Frieser, "Noise Spectrum of Developed Photographic Layers Exposed by Light, X-rays, and Electrons," *Phot. Sci. & Engr.*, **3**:4, p. 164 - 169 (1959).

82. H.J. Zweig, "The Relation of Quantum Efficiency to Energy- and Contrast-Detectivity for Photographic Materials," *Phot. Sci. & Engr.*, **5**:3, p. 142 - 148 (1961).

83. J.A. Eyer, "The Influence of Emulsion Granularity on Quantitative Photographic Radiometry," *Phot. Sci. & Engr.*, **6**:2, p. 71 - 74 (1962).

84. E.C. Doerner, "Wiener Spectrum Analysis of Photographic Granularity," *J. Opt. Soc. Amer.*, **52**, p. 669 - 672 (1962).

85. E. Klein & G. Langer, "Relations between Granularity, Graininess and the Wiener Spectrum of the Density Deviations," *J. Phot. Sci.*, **11**, p. 177 - 185 (1963).

86. J.H. Altman, "The Measurement of RMS Granularity," *Appl. Opt.*, **3**:1, p. 35 - 38 (1964).

87. D. Zwick, "Quantitative Studies of Factors Affecting Granularity," *Phot. Sci. & Engr.*, **9**:3, p. 145 - 148 (1965).

88. M. DeBelder & J. DeKerf, "The Determination of the Wiener Spectrum of Photographic Emulsion Layers with Digital Methods," *Phot. Sci. & Engr.*, **11**:6, p. 371 - 378 (1967).

89. A. Guttman, "Background - Light Sensitization of a Fast Emulsion," *Phot. Sci. & Engr.*, **12**:3, p. 146 - 153 (1968).

90. L. Brewart, "Wiener Spectrum of Experimental Emulsions with Cubic Homogeneous Grains, Comparison of the Spectra with the Wiener Spectra of Commercial Emulsions," *J. Phot. Sci.*, **17**, p. 41 - 47 (1969).

91. E.A. Trabka, "Relationship between rms Density and Transmittance Fluctuations of Photographic Film," *J. Opt. Soc. Amer.*, **59**, p. 662 - 663 (1969).

92. H.C. Schmitt, Jr. & J.H. Altman, "Method of Measuring Diffuse RMS Granularity," *Applied Optics*, **9**:4, p. 871 - 874 (1970).

93. D.H.R. Vilkomerson, "Measurements of the Noise Spectral Power Density of Photosensitive Materials at High Spatial Frequencies," *Applied Optics*, **9**:9, p. 2080 - 2087 (1970).

94. S.A. Benton & R.E. Kronauer, "Properties of Granularity Wiener Spectra," *J. Opt. Soc. Amer.*, **61**:4, p. 524 - 529 (1971).

95. E.A. Trabka, "Crowded Emulsions: Granularity Theory for Monolayers," *J. Opt. Soc. Amer.*, **61**:6, p.800-810 (1971).

96. R.H. Ericson & J.C. Marchant, "RMS granularity of monodisperse photographic emulsions," *Phot. Sci. & Engr.*, **16**:4, p. 253 - 257 (1972).

97. E.A. Trabka & W.H. Lawton, "Colour Granularity: A Layered Model," *J. Photogr. Sci.*, **22**, p. 131 - 136 (1974).

98. R. Shaw, "Image Noise Evaluation," *Proceedings of the SID*, **21**:3, p. 293 - 304 (1980).

99. D. Hoeschen & W. Mirande, "Measurement of Wiener Spectra with a Linear Microdensitometer," *Phot. Sci. & Engr.* **24**:5, p. 257 - 263 (1980).

100. D. Hoeschen, "The Measurement of Wiener Spectra and Granularity of Black and White Films with a Laser Microdensitometer," *Photographic Image Quality*, Oxford (1980).

101. H.M. Graves & A.E. Saunders, "The Noise-Power Spectrum of Colour Negative Film with Incorporated Couplers," *Proceedings of the Symposium on Photographic and Electronic Image Quality*, p. 21 - 31, Cambridge (1984).

102. A.B. Keen & A.E. Saunders, "Noise Analysis in Analogue Granularity Measurements," *Proceedings of the Symposium on Photographic and Electronic Image Quality*, p. 67 - 74, Cambridge (1984).

103. R.J. Geluk, "Performance Measurement of Photographic Materials using Television Techniques," *Proceedings of the Symposium on Photographic and Electronic Image Quality*, p. 75 - 79, Cambridge (1984).

104. R. Green, "Improvement in Quality of Colour Video Images by Non-linear Filtering," *Proceedings of the Symposium on Photographic and Electronic Image Quality*, Cambridge p. 80 - 85, (1984).

105. C.B. Rider, "Signal-to-Noise Considerations in Analogue Granularity Measurements," *Proceedings of the Symposium on Photographic and Electronic Image Quality*, p. 86 - 98, Cambridge (1984).

106. J.R. Jarvis, "A Granularity Theory for DIR-Incorporated Colour Negative Materials," *Proceedings of the Symposium on Photographic and Electronic Image Quality*, p. 172 - 175, Cambridge (1984).

107. P.G. Engeldrum & G.E. McNeill, "Some Experiments on the Perception of Graininess in Black and White Photographic Prints," *J. Imaging Sci.*, **29**:1, p. 18 - 23 (1985).

108. H.M. Graves & A.E. Saunders, "The Noise-Power Spectrum of Colour Negative Film with Incorporated Couplers," *J. Photogr. Sci.*, **33**, p. 145 - 153 (1985).

109. G.D. Boreman, "Fourier spectrum techniques for characterization of spatial noise in imaging arrays," *Optical Engineering*, **26**:10, p. 985 - 991 (1987).

110. P.D. Burns, "Image Signal Modulation and Noise Characteristics of Charge-Coupled Device Imagers," *SPIE Vol. 1071 Optical Sensors and Electronic Photography*, (1989).

111. A. Juenger & E.W. Higgins, "A Graininess Metric for Electronic Still Photography," *Proceedings, IS&T's 46th Annual Conference* (1993).

112. *Root Mean Square (rms) Granularity of Film (Images on One Side Only) - Method for Measuring*, American National Standards Institute PH2.40 - 1985 (Reaffirmed 1991).

113. G.D. Boreman & P.L. Heron, "Description of Fixed-Pattern Noise in CCD's Using the Spatial Power Spectrum," manuscript.

Psychological Scaling & Subjective Testing:

114. H. Frieser & K. Biedermann, "Experiments on Image Quality in Relation to Modulation Transfer Function and Graininess of Photographs," presented at the SPSE Annual Conference in Boston, (1962).

115. M.C. Goddard & R.G. Gendron, "Variations of SMT Acutance with System Elements," *Phot. Sci. & Engr.*, **10**:2, p. 77 - 80 (1966).

116. F. Scott, "The Search for a Summary Measure of Image Quality - A Progress Report," *Phot. Sci. & Engr.*, **12**:3, p. 154 - 164 (1968).

117. R.P. Chambers & J.S. Courtney-Pratt, "Experiments on the Detection of Visual Signals in Noise Using Computer Generated Signals," *Phot. Sci. & Engr.*, **13**:6, p. 286 - 298 (1969).

118. G.C. Higgins, "Methods for Analyzing the Photographic System, Including the Effects of Nonlinearity and Spatial Frequency Response," *Phot. Sci. & Engr.*, **15**:2, p. 106 - 118 (1971).

119. T.W. Barnard, "Image evaluation by means of target recognition," *Phot. Sci. & Engr.*, **16**:2, p. 144 - 150 (1972).

120. E.M. Granger & K.N. Cupery, "An optical merit function (SQF), which correlates with subjective image judgments," *Phot. Sci. & Engr.*, **16**:3, p. 221 - 230 (1972).

121. D.M. Zwick, "Film graininess and density - A critical relationship," *Phot. Sci. & Engr.*, **16**:5, p. 345 - 348 (1972).

122. W.N. Charman, "Visual Factors in Photographic Detection, Recognition, and Resolution Tasks," *Phot. Sci. & Engr.*, **19**:4, p. 228 - 234 (1975).

123. D. Zwick & D.L. Brothers, Jr., "RMS Granularity: Determination of Just-Noticeable Differences," *Phot. Sci. & Engr.*, **19**:4, p. 235 - 238 (1975).

124. G.T. Yonemura, "An Image Quality Criterion for the Identification of Faces," *Selected Readings in Image Evaluation*, R. Shaw, ed., p. 488 - 492, SPSE (1976).

125. G. Westheimer, "Spatial frequency and light spread descriptions of visual acuity and hyperacuity," *J. Opt. Soc. Amer.* **67**:2, p. 207 - 212 (1977).

126. R.F. Quick, Jr., W.W. Mullins, & R.N. Lucas, "Contrast Thresholds of Random Patterns," *Phot. Sci. & Engr.* **22**:2, p.72 - 75 (1978).

127. H.J. Metz, S. Ruchti, & K. Seidel, "Comparison of Image Quality and Information Capacity for Different Model Imaging Systems," *J. Photogr. Sci.*, **26**, p. 229 - 233 (1978).

128. J.R. Hamerly & R.M. Springer, "Raggedness of edges," *J. Opt. Soc. Amer.* **71**:3, p.285 - 288 (1981).

129. C.J. Bartleson, "The Combined Influence of Sharpness and Graininess on the Quality of Colour Prints," *J. Photogr. Sci.*, **30**, p. 33 - 38 (1982).

130. G.P. Corey, M.J. Clayton, & K.N. Cupery, "Scene Dependence of Image Quality," *Phot. Sci. & Engr.*, **27**, p. 9 - 13 (1983).

131. J.R. Hamerly, "Just-Noticeable Differences for Solid Area Noise," *J. Appl. Phot. Engr.* **9**:1, p.14 - 17 (1983).

132. K. Biedermann & Y. Feng, "Quality Criteria for Photographic Images and Lenses," *Proceedings of the Symposium on Photographic and Electronic Image Quality*, p. 32 - 40, Cambridge (1984).

133. D.M. Zwick, "Psychometric Scaling of Terms Used in Category Scales of Image Quality Attributes," *Proceedings of the Symposium on Photographic and Electronic Image Quality*, p. 46 - 55, Cambridge (1984).

134. Y. Miyake, S. Inoue, S. Kubo, Y. Tamoto, "Evaluation of Image Quality of Digital Pictures Obtained by Drum Scanner and Photo-printer," *Proceedings of the Symposium on Photographic and Electronic Image Quality*, p. 62 - 66, Cambridge (1984).

135. K. Birgmeir, "Comparison of the Image Quality of Conventionally and Electronically Produced Prints," *Proceedings of the Symposium on Photographic and Electronic Image Quality*, p. 108 - 118, Cambridge (1984).

136. K.M. Hanson, "Image Quality Indices based upon the Performance of Specific Tasks by the Ideal Observer," *Proceedings of the Symposium on Photographic and Electronic Image Quality*, p. 166, Cambridge (1984).

137. W.E. Glenn, K.G. Glenn, & C.J. Bastian, "Imaging System Design Based on Psychovisual Data," *Proceedings of the SID*, **26**:1, p. 71 - 78 (1985).

138. C.J. Bartleson, "Predicting Graininess from Granularity," *J. Photogr. Sci.*, **33**, p. 117 - 126 (1985).

139. Y. Miyake, S. Inoue, M. Inui, S. Kubo, "An Evaluation of Image Quality for Quantized Continuous Tone Image," *J. Imaging Tech.*, **12**:1, p. 25 - 34 (1986).

140. J. Bowman, J. Bullitt, F.R. Cottrell, B. Hultgren, "Color Print Image Quality I: Scaling Techniques for Image Quality," *Paper Summaries, 42nd Annual Conference of the SPSE*, p. 465 (1989).

141. B. Hultgren, J. Bowman, J. Bullitt, F.R. Cottrell, "Color Print Image Quality II: The Combined Influence of Sharpness and Grain," *Paper Summaries, 42nd Annual Conference of the SPSE*, p. 466 (1989).

142. J. Bullitt, J. Bowman, F.R. Cottrell, B. Hultgren, "Color Print Image Quality III: Exposure and Color Balance," *Paper Summaries, 42nd Annual Conference of the SPSE*, p. 468 (1989).

Detective Quantum Efficiency:

143. L. Silberstein, "Quantum Theory of Photographic Exposure," *Phil. Mag.*, 44, p. 257 - 273 (1922)

144. A. Rose, "A Unified Approach to the Performance of Photographic Film, Television Pickup Tubes, and the Human Eye," *J. SMPE*, **47**, p. 273 - 294 (1946).

145. A.Rose, "Television Pickup Tubes and the Problem of Vision," *Advances in Electronics*, L. Marton, ed., **1**, p. 131 - 166, Academic Press, New York (1948).

146. J.H. Webb, "Absolute Sensitivity Measurements on Single-Grain-Layer Photographic Plates for Different Wave-Lengths," *J. Opt Soc. Amer.*, **38**:4, p. 312 - 323 (1948)

147. R.C. Jones, "On the Quantum Efficiency of Photographic Negatives," *Phot. Sci. & Engr.*, **2**:2, p. 57 - 65 (1958).

148. A. Marriage, "How Many Quanta?" *J. Phot. Sci.*, **9**, p. 93 - 100 (1961)

149. H.J. Zwieg, K.F. Stultz, and D.L. MacAdam, "Effect of Complex Granularity Patterns on the Determination of Quantum Efficiency," *J. Phot. Sci.*, **9**, p. 273 - 274 (1961).

150. H.F. Nitka, "Sensitivity and Detail Rendition in the Recording of Light Images and Electron Beams," *Phot. Sci. & Engr.*, **7**:3 p. 188-195 (1963).

151. R. Shaw, "The Equivalent Quantum Efficiency of the Photographic Process," *J. Phot. Sci.*, **11**, p.199 - 204 (1963).

152. H.J. Zwieg, "Performance Criteria for Photodetectors - Concepts in Evolution," *Phot. Sci. & Engr.*, **8**:6, p. 305 - 311 (1964).

153. R. Shaw, "Image Characteristics of Model Photodetectors," *J. Phot. Sci.*, **15**, p. 78 - 83 (1967).

154. R. Shaw & A. Shipman, "Practical Factors Influencing the Signal-to-Noise Ratio of Photographic Images," *J. Phot. Sci.*, **17**, p. 205 - 210 (1969).

155. A. Shepp & W. Kammerer, "Increased Detectivity by Low Gamma Processing," *Phot. Sci. & Engr.*, **14**:5, p. 363 - 368 (1970).

156. H.E. Spencer, "Calculated Sensitivity Contributions to Detective Quantum Efficiency in Photographic Emulsions," *Phot. Sci. & Engr.*, **15**:5, p. 468 - 471 (1971).

157. R. Shaw, "Multilevel grains and the ideal photographic detector," *Phot. Sci. & Engr.*, **16**:3, p. 192 - 200 (1972).

158. J.F. Hamilton, "Simulated detective quantum efficiency of a model photographic emulsion," *Phot. Sci. & Engr.*, **16**:2, p. 126 - 130 (1972).

159. R. Shaw, "Image evaluation as an aid to photographic emulsion design," *Phot. Sci. & Engr.*, **16**:6, p. 395 - 405 (1972).

160. G.R. Bird, "Noiseless chemical amplifiers and the ultimate capabilities of organic imaging systems," *Phot. Sci. & Engr.*, **17**:3, p. 261 - 267 (1973).

161. R. Shaw, "Photon noise amplification due to photographic defects," *Phot. Sci. & Engr.*, **17**:6, p. 491 - 494 (1973).

162. R. Shaw, "The influence of fog grains on detective quantum efficiency," *Phot. Sci. & Engr.*, **17**:6, p. 495 - 498 (1973).

163. M.R.V. Sahyun, "Relationship Between Kinetics of Development of a Silver Halide Photographic Material and its Quantum Efficiency," *Phot. Sci. & Engr.*, **19**:1, p. 38 - 43 (1975).

164. R. Shaw, "Evaluating the efficiency of imaging processes," *Rep. Prog. Phys.*, **41** p. 1103-1155 (1981)

165. A.E. Saunders, "On the Design of Astronomical Plates," *Proceedings of the Symposium on Photographic and Electronic Image Quality*, p. 142 - 145, Cambridge (1984).

166. R. Shaw & R.L. VanMetter, "The role of screen and film in determining the noise equivalent number of quanta recorded by a screen-film system," *SPIE Vol. 535 Application of Optical Instrumentation in Medicine XIII*, p. 184 - 194 (1985).

167. P.D. Burns, "Analysis of the Image Signal Modulation and Noise Characteristics of Laser Printers," *J. Imaging Sci.*, **31**:2, p. 74 - 81 (1987).

168. R. Shaw, "Image Analysis for Laser-Written Hardcopy," *Proceedings of the International Conference on Lasers* (1987).

169. R. Shaw, "Quality criteria for quantized images," *SPIE Vol. 901 Image Processing, Analysis, Measurement, and Quality*, p. 139 - 143 (1988).

170. P.D. Burns, "Signal-to-Noise Ratio Analysis of Charge-Coupled Device Imagers," *SPIE Vol. 1242* (1990).

Information Theory:

171. P. Mertz & F. Gray, "A Theory of Scanning and Its Relation to the Characteristics of the Transmitted Signal in Telephotography and Television," *Bell System Technical Journal*, **13**, p. 464 - 515 (1934).

172. C.E. Shannon, "A Mathematical Theory of Communication," *Bell System Technical Journal*, **27**, p. 379 - 423 (1948).

173. C.E. Shannon, "Communication in the Presence of Noise," *Proc. IRE*, **37**, p. 10 - 21 (1949).

174. D.A. Huffman, "A Method for the Construction of Minimum-Redundancy Codes," *Proc. IRE*, **40**, p. 1098 - 1101 (1952).

175. P.B. Felgett & E.H. Linfoot, "On the Assessment of Optical Images," *Phil. Trans. Roy. Soc. London, Ser. A*, **247**, p. 369 - 407 (1955).

176. H.J. Zwieg, G.C. Higgins, & D.L. MacAdam, "On the Information Detecting Capacity of Photographic Emulsions," *J. Opt. Soc. Amer.*, **48**, p. 926 - 933 (1958).

177. R. Shaw, "The Application of Fourier Techniques and Information Theory to the Assessment of Photographic Image Quality," *Phot. Sci. & Engr.*, **6**:5, p. 281 - 286 (1962).

178. J.H. Altman & H.J. Zweig, "Effect of Spread Function on the Storage of Information on Photographic Emulsions," *Phot. Sci. & Engr.*, **7**:3, p. 173 - 177 (1963).

179. R. Shaw, "Photon Fluctuations, Equivalent Quantum Efficiency, and the Information Capacity of Photographic Images," *J. Phot. Sci.*, **11**, p. 313 - 320 (1963).

180. C.J. Bartleson & R.F. Witzel, "Source Coding of Image Information," *Phot. Sci. & Engr.*, **11**:4, p. 263 - 269 (1967).

181. D.H. Lehmbeck, "Experimental Study of the Information Storing Properties of Extended Range Film," *Phot. Sci. & Engr.*, **11**:4, p. 270 - 278 (1967).

182. J. Riesenfeld, "Relationships Between Information Capacity and Resolving Power," *Phot. Sci. & Engr.*, **11**:6, p. 415 - 418 (1967).

183. F.T.S. Yu, "Markov Photographic Noise," *J. Opt. Soc. Amer.*, **59**:3, p. 342 - 344 (1969).

184. R. Shaw & P.D. Burns, "Noise Requirements for the Recording Medium of a Laser Printing Device," *SPSE - Advances in Non-Impact Printing Technologies*, (1984).

185. R.E. Burge, "Image Fidelity and Data Compression," *Proceedings of the Symposium on Photographic and Electronic Image Quality*, p. 99, Cambridge (1984).

186. P.G. Powell & B.E. Bayer, "A Method for the Digital Enhancement of Unsharp, Grainy Photographic Images," *Proceedings of the Symposium on Photographic and Electronic Image Quality*, p. 119 - 125, Cambridge (1984).

187. G. Fischer & K.R. Scheuter, "Frequency Modulation Picture Recording with Random Pixel Distribution," *Proceedings of the Symposium on Photographic and Electronic Image Quality*, p. 154 - 160, Cambridge (1984).

Microdensitometry:

188. R.A. Jones & John F. Coughlin, "Elimination of Microdensitometer Degradation from Scans of Photographic Images," *Applied Optics*, 5:9, p. 1411 - 1414 (1966).

189. D. Galburt, R.A. Jones, & J. W. Bossung, "Critical Design Factors Affecting the Performance of a Microdensitometer," *Phot. Sci. & Engr.*, **13**:4, p. 205 - 209 (1969).

190. T.H. Lee, T.J. Tredwell, B.C. Burkey, T.M. Kelly, R.P. Khosla, D.L. Losee, R.L. Nielsen, & W.C. McColgin, "A 360,000 Pixel Charge-Coupled Color Image Sensor for Imaging Photographic Negatives," *Proceedings of the Symposium on Photographic and Electronic Image Quality*, p. 100 - 107, Cambridge (1984).

191. D. Difrancesco, "High Resolution Three Color Laser Scanner for Motion Pictures," *Proceedings of the Symposium on Photographic and Electronic Image Quality*, p. 126 - 135, Cambridge (1984).

192. T.J. Tucker & A.E. Saunders, "A Video Technique for Photographic Image Structure Measurements," *Proceedings of the Symposium on Photographic and Electronic Image Quality*, p. 136 - 141, Cambridge (1984).

193. Pei-jie Xia & Yu-chen Liu, "The Effect of Shape of Sampling Aperture on Granularity Measurement of Patterned Silver Halide Grain Layers," *Proceedings of the Symposium on Photographic and Electronic Image Quality*, p. 176 - 185, Cambridge (1984).

194. He Guang-qian, Zhang Jing-xian, & Mao Xiang, "Diffuse RMS Granularity Measurements for B/W Films," *Proceedings of the Symposium on Photographic and Electronic Image Quality*, p. 186 - 188, Cambridge (1984).

195. D. Hertel, D. Schellbach, K. Töpfer, & E. Görgens, "Automatische Bildqualitätsanalyse photographischer Aufzeichnungsmaterialien mit CCD-Zeilerkamera," *J. Inf. Rec. Mater.*, **16**:3, p.185 - 201 (1988).

196. K. Töpfer, E. Görgens, D. Hertel, U. Dieckmann, & H. Böttcher, "Experimental Investigations on the Image Quality of Commercial Silver Halide Films," *J. Photogr. Sci.*, **37**, p.38 - 43 (1989)

197. D. Hertel, K. Töpfer, H. Böttcher, "Image Quality Investigations by Means of Photodetector Arrays - An Effective Method and Some Aspects of its Experimental Realization," *Proceedings, IS&T's 46th Annual Conference* (1993).